# Synthesis and Evaluation of Novel 3,2-Hydroxypyridinone Based „Smart" Contrast Agents for Functional Magnetic Resonance Imaging

**Dissertation**

der Mathematisch-Naturwissenschaftlichen Fakultät

der Eberhard Karls Universität Tübingen

zur Erlangung des Grades eines

Doktors der Naturwissenschaften

(Dr. rer. nat.)

vorgelegt von

Karolina Jankowska

aus Konskie

Tübingen

2013

Hereby I declare the fact that I am writing this work and no different than the indicated aids had been used.

To Ulrich, Aneta & Ilgar.

Without you this would not have been possible.

# Acknowledgments

# Abbreviations

| | |
|---|---|
| 1,2-HOPO | 1,2-hydroxypyridinone |
| 1-Me-HOPO | 1-methyl-3,2-hydroxypyridinone |
| 3,2-HOPO | 3,2-hydroxypyridinone |
| AA | arachidonic acid |
| AAZTA | 6-amino-6-methylperhydro-1,4-diazepinetetraacetic acid |
| APTRA | 2-aminophenol-N,N,O-triacetic acid |
| asp | aspartic acid |
| BAC | bis(acetate) |
| BAPTA | 1,2-bis(o-aminophenoxy)ethane-N,N,N',N'-tetraacetic acid |
| BMS | bulk magnetic susceptibility measurements |
| Boc | *tert*-butylcarbamate |
| BP2A | 2,11-Diaza[3.3](2,6)pyridinophane-N,"-diacetic acid |
| Bu | butyl |
| CA | contrast agent |
| calc. | calculated |
| CaM | calmodulin |
| Cbz | benzyl carbamate |
| CDCl$_3$ | deuterated chloroform |
| CDI | 1,1'-carbonyldiimidazole |
| CEST | chemical exchange saturation transfer |
| cyclen | 1,4,7,10-tetraazacyclododecane |
| d | dublet |
| DCC | N,N-dicyclohexylcarbodiimide |

| | |
|---|---|
| DCM | dichloromethane |
| DIPEA | ethyldiisopropylamine |
| DMAP | 4-(dimethylamino)pyridine |
| DMF | N,N-dimethylformamide |
| DMSO | dimethylsulfoxide |
| DO3A | 2,2',2''-(1,4,7,10-tetraazacyclododecane-1,4,7-triyl)triacetic acid |
| DOTA | 1,4,7,10-tetraazacyclododecane-1,4,7,10-tetraacetic acid |
| DTPA | diethylenetriaminepentaacetic acid |
| DTPA-BMA | diethylenetriaminepentaacetate-bis(methylamide) |
| EA | esteramide |
| EDC | N-(3-Dimethylaminopropyl)-N′-ethylcarbodiimide |
| EDTA | ethylenediaminetetraacetate |
| eq. | equation |
| eq | equivalent |
| ESI | electrospray ionisation |
| Et | ethyl |
| FAB | fast atom bombardment |
| Fig. | figure |
| $GdCl_3$ | gadolinium chloride |
| HEPES | 4-(2-Hydroxyethyl)piperazine-1-ethanesulfonic acid |
| HOPY | 6-carboxyamido-5,4-hydroxypyrimidone |
| HPLC | high performance liquid chromatography |
| HR-MS | high resolution mass |
| HSA | human serum albumin |
| Hz | hertz |
| IAM | 2-hydroxyisophthalamide |

| | |
|---|---|
| ICP-MS | inductively coupled plasma mass spectrometry |
| $J$ | coupling constant |
| $k_{ex}$ | solvent exchange rate |
| $m$ | *meta* position |
| M | molar |
| m | multiplet |
| $M_0$ | equilibrium at applied magnetic field $B_0$ |
| MAM | maltol |
| Me | methyl |
| Me-MAM | 6-methylmaltol |
| MeOH | methanol |
| min | minutes |
| MOM | methoxy-methyl |
| MRI | magnetic resonance imaging |
| $M_z$ | longitudinal magnetization, |
| NBA | 3-nitrobenzyl alcohol |
| $^n$BuLi | *n*-butyllithium |
| NMR | nuclear magnetic resonance |
| NMRD | nuclear magnetic relaxation dispersion |
| $p$ | *para* position |
| PCT2A | pyridine-containing macrocycle biacetate |
| PCTA | pyridine-containing macrocycle triacetate |
| PEG | polyethylene glycol |
| PFP TFA | perfluorophenyl 2,2,2-trifluoroactetate |
| pht | phthalimide |
| PLL | poly-L-lysine |
| py | pyridine |

| | |
|---|---|
| q | hydration number |
| q | quartet |
| quin | quintet |
| Ra-Ni | Raney nickel |
| r.t. | room temperature |
| $r_1$ | longitudinal relaxivity |
| $r_2$ | transverse relaxivity |
| RF | radio frequency |
| ROI | region of interest |
| RT | retention time |
| s | singlet |
| SAM | salicylamide |
| SEAP | secreted alkaline phosphatase |
| $SiO_2$ | silica gel |
| SPIOs | super paramagnetic iron oxide particles |
| t | time |
| T | tesla |
| t | triplet |
| $T_1$ | longitudinal (or spin – lattice) relaxation time |
| $T_2$ | transverse (or spin-spin) relaxation time |
| TACN | triazacyclonanone |
| TAM | terephathalamide |
| $^t$Bu | *tert*-butyl |
| TFA | trifluoroacetic acid |
| THF | tetrahydrofurane |
| TMEDA | 1,1',2,2'-tetra-methylethylenediamine |
| TREN | tris(2-aminoethyl)amine |

| | |
|---|---|
| TsOH | *p*-toluenesulfonic acid |
| tyr-gal | tyrosine-galactose |
| UV-VIS | ultraviolet-visibile |
| $\delta$ | chemical shift |
| $\lambda$ | wavelenght |
| $\tau_M$ | mean water residence time, reciprocal of $k_{ex}$ |
| $\tau_r$ | rotational correlation time |

# Table of Contents

# Chapter 1

# Literature

# 1. Introduction

During the last 20 years magnetic resonance imaging (MRI) became a very popular diagnostic and research tool in medicine and neuroscience. The admiration of physicians and researchers alike is well deserved thanks to the high quality three dimensional images of the soft tissue obtained in a non-invasive manner. A lack of harmful radiation and no need for additional equipment also add to the advantages of MRI.[1,2] The contrast of the MR images is generated when the spins of water protons present in every tissue are realigning back with the external magnetic field after applying a magnetic pulse.[3] In addition to endogenous contrast difference, the contrast of the MR images can be enhanced by chemical substances called contrast agents (CA). CAs are paramagnetic materials which influence the longitudinal and transverse relaxation rates of bulk solvent protons in their vicinity.[4] Unfortunately, paramagnetic ions, like $Gd^{3+}$, $Fe^{3+}$ or $Mn^{2+}$, are toxic and cause severe kidney failure, cell death or disturb ion balance. Therefore, to diminish toxicity, the ions are entrapped within organic ligands. Interestingly, the purpose of ligands is not only limited to neutralization of harmful ions but also may alter paramagnetic properties of the metal ion. Moreover, the ligands also allow further functionalization of CAs. This would allow targeting of desired ions, biologically significant molecules, e.g. neurotransmitters, or particular cells and tissue types, e.g. tumours.

## 1.1. Basics of MRI signal acquisition and the importance of relaxivity

Spins of all nuclei in their resting state are always aligned with an external magnetic field $B_0$. This alignment can be easily disturbed by application of a radio frequency (RF) pulse carrying enough energy for the nuclei spins to change their orientation and transit to a higher energy level. For protons this would be particularly the Larmor frequency which is proportional to the strength of the applied magnetic field and the gyromagnetic constant of the hydrogen nuclei. After the RF pulse is removed, the nuclei spins are realigning back with the external magnetic field and two processes are occurring during that time: spin-lattice ($R_1$) and spin-spin ($R_2$) relaxation.

The longitudinal (or spin – lattice) relaxation time $T_1$ is a time constant describing how fast the spin of a nucleus is realigning with the outer magnetic field by a factor of e after applying a magnetic pulse of a frequency which is at least equal to the energy difference between spin states (Fig. 1a).[5]
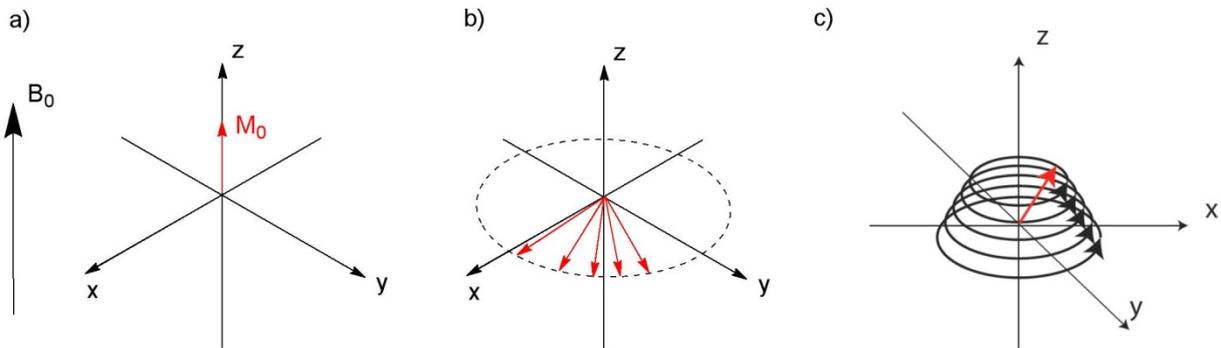
It is defined by eq. 1:

$$M_z = M_0 \left(1 - e^{\frac{-t}{T_1}}\right)$$
(1)

where $M_z$ is the longitudinal magnetization, $M_0$ is the equilibrium at applied magnetic field $B_0$ and t is time after which the spin is fully realigned with $B_0$.

When nuclei spins are returning to the equilibrium state, the vectors are rotating around the Z axis (Fig. 1b) and they start to dephase due to the fact that every spin packet is interacting with other spins and starts to rotate at its own Larmor frequency. This is known as a transverse relaxation and is characterized by constant $R_2$. The transverse (or spin-spin) relaxation time $T_2$ is the time required to reduce the transverse magnetization $M_{XY}$ by a factor of e (eq. 2):

$$M_{XY} = M_{XY0} e^{\frac{-t}{T_2}}$$
(2)

Both $T_1$ and $T_2$ processes occur simultaneously, providing that $T_2 \leq T_1$. Fig. 1c presents how both longitudinal and transverse relaxations are influencing each other.

The relaxation rate ($\frac{1}{T_i}, i = 1,2$) in presence of a CA is defined as a sum of paramagnetic (p) and diamagnetic (d) relaxation rates of solvent nuclei, as presented in eq. 3:

$$\frac{1}{T_i} = \left(\frac{1}{T_i}\right)_d + \left(\frac{1}{T_i}\right)_p , (i = 1,2) \tag{3}$$

The diamagnetic contribution is a constant value for a specified solvent in absence of paramagnetic contrast agent. The paramagnetic contributions are dependent on concentration of the paramagnetic metal centre [Gd] as presented in eq. 4:

$$\frac{1}{T_i} = \left(\frac{1}{T_i}\right)_d + r_i[Gd] , (i = 1,2) \tag{4}$$

Therefore the most important value, relaxivity $r_i$, is defined as the slope of the function of relaxation rate versus concentration and is expressed in mM$^{-1}$s$^{-1}$ (Fig. 2).
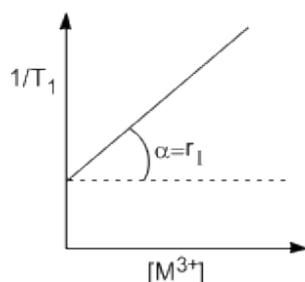


**Figure 2**

Other parameters determining the paramagnetic relaxation rate are the inner- and outer-sphere relaxation rates (eq. 5)

$$\left(\frac{1}{T_i}\right)_p = \left(\frac{1}{T_i}\right)_{inner-sphere} + \left(\frac{1}{T_i}\right)_{outer-sphere} , (i = 1,2) \tag{5}$$

The inner sphere relaxation rate is the change in relaxation rate of the solvent nuclei directly bound to the metal centre of the CA and the outer sphere relaxation rate

describes relaxivity changes of the nuclei in the second or further coordination sphere.

The inner sphere relaxation rate is dependent on the hydration number of a CA (q), the rotational correlation time $\tau_r$ and the solvent exchange rate $k_{ex}$ which is the reciprocal of the waters' molecule mean life time $\tau_M$ as shown in eq. 6.[6]

$$\left(\frac{1}{T_i}\right) = qP_m \left[\frac{1}{(T_{im}+\tau_M)}\right] , (i = 1,2) \tag{6}$$

The hydration number, q, is the number of water molecules directly bound to the metal ion. The rotational correlation time $\tau_r$ describes how fast the CA tumbles in the solution and the solvent exchange rate, $k_{ex}$, tells how fast protons of water molecules directly coordinated to the metal centre are exchanging with protons of the bulk solvent. All three parameters are presented in Fig. 3.
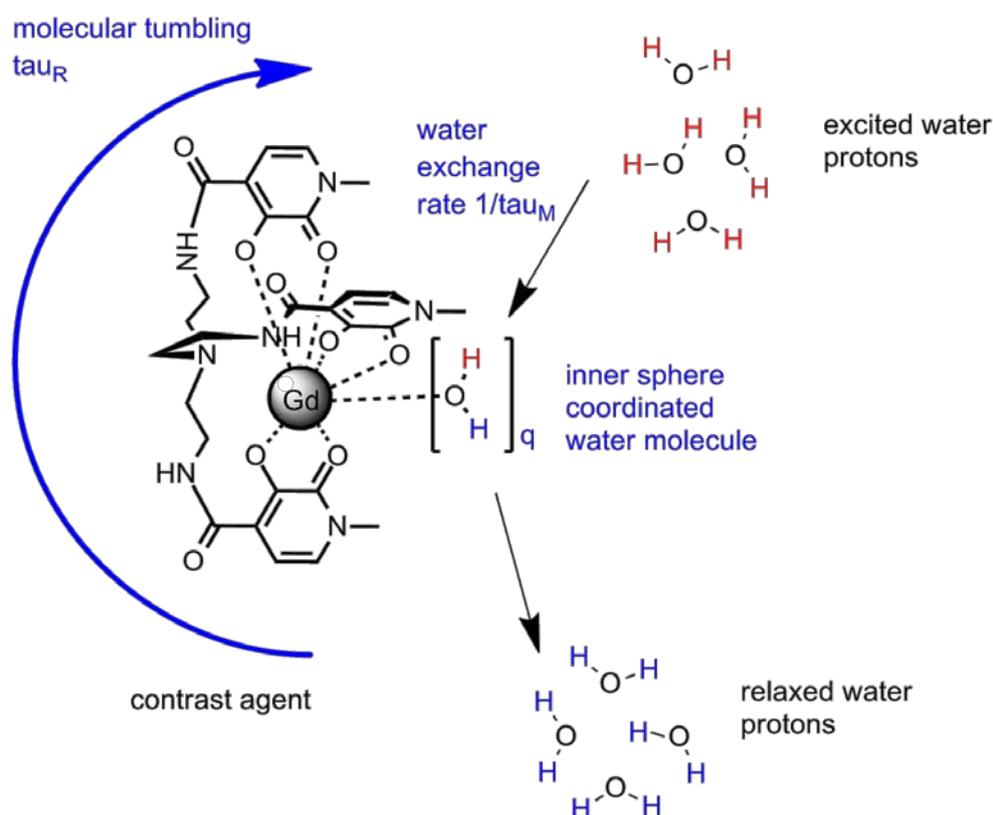


Figure 3 The crucial parameters responsible for the performance of a CA.

The outer sphere relaxation rate is dependent on the concentration of the CA, the distance between the complex and the closest water molecule and the diffusion constants of the complex and water itself.

## 1.2. Relaxivity is critical for contrast agents (CAs)

Commercially available CAs possess very important high thermodynamic stability (high stability constant of the complex) and kinetic inertness (no dissociation of the agent in biological media),[7-9] but they lack relaxivity values that would allow their application at higher magnetic fields (above 100 MHz), where the dominating relaxivity mechanisms are based on hydration number, q, and water exchange rate, $k_{ex}$. Therefore agents which present higher relaxivity are needed.

There are different ways to increase the efficiency of a CA, based on parameters influencing relaxivity:

- modulate the hydration number q;

- increase the water exchange rate $k_{ex}$;

- decrease the correlation time $\tau_r$;

The most profitable approach is to increase the hydration number q. There are several systems which exhibit a q>1 but their stability is jeopardized due to decreased denticity.[10] The trade-off between stability and high number of coordinated water molecules is a true challenge. Nevertheless, there are systems which are stable despite the decreased denticity allowing at least two water molecules coordinated in the inner sphere (Fig. 4a).

The second most popular system, right after 1,4,7,10-tetraazacyclododecane-1,4,7,10-tetraacetic acid (DOTA), is 2,2',2''-(1,4,7,10-tetraazacyclododecane-1,4,7-triyl)triacetic acid (DO3A), both presented in Fig. 4a. In comparison to DOTA, DO3A has one coordinating site less and therefore a higher hydration number (q=2),[11] while it still exhibits high thermodynamic stability and kinetic inertness.[12] Yet, although this group of compounds shows desirable characteristics, it does not exhibit significant increase in relaxivity despite a 100% increase in q.

**a) optimized q**
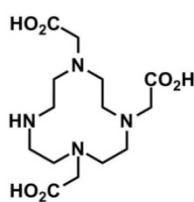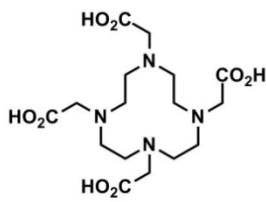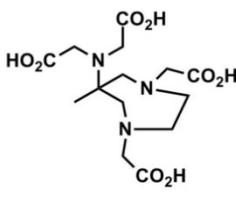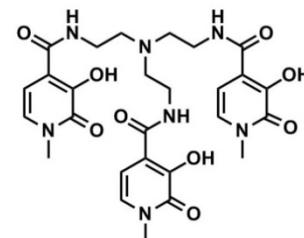


DO3A  DOTA  AAZTA  HOPO
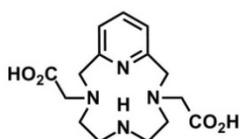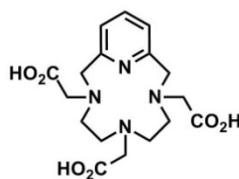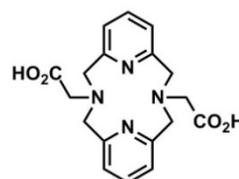
PC2A  PCTA  BP2A

**b) adjusted $k_{ex}$**
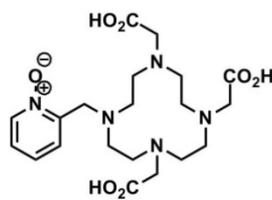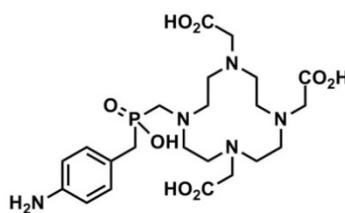


DO3A-pyNox  DO3AP$^{ABn}$

**c) slowed down $\tau_R$**
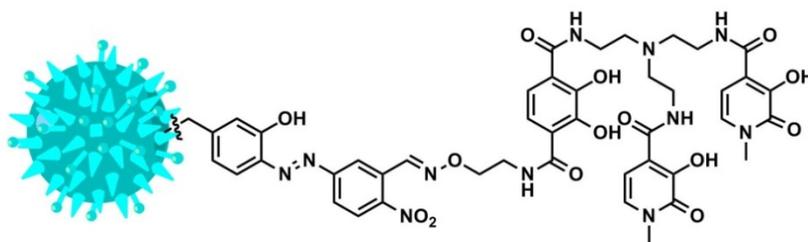


HOPO conjugated to a MS2 virus capsid

**Figure 4 Examples of ligands used for preparation of CAs with increased the relaxivity.**

Derivatives of 6-amino-6-methylperhydro-1,4-diazepinetetraacetic acid (AAZTA, Fig. 4a) are another class of contrast agents allowing an access of 2 water molecules to the metal centre without toxicological issues.[13] Moreover, it allows additional alterations and shows satisfying longitudinal relaxivity ($r_1$=8-12 mM$^{-1}$s$^{-1}$).[14]

An alternative class of CAs is a group of 1,4,7,10-tetraazacyclododecane, cyclen, derivatives containing pyridine moieties build in the macrocyclic ring. This particular system shows multiple water molecules coordinated in the inner sphere of the metal ion, with up to 4 coordinated water molecules. The family consists of pyridine-containing macrocycle triacetate (PCTA), pyridine-containing macrocycle biacetate (PC2A) and 2,11-diaza[3.3](2,6)pyridinophane-N,N'-diacetic acid (BP2A)[15] (Fig. 4a). The most stable of them is the Gd$^{3+}$-PCTA complex due to its heptadenticity.[16] Gd$^{3+}$ complexes of PC2A and BP2A present much worse stability.[17] Nevertheless, despite the double longitudinal relaxivity in comparison to DOTA ($r_1$=4.5 mM$^{-1}$s$^{-1}$), this group of CAs proved problematic for further synthetic modifications without disturbing the stability.

Finally, there is one more category of contrast agents based on pyridine derivatives. Hydroxypyridinone (HOPO, Fig. 4a) based systems present high thermodynamic stability, high hydration number and high longitudinal relaxivity,[6] making them potentially well suited for use as MRI CAs. Since the aim of this thesis was to synthesize HOPO-based Ca$^{2+}$-responsive MRI CAs, the properties of HOPO CAs will be presented in more detail in later sections.

Modulation of the exchange rate of water protons $k_{ex}$ is an alternative method to increase relaxivity. This can be achieved by a steric hindrance of the metal centre at the water binding sites. One has to keep in mind however, that by optimizing this parameter, a trade off with stability exists as shown by Merbach and co-workers.[18,19] Examples presenting a balance between stability and water exchange rate $k_{ex}$ are reported. For example, DO3A derivatives containing pyridine N-oxide[20] or phosphinic[21] pendants (both in Fig. 4b) showed to have respectively 6 and 15 times higher $k_{ex}$ and therefore longitudinal relaxivity was 2 and 15% higher. Also, previously described AAZTA and PCT agents show almost 3 times higher water exchange rate. Additionally, attaching a phosphinic pendant to a PCT CA further increases the $k_{ex}$.[22]

The tumbling rate of the CA has also influence on its relaxivity. Slowing down the $\tau_R$, resulting in increasing relaxivity, can be achieved by attaching a single or multiple CAs to a cargo molecule like a peptide,[23] virus[24] (Fig. 4c) or a synthetic dendrimer.[25] There is, however, one condition which has to be fulfilled – the linkage between the cargo molecule and the Gd-complex should be rigid. Otherwise the local movement of the CA will diminish the enhancement in relaxivity gained by slow global rotation.[24,25]

## 1.3. Responsive/smart contrast agents (S)CAs

A contrast agent modified with a functional moiety able to detect a variation of a given physicochemical parameter of the tissue is called a responsive CA.[4] An analyte to which a responsive CA reacts may be an ion, metabolite or a receptor on a cell membrane.

There are two main strategies to modulate CAs' response towards detected ion. The first one involves a change in the number of water molecules in the presence and absence of the analyte (Fig. 5a). When the specific ion is present, the functional moiety is coordinating to it and the access of water molecules to a metal centre is left open. This results in a higher q, which translates to higher relaxivity and therefore a brighter MR image is observed. On the other hand, in the absence of the ion, the responsive part is coordinating to the metal ion and therefore obstructing admission of water. The lower q in this case results in lower relaxivity and a darker MR image. An example of such an agent was published by Dhingra *et al.*[26] In their study, the utilised *o*-aminophenol-N,N,O-triacetic acid (APTRA) derivative responsible for $Ca^{2+}$ chelation was coordinating to $Gd^{3+}$ in absence of calcium and allowed the access of water molecules to the metal centre when $Ca^{2+}$ was present giving 100% of relaxivity change.
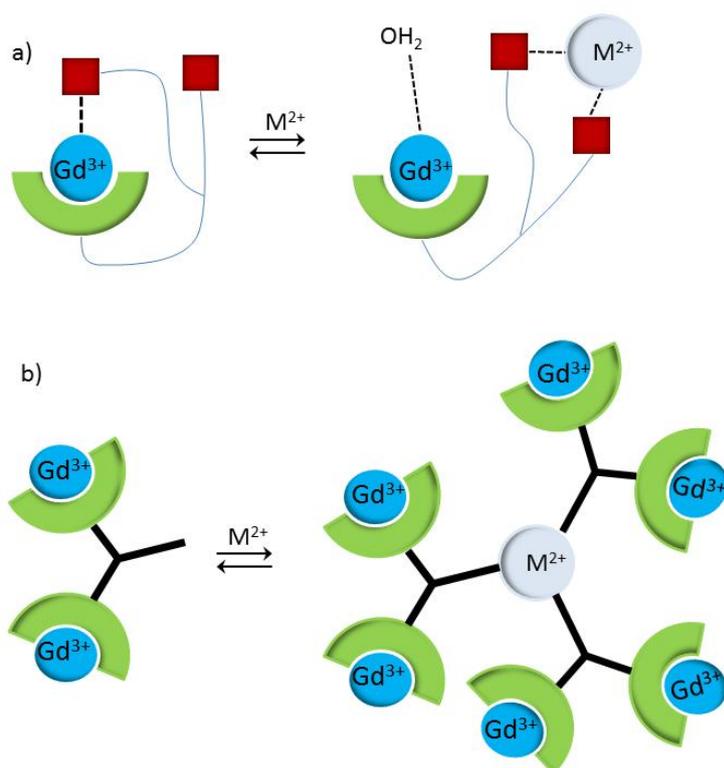
**Figure 5 Two possible mechanism of behaviour of an SCA in presence of an analyte**

The second strategy is based on aggregation of CAs around the analyte (Fig. 5b). The CAs form a bigger structure which has a slower tumbling rate and thus higher relaxivity. This method finds its application only at lower magnetic fields (up to 100 MHz) where the tumbling rate has a significant impact on the relaxation rate. An example was presented by Jassanof *et al.*[27] In this case super-paramagnetic iron oxide nanoparticles (SPIOs) modified with calmodulin (CaM) and M13-protein aggregate in presence of $Ca^{2+}$ ions.

Yet another type of responsive agents is the Chemical Exchange Saturation Transfer (CEST) CA family. CEST agents are complexes of organic ligands with lanthanide ions different from $Gd^{3+}$. This type of agents contains protons (protons from amides, amines, alcohols) which undergo slow exchange with protons of the bulk solvent. The spins of these protons can be saturated by a low-power pulse so that they will align against the vector of an applied magnetic field. The saturation and further chemical exchange will result in a decrease of the bulk solvent protons signal intensity (Fig. 6) observed in an MR image as its darkening.[28]
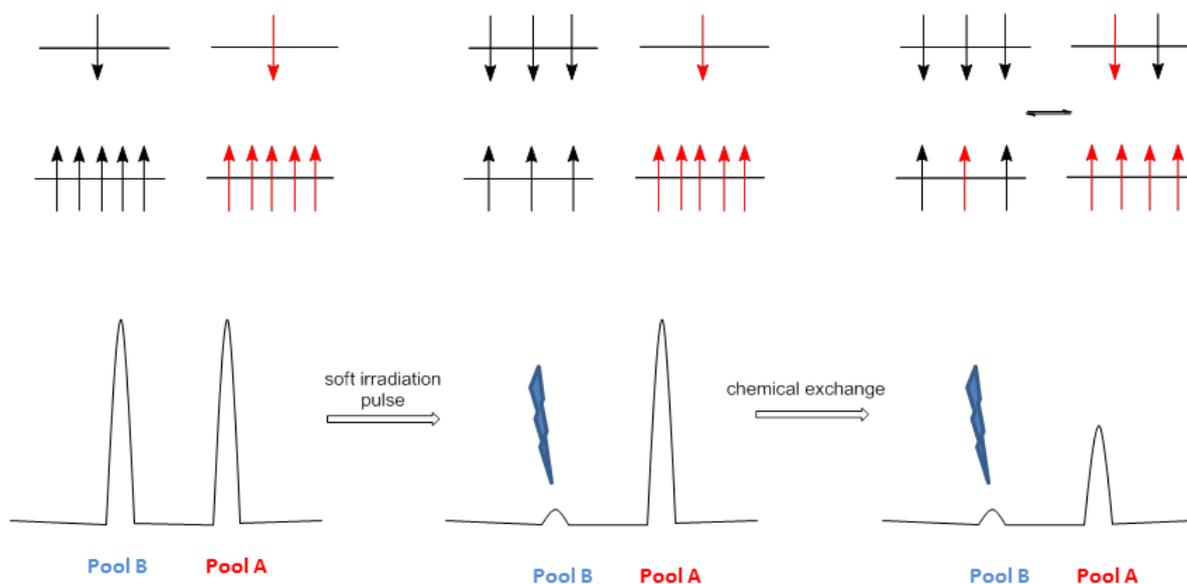
**Figure 6 Cartoon depicting mechanism how a CEST agent works before and after application of RF pulse.**

An example of a CEST agent was published by Chauvin *et al.*[29] where due to enzymatic reaction an amine group is formed and the CEST phenomenon can occur.

CEST agents show two significant advantages over traditional paramagnetic CAs. Firstly, their signal can be adjusted by an appropriate pulse sequence and switched on and off according to needs. Secondly, they can be used as ratiometric probes. If a mixture of two isostructural agents is applied, one works as a responsive agent while the other provides information about concentration and distribution as shown by Aime and co-workers.[30] In their study, they used the same ligand but loaded it with two different lanthanides responsible for activation of agent at two different pulse frequencies. With europium doped ligand they could evaluate the distribution of the agent itself without observing the CEST effect. When the metal was exchanged for ytterbium, the agent allowed monitoring of pH.

## 1.3.1. CAs responsive to biologically relevant ions

## 1.3.1.1. Detecting Ca$^{2+}$

Calcium plays an important role in neuronal signalling among others through its involvement in the presynaptic release of neurotransmitters, the change of the postsynaptic potential via ion channels and its prominent role as a second messenger, influencing various intracellular processes.[31] Calcium responsive agents utilize a variety of known calcium chelators, from simple ethylenediaminetetraacetate (EDTA) through multifunctional 2-aminophenol-N,N,O-triacetic acid (APTRA) to the often used 1,2-bis(o-aminophenoxy)ethane-N,N,N',N'-tetraacetic acid (BAPTA) (Fig. 7) which is known for its $Ca^{2+}$ selectivity.



**EDTA**

**EGTA**

**BAPTA**

**APTRA**
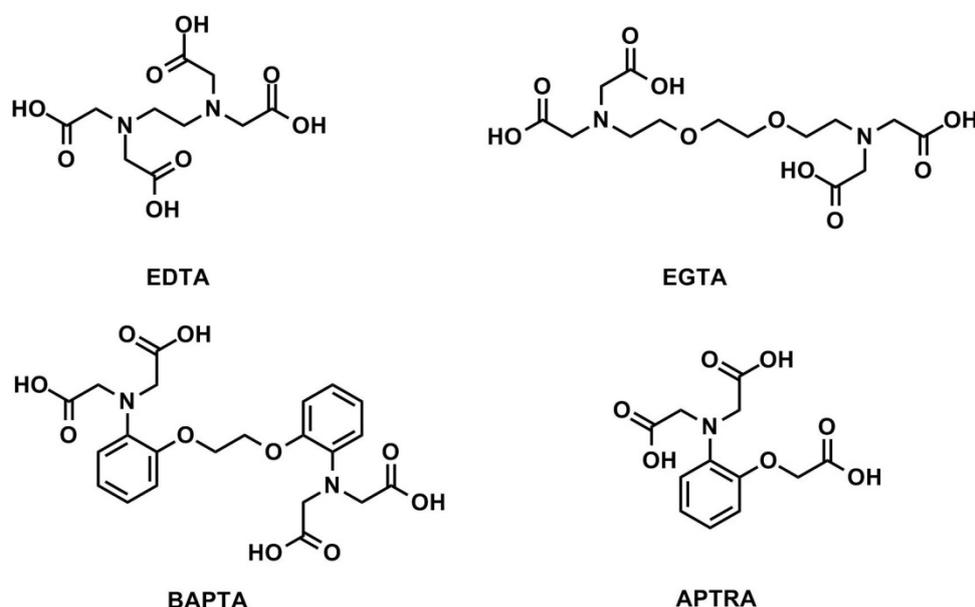
**Figure 7 Ligands used for chelating Ca$^{2+}$**

The first $Ca^{2+}$-responsive CA for MRI was published by Meade and co-workers.[32] Two macrocyclic MR-reporters were linked together with BAPTA acting as the calcium chelator (Fig. 8). The approximately 80% increase in longitudinal relaxivity $r_1$ upon addition of $Ca^{2+}$, high selectivity vs. $Mg^{2+}$ and pH-independent response allowed this compound to serve as an ideal template for future design of responsive MRI agents.

Following the bis-macrocyclic pattern Dhingra *et al.*[33] synthesized an agent with BAPTA bis-amide as a $Ca^{2+}$ chelator. However, the $r_1$ response turned out to be too low (10-15%) for detection with MRI. Nevertheless, the $Ca^{2+}$-chelator retained its selectivity towards $Ca^{2+}$ vs. $Mg^{2+}$. Angelovski *et al.*[34] also presented similar probes

with an EGTA bis-amide derivative for sensing $Ca^{2+}$. The agents showed up to 80% longitudinal relaxivity change in presence of $Ca^{2+}$ and remained insensitive towards $Mg^{2+}$.

The bis-macrocylic pattern has the advantage of a double amount of $Gd^{3+}$ present in an agent which allows higher MR signal intensity. But, Dhingra and co-workers[26] showed that mono-macrocyclic probes can be effective as well. Their APTRA derivative linked to a 2,2',2''-(1,4,7,10-tetraazacyclododecane-1,4,7-triyl)triacetic acid (DO3A, Fig. 4) moiety demonstrated 97% change in $r_1$ in water and up to 36% in biological media. But, the modification of APTRA moiety jeopardized the agents' selectivity for $Ca^{2+}$ and signal change can be also obtained for $Zn^{2+}$ and $Mg^{2+}$.
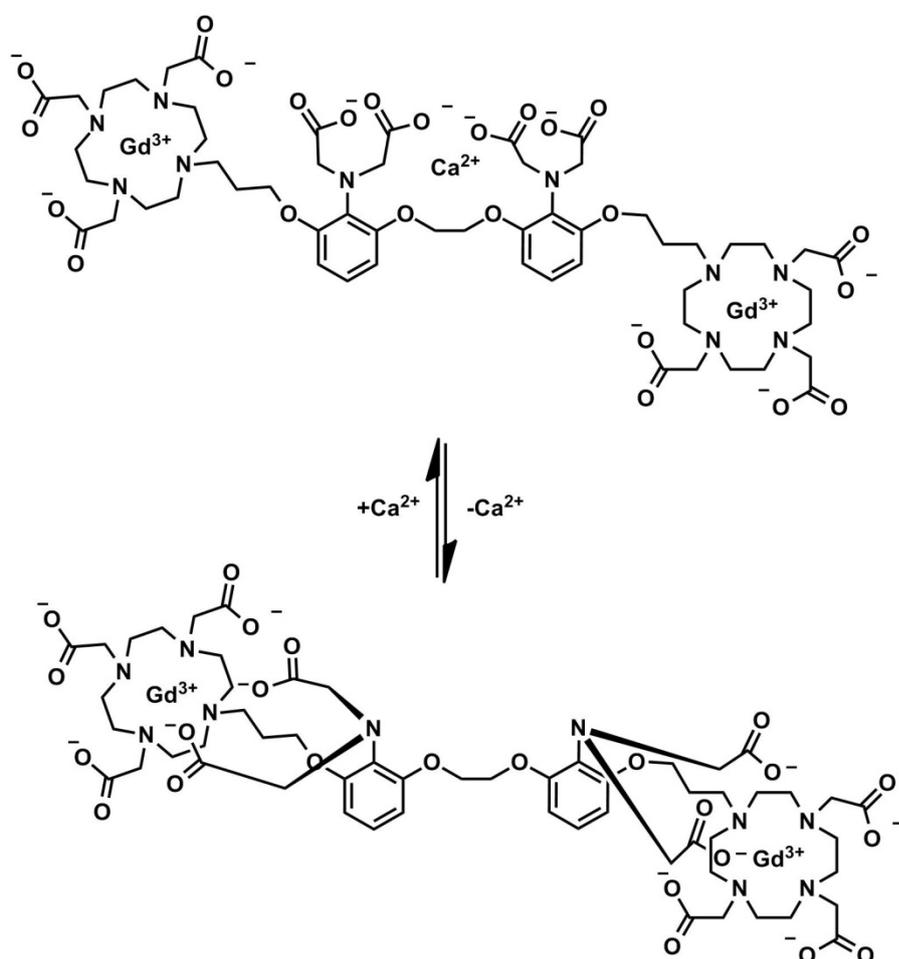


**Figure 8 The first "flipping" mechanism proposed by Meade _et al._[32]**

Another approach for sensing $Ca^{2+}$ was presented by the above mentioned group of Jasanoff.[27] In their study the SPIOs aggregate around calcium ions causing a 5-fold change in transverse relaxivity $r_2$ (iron oxide is a $T_2$ agent). This gives approximately two times higher signal increase in comparison with the $T_1$ agents presented before based on cyclen.

## 1.3.1.2. Sensing $Zn^{2+}$

In the human body concentration of zinc is highest in the brain where it has been shown to locally modulate gated membrane channels, transporters and receptors.[35-37] Moreover, its deregulation has been linked to neurodegenerative diseases such as Alzheimer's.[38]

The first published $Zn^{2+}$ sensor based on a DTPA core with pyridine derivatives as sensing moieties[39] provided a 30% response to the ions. The drawback occurred after addition of excess of $Zn^{2+}$ when the longitudinal relaxivity returned to the starting value. When excess of $Zn^{2+}$ is added, access of water to the metal centre is not obstructed anymore as zinc ions are chelated by the pyridines pending on the same nitrogen atom instead of the two on the opposite sides of the agent. This way the same relaxivity value can be obtained for two different $Zn^{2+}$ concentrations. To overcome this issue another sensor was synthesized by the same group.[35] Two out of four pyridine moieties were substituted with carboxylate groups. This way the longitudinal relaxivity change remained at 30% and the agent was still selective to $Zn^{2+}$ vs. $Ca^{2+}$ or $Mg^{2+}$.

The work presented by Meade et al.[40] showed on four examples how important is the choice of chelating parts responsible for detection of $Zn^{2+}$. The best presented agent, containing two carboxylate groups, showed 120% change in $r_1$ upon addition of equimolar amount of $Zn^{2+}$. Another agent with one of the carboxylates substituted with a pyridine moiety, exhibited 100% response. The two remaining molecules, with only one carboxylate or with only two pyridine derivatives, did not show any response towards zinc ions.

## 1.3.1.3. $Fe^{2+/3+}$ as a target for SCAs

Iron is the most abundant transition metal in the brain and it is utilized as a crucial component of oxygen transport and metabolism. Iron deficiency and excess has been shown to play a role in neurodegenerative diseases like Alzheimer's, Huntington's or Parkinson's.[41]

The great majority of $Fe^{2+/3+}$-responsive agents is based on aggregation of the probe around an analyte. The response is generated by a slowed tumbling rate of the aggregate in comparison to the single agent. As detecting moieties, derivatives of pyridine[42,43] and phenantroline[44,45] have been incorporated. In all cases, the connection between the $Gd^{3+}$-chelate and the responsive part has been maximally rigidified to ensure the highest response.

Ruloff and co-workers[42] presented an agent with mononuclear DTPA-$Gd^{3+}$ core, which showed $r_1$ increase of 140% upon addition of $Fe^{2+}$. A year later Livramento *et al.*[43] reported a binuclear agent with starting longitudinal relaxivity 12 $mM^{-1}s^{-1}$ which increased to 33.6 $mM^{-1}s^{-1}$ in presence of $Fe^{2+}$. In 2006 two other $Fe^{2+}$-sensing agents have been published. Paris *et al.*[45] presented a mononuclear agent with a DO3A-$Gd^{3+}$ centre. The $r_1$ increased by 90% in the presence of the analyte, but no selectivity for $Fe^{2+}$ vs. $Ni^{2+}$ was observed. Parac-Vogt[44] focused on a mononuclear DTPA-core and achieved 140% signal raise with final longitudinal relaxivity value similar to the one obtained by Paris (9.5 vs. 10.5 $mM^{-1}s^{-1}$ respectively).

## 1.3.1.4. Sensing changes in pH

Keeping a proper pH is crucial to maintain human body's proper functioning. It regulates water balance and in the brain controls storage of transmitters in vesicles.[46] Any changes occurring in the pH balance may be a signal of a disease, e.g. tumour.[47]

Over the years only a few examples of pH-responsive contrast agents were reported. Strategies employed both low- and high-molecular weight compounds, but only one reached the stage of in vivo evaluation. Sherry and co-workers[48] reported a

1,4,7,10-tetraazacyclododecane-1,4,7,10-tetraacetic acid (DOTA Fig. 4a) derivative with non-coordinating phosphonate arms which showed a longitudinal relaxivity $r_1$ dependent on pH changes. The probe exhibited a 100% increase in $r_1$ in pH range between 3 and 6 and an even higher increase of 150% between pH 6 and 9. Generally, the lower pH is biologically more relevant. A few years later the probe was tested in vivo.[49] Pharmacokinetics and in vivo pH response have been investigated. In this report two groups of mice were compared: control animals and mice with increased pH of kidneys and neighbouring tissues. $T_1$ weighted images were obtained and the calculated pH maps of the control and the treated animals showed an enhanced contrast in regions with abnormal pH.

### 1.3.2. SCAs for detection of enzymes and metabolites

For modern biology very useful tools are CAs that are able to report on enzymatic activity and its products – metabolites. Such probes allow understanding how processes at cellular level are translated into physiological functions occurring in whole organisms.

Li *et al.*[50] reported a chemical exchange saturation transfer (CEST) agent allowing the detection of the esterase enzyme. The reported probe had a DOTA-type MRI reporter with an attached tri-methyl lock (TML)-ester. The mechanism herein is based on different shifts of protons of the starting amide and the resulting amine after enzymatic cleavage. The work showed that in the absence of esterase, only one CEST effect is present (10%). After addition of the enzyme this signal is diminishing (8.5%) and a peak from amine appears (3%) quite distinct from the starting material, resulting in a ratio of the effects of around 30%. In vivo studies were also performed. In cell culture medium the CEST effect showed higher values, 12% immediately after addition of the agent and 8.7 and 6% after 24h for starting amide and formed amine respectively. This provided an effect ratio of 66%, twice as high in comparison to the *in vitro* measurement. Although, both CEST effects from amide and amine showed dependence on concentration of the agent and $T_1$ relaxation, the ratio itself did not exhibit such reliance. Nevertheless, pH and

temperature need to be controlled as changes in one or both of those parameters leads to disturbance in the amide to amine ratios.

Meade and Arena reported detection of β-galactosidase in two different manners. Meade[51] presented a DOTA-type MR-reporter where attached galactopyranose is obstructing the access of water molecules to the $Gd^{3+}$ and significantly increasing relaxation time of the CA. In presence of the enzyme, the sugar ring is cleaved and $T_1$ decreases by 20%. A few years later this agent was tested *in vivo*.[52] Arena and co-workers[53] exploited an aggregation mechanism in their work. They used a DOTA-derivative containing a tyrosine group where the terminal –OH functionality is protected by a galactose moiety (DOTA-tyr-gal). When the galactose part is cleaved, the tyrosine facilitates oligomerization, the agent aggregates and its tumbling rate changes increasing longitudinal relaxivity. Having proved that DOTA-tyr-gal was not reacting to tyrosinase, DOTA-tyr-gal was activated with a solution of β-galactosidase. The decrease in $r_1$ showed an end value exactly of the control DOTA-tyr, both in phosphate buffer and in serum. After addition of both enzymes to DOTA-tyr-gal, an increase in longitudinal relaxivity was observed, similar in values to the response of DOTA-tyr alone.

A third approach, opposite from the one presented above, was reported by Westmeyer *et al.*[54] The authors showed how mammalian secreted alkaline phosphatase (SEAP) activity can be indirectly monitored by a disaggregation of super paramagnetic iron oxide particles (SPIOs). SPIOs were linked with an adenosine binding moiety. After adenosine is formed as a result of SEAP cleavage, the binding part of SPIOs is coordinating to the formed adenosine, releasing the second part of the agent. Lowering of the molecular weight leads to in faster tumbling rate and therefore in lower $R_2$ values. Thus, the MR image brightens in comparison to the one in absence of SEAP. Noteworthy is the fact that the SPIOS disaggregation can be reversed upon removal or destruction of adenosine.

For brain activity lactate and glucose as metabolites are important. The two probes have been shown to be able to detect lactates and glucose based on CEST mechanism.

In 2002 Aime and co-workers[55] reported a CEST agent able to detect lactate *in vitro*. They used a DO3A-derivative with *m*-methoxybenzyl arm containing six

exchangeable amide protons. Upon binding to lactate, the saturation transfer intensity dropped from 60% to 0%. The plateau was reached approximately at 1:1 binding ratio. Yet, no in vivo measurements have been performed.

Two years later Trokowski et al.[56] presented another CEST agent for detection of glucose. Two DOTA-tetraamides with two arms containing boronic acids, in *trans* and *cis* position, as a reporting moiety for glucose and one DOTA derivative with only one reporting arm were effectively synthesized. It was shown that the mono-phenylboronic acid derivative was selective for fructose versus glucose. While both bis-phyenylboronic acid derivatives of DOTA preferred glucose over fructose, the *trans* isomer was more selective. Performed phantom MRI images clearly showed increased darkening with increasing amount of glucose due to occurring CEST effect. While mono-phyenylboronic DOTA didn't show any visual differences between addition of glucose, fructose and galactose, the trans-bis-phenylboronic acid DOTA did not respond to galactose and clearly preferred glucose over fructose. Noteworthy is the fact that the free ligands also showed binding to glucose and fructose.

### 1.3.3. Detection of neurotransmitters

Neurotransmitters are the type of analyte which is very difficult to detect non-invasively, mainly due to their low concentrations (from nM to low µM). A more feasible way to detect a neurotransmitter release is to monitor other constituents stored in vesicles,[57] e.g. $Zn^{2+}$. Nevertheless, there are reported probes able to detect neurotransmitters. Two examples of such probes presented below were designed to detect dopamine. Dopamine is a neurotransmitter involved in learning, reward and motor coordination. Moreover, dopamine exists in concentration range that is detectable by MRI (1 µM to tens of µM).

Jasanoff et al.[58] focused on extracting from *Bacillus megaterium* a heme domain containing a single iron atom which was responsible for generating an MR signal. First experiments showed decrease for both natural and unnatural substrates for this domain, which encouraged the investigators to further modify the ligand. Two mutant proteins have been evolved, BM3h-8C8 and BM3h-B7. Both of them

demonstrated an 85% decrease in relaxivity upon binding with dopamine in water. Next, binding specificities were investigated and showed that only serotonin and norepinephrine can compete with dopamine. Nevertheless, decrease in relaxivity presented by them was at least half lower in comparison with performance of dopamine. The new CAs were also tested in a cell culture, where BM3h-8C8 showed 37% and BM3h-B7 54% decrease in longitudinal relaxivity upon release of dopamine. For in vivo imaging of a living rat brain mutant BM3h-8C8 was chosen and proved to decrease intensity enhancement of about 50% upon injection of dopamine in 1.5 mm radius of region of interest (ROI). The mutant exhibited 3% signal decrease upon $K^+$ stimulation.

Another work of Jasanoffs' group[59] reports the same heme domain where iron is substituted for manganese. The wild type of the protein showed only minor response towards its natural ligand - arachidonic acid (AA), therefore a mutant Mn-C1634 was prepared. The latter showed a 63% signal decrease upon binding to AA. Binding specificity was examined and proved lack of competitors for AA. Therefore the Mn-C1634 is a potential promoter to establish a new class of responsive CAs.

### 1.3.4. Targeted CAs

Yet another class of smart contrast agents (SCAs) is composed of probes containing a functional moiety able to detect a particular receptor side and provide accumulation of CA at one particular place.[2]

Tei *et al.*[60] synthesized two biotin based CAs with one and three Gd-DOTA chelates. The increase in relaxivity upon binding to avidin was significant. In vitro phantom measurements in two cell lines showed brightening of images in case of tubes containing a biotinylated peptide sequence known for selective binding to tumour cells.

Biotin moiety was also used by Mishra *et al.*[61] in their work on longitudinal brain connectivity studies. The reported molecule consists of biocytin conjugated to a DOTA-type MR-reporter. Facile probe preparation and favourable characteristics showed the potential of this molecule. High longitudinal relaxivity for a monoaqua complex is increasing up to 43% upon binding to avidin. Cell studies showed no

cytotoxic effect or reduction of metabolic activity up to 100 μM concentrations. Cellular internalization was confirmed by MRI and fluorescence microscopy. MR images in rat brain (injected in one half and saw in the other) clearly show distribution to the other brain hemisphere after 24h. Histological results revealed retrograde transport along axons with anatomical details, e.g. cells projecting to the injection site or axonal trajectories of connected neurons.

Neuronal connectivity in vivo was also studied by Mamedov *et al*[62]. Following a concept of Ungerleider *et al*[63], the authors presented a multimodal probe consisting of an optical and an MR reporter, both coupled to a dextrane core known for its labelling properties of neurons. As the MR part, Gd-AAZTA complex was chosen due to its high longitudinal relaxivity and thermodynamic stability. Rhodamine derivative served as an optical factor. The measured longitudinal relaxivity at 7T in water showed $r_1$ value 9.5 mM$^{-1}$s$^{-1}$, which is twice as high as commercially available DOTA. Unlike DO3A-type conjugates, in the AAZTA-dextran conjugate no decrease in relaxivity in cell medium was observed. Fluorescence microscopy studies showed specific uptake in neurons.

As one can see, the majority of the presented reports is based on DOTA and DO3A type gadolinium complexes as MR reporters. While both of them show high thermodynamic stability and kinetic inertness, they also demonstrate some critical drawbacks. DOTA shows relatively low longitudinal relaxivity values, which translates to lower contrast enhancement of MR images. DO3A leaves more space on metal centre for water molecules to coordinate, but also for other coordinating ligands like endogenous anions. Displacement of water molecules by phosphonates or carbonates has influence on the $r_1$ values.[7,64] The question is, if the trade-off between relaxivity and response to biologically abundant anions is really the only option. An answer to that problem could be a different system chelating Gd$^{3+}$, e.g. HOPO.

## 1.4. 3,2-Hydroxypyridinone (HOPO) based CAs

In 1995 HOPO derivatives were published for the first time as a potential CA.[65] Already the first complex showed extraordinary longitudinal relaxivity of 10.5 mM$^{-1}$s$^{-1}$ (37°C, 20 MHz). The occurring drawback of low water solubility[66] was solved and every further generation of HOPO CAs showed greater potential for MRI application. In this chapter an overview of HOPOs' characteristics is given. Starting from the very first compound to the latest reports of virus and dendrimer conjugates, properties from relaxivity and water solubility, through interactions with ions to stability constants are presented.

Originally HOPO CAs contained two parts: HOPO itself and a scaffold. The HOPO part is responsible for coordinating Gd$^{3+}$. Due to the fact that three HOPO rings pending on an amine scaffold are creating a hexadentate ligand, there is still enough space to coordinate two water molecules to the metal centre. Moreover, HOPO rings provide one type of donor atoms, namely oxygen donor atoms which are preferred by Gd$^{3+}$. This ensures thermodynamic stability comparable with the commercial CAs, e.g. DOTA. The aim of the scaffold is to keep chelating moieties together and guarantee stable interactions between HOPO moieties and Gd$^{3+}$. In addition, the scaffold allows tuning of the q number (Fig. 9).
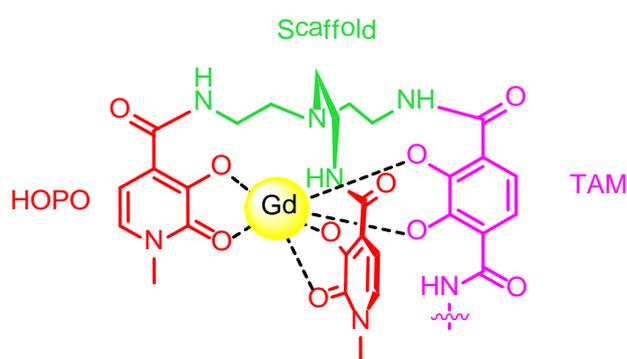


**Figure 9 A cartoon depicting three moieties creating a HOPO CA**

Due to the toxicity of free Gd$^{3+}$, ligands used to entrap it should form a stable complex with it. Stability of CAs is often presented as logK. Stability of HOPO-based CAs is always presented as a pGd value (eq. 7):

$$pGd = -\log[Gd^{3+}]_{free} \tag{7}$$

where $[Gd^{3+}]_{free}$ is the concentration of free $Gd^{3+}$ in presence of the HOPO ligand. The higher the pGd value, the more stable is the complex.

### 1.4.1. The chelating moieties

The library of HOPO-based CAs consists of over 30 complexes. The majority of them contains two types of chelators: 3,2-HOPO and a terephtalamide (TAM) part. The TAM moiety provides an opportunity for further functionalization of the CA. Nevertheless, CAs consisting of different co-chelators are reported.

The first "mixed" HOPO CAs appeared in the year 2000, when four potential substitutes for one of the HOPO moieties were screened.[67] Three aromatic candidates are salicylamide (SAM), 2-hydroxyisophthalamide (IAM) and 2,3-dihydroxyterephthalamide (TAM) (Fig. 10). Additionally bis(acetate) (BAC) (Fig. 10) was considered as a chelator which can be further functionalized. CAs with all aromatic substituents had q=2 while the q of BAC containing ligand was only 1. This reflected on the longitudinal relaxivity values. TAM, IAM and SAM had relaxivities of 8.8, 7.2 and 7.7 $mM^{-1}s^{-1}$, respectively, while BAC exhibited $r_1$ of only 5.6 $mM^{-1}s^{-1}$ (20 MHz).

A year later a new class of heterocyclic moieties was investigated.[68] The aim of 6-carboxyamido-5,4-hydroxypyrimidones (HOPY) (Fig. 10) was to improve solubility and allow further modifications at the two ring positions, while maintaining structural characteristics and the stability of the original HOPO agents. The solubility of the Gd-HOPY complex was greatly improved along with the selectivity towards $Gd^{3+}$ vs. $Zn^{2+}$ and $Ca^{2+}$. Its longitudinal relaxivity with value 9 $mM^{-1}s^{-1}$ (20 MHz) was slightly lower than that of the parent heterocycle at pH=7.2. The maximum of $r_1$ was found to be at pH=2.5. Despite these favourable characteristics it turned out, however, that the complex of $Gd^{3+}$ with HOPY was less stable in comparison to the HOPO analogues.

The next examined CA contained three identical chelators – maltols (MAMs).[69] MAMs, popular food additives, are monoanionic, hard oxygen donor ligands like parent HOPOs. The additional advantages of Gd-MAM complexes are high solubility and biocompatibility. Therefore two $Gd^{3+}$ complexes with MAM and 6-

methylmaltol (Me-MAM) were prepared and their characteristics examined. Relaxivities occurred to be slightly lower than for the HOPO archetype, but both molecules had q=2. Stability constants of the new complexes were not reported.

In 2007 an isomer of 3,2-HOPO, 1,2-HOPO was brought to the field of CAs.[70] Relaxivity was again slightly lower than the one of parent 3,2-HOPO (8.5 vs. 10.5, respectively, at 20 MHz) but the lower anion affinity and higher stability of the complexes in acidic media justified further research on solubility enhancement.[71]

Despite the great potential of all investigated potential chelators, the majority of research involving HOPO CAs is conducted with 1-Me-HOPO and TAM moieties as vectors for further functionalization. This choice was made based on the short, clean and efficient synthesis of both chelating parts.[65,72]



[Gd{tren(1-Me-3,2-HOPO)$_3$}(H$_2$O)$_2$]    [Gd{tren(1-Me-3,2-HOPO)$_2$(tam-Me)}(H$_2$O)$_2$]    [Gd{tren(1,2-HOPO)$_3$}(H$_2$O)$_2$]

[Gd{tren(6-Me-3,2-HOPO)$_3$}(H$_2$O)$_2$]     [Gd{tren(5,4-HOPY)$_3$}(H$_2$O)$_2$]

[Gd{tren(mam)$_3$}(H$_2$O)$_2$]    [Gd{tren(Me-mam)$_3$}(H$_2$O)$_2$]    [Gd{tren(1-Me-3,2-HOPO)$_2$(sam)}(H$_2$O)$_2$]

[Gd{tren(1-Me-3,2-HOPO)$_2$(iam)}(H$_2$O)$_2$]    [Gd{tren(1-Me-3,2-HOPO)$_2$(bac)}(H$_2$O)$_2$]
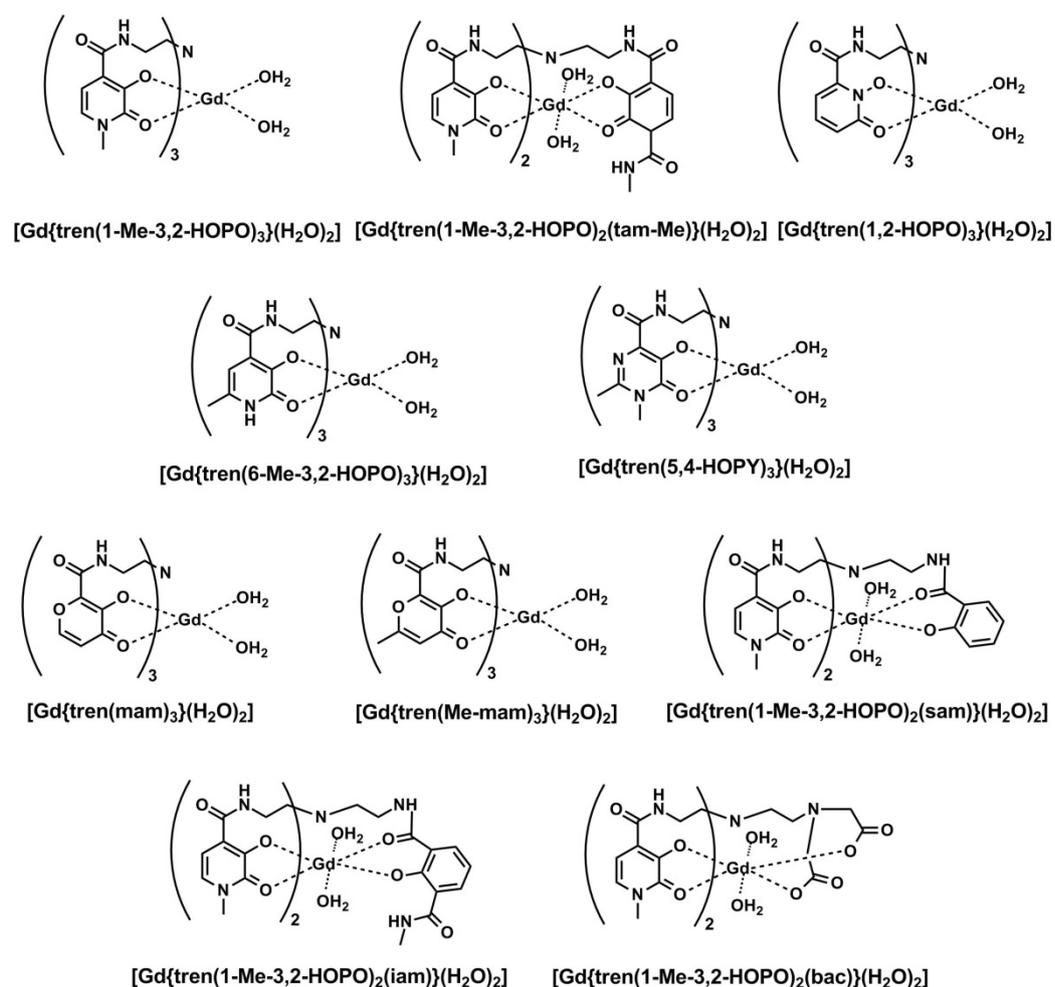
**Figure 10 Cornucopia of HOPO-based CAs created with different chelating moieties**

## 1.4.2 The scaffold

Over the course of 20 years of researching HOPOs as MRI CAs several scaffolds were investigated to improve further solubility of the complexes along with their longitudinal relaxivities.
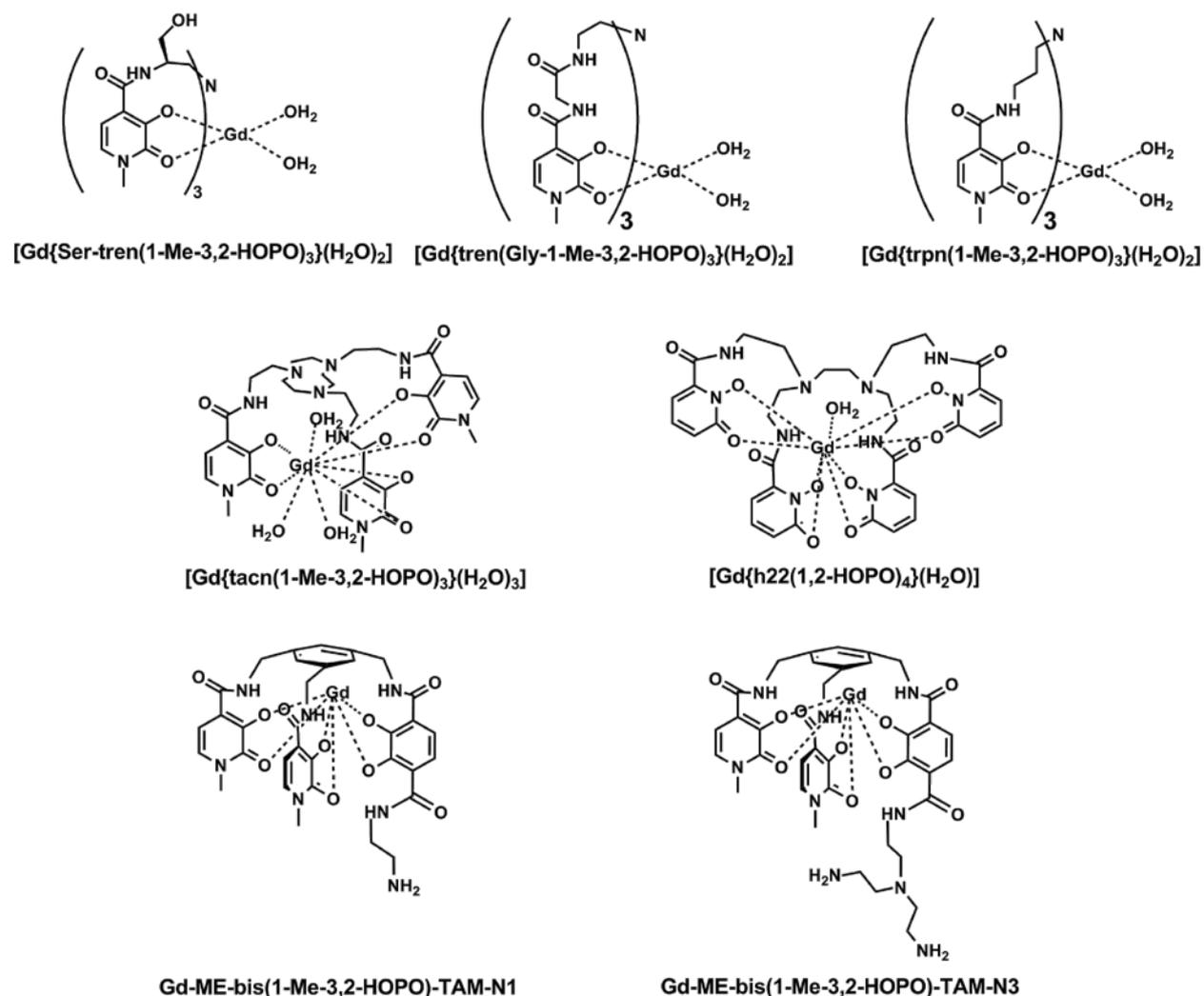


**Figure 11 Examples of HOPO CAs with various amine scaffolds**

The first report on this topic was published in early 2000s[73,74] wherein the original TREN scaffold was substituted with a chiral serine backbone (Fig. 11). Solubility was improved and increased to 15 mM vs. 0.1 mM for the archetype. The longitudinal relaxivity was slightly lower, 9 mM$^{-1}$s$^{-1}$, as was stability.

The next candidates for screening as potential scaffolds were TREN with a glycine spacer and lengthening of the TREN scaffold to a propylene motif.[75] The increase in distance between the HOPO moieties and $Gd^{3+}$ ion decreased the stability of the complex. Both new agents had stability three to four units lower than the parent HOPO: pGd of 16.7, 15.6 and 19.2, respectively. The longitudinal relaxivity of the more stable homologue with glycine spacer was 6.6 $mM^{-1}s^{-1}$ which is just above the range of Gd-DOTA agents ($r_1$=4.2 $mM^{-1}s^{-1}$) and almost 50% lower than the original HOPO agent.

In 2007 another scaffold was published.[76] Cyclic triazacyclonanone (TACN) was chosen due to its size. It is big enough to ensure three water molecules within the agent cavity and therefore increase solubility without affecting the stability of the CA. Measured relaxivity values were 13.1 $mM^{-1}s^{-1}$ in water and 17 $mM^{-1}s^{-1}$ in serum (20 MHz), respectively 30 and 70% higher than the HOPO archetype.

In the same year another attempt was made to change the scaffold and increase denticity of the ligand.[77] This study was performed on the 1,2-HOPO isomer and showed only one water molecule coordinated to the metal centre. This was the first symmetrical agent.[78] The 1,2-HOPO-based CA containing a scaffold with four pending amines showed very good $r_1$, 7.9 $mM^{-1}s^{-1}$, and twice as high selectivity towards $Gd^{3+}$ than $Zn^{2+}$ and $Ca^{2+}$. Due to increased denticity the stability also increased. Moreover, it was shown that the new agent exhibits no affinity for carbonates, biphosphates or fluorides.

In 2009 yet another class of HOPO CAs with an aromatic scaffold emerged.[79] Their $r_1$ values of 10 and 12 $mM^{-1}s^{-1}$ (20 MHz), for Gd-ME-bis(1-Me-3,2-HOPO)-TAM-N3 and Gd-ME-bis(1-Me-3,2-HOPO)-TAM-N1 (Fig. 11) respectively, were promising and indicated hydration number q=3 and 2, respectively. Yet, nuclear magnetic relaxation dispersion (NMRD) profiles could be fitted with only fractional q close to 0. Therefore, the high $r_1$ was attributed to aggregation of mesityl capped HOPO CAs. Moreover, solubility was established to be below 10 µM in water.[80] The solution of this issue will be presented in the following section dedicated to the effect of substituents.

### 1.4.3 The effect of substituents

The effect of substituents on one of the HOPO or TAM moieties was also studied. Pendants such as polyamines, polyacids and polyethers were examined in terms of modulation relaxivity and/or solubility (Fig. 12).



[Gd{tren(1-Bn-6-Me-3,2-HOPO)$_2$(TAM-Me)}(H$_2$O)$_2$] [Gd{tren(6-Me-3,2-HOPO)$_2$(TAM-tri)}(H$_2$O)$_2$] [Gd{tren(1-moe-3,2-HOPO)$_3$}(H$_2$O)$_2$]



[Gd{tren(1-Me-3,2-HOPO)$_2$(tam-R)}(H$_2$O)$_2$]

**Figure 12 Examples of pendants placed on HOPO or TAM moieties.**

The first report is from 2000[81] where the N-substituted pyridinone was synthesized without autoclaves[65] with a different functionality than the methyl group. The stability of pGd=19.8 was slightly higher than the first HOPO-Gd complex but still comparable with the clinically approved Gd-DTPA (pGd=19.1). The solubility was increased to approximately 1 mM which is suitable for clinical applications. The longitudinal relaxivity was not reported.

Four years later a compendium comparing various aromatic and polyethylene glycol (PEG) pendants was published.[82] In the course of research on PEG pendants

on HOPO CAs it occurred that PEG chains longer than 4 units are coordinating to the $Gd^{3+}$ centre displacing one water molecule. For very long chains (PEG 42 and 122) this effect was compensated by increased water exchange rate $k_{ex}$ and resulted in $r_1$ close to the parent HOPO CA (9.1 $mM^{-1}s^{-1}$ for PEG 42 and 122).

Yet, such effect is not observed for pendants shorter than 42 PEG units, where the q number is decreased but no significant contribution to $k_{ex}$ is observed. A good example of a destructive influence of an inappropriate chain length is shown in case of $[Gd\{tren(1\text{-}Bn\text{-}6\text{-}Me\text{-}3,2\text{-}HOPO)_2TAM\}(H_2O)_2]$. The compound alone shows $r_1$ 10.4 $mM^{-1}s^{-1}$ (20 MHz) however, with PEG11 pending from TAM moiety relaxivity is reduced by 15%.

In a report from 2006 the influence of various amine, acid and ether functionalities on solubility and relaxivity of HOPO CAs was investigated.[83] It was shown that the nature of the substituent can stabilize a coordination of the third water molecule via hydrogen bonding increasing the same the relaxivity.

## 1.4.4. HOPO CAs attached to macromolecules

The example of the PEG chains showed that increase in size allows modulation of $r_1$. In the next sections the covalent and non-covalent attachment to a bigger cargo molecule and the resulting longitudinal relaxivity $r_1$ adjustment will be described.

## 1.4.4.1. Dendrimers

Dendrimers are monodisperse nanosized polymeric molecules consisting of a large number of perfectly branched monomers that spread radially from a central core.[84] The first report about dendrimeric HOPO agents appeared in 2005.[85] A dendrimer utilized in this study was based on aspartic acid (Fig. 13). Only one Gd-HOPO-TAM complex was attached. Thanks to the shortest possible linker between branches of the dendrimer the $\tau_r$ increased two times as well as the relaxivity. Moreover, the 12 hydroxyl groups ensured significant increase in solubility in comparison to the parent HOPO CA.
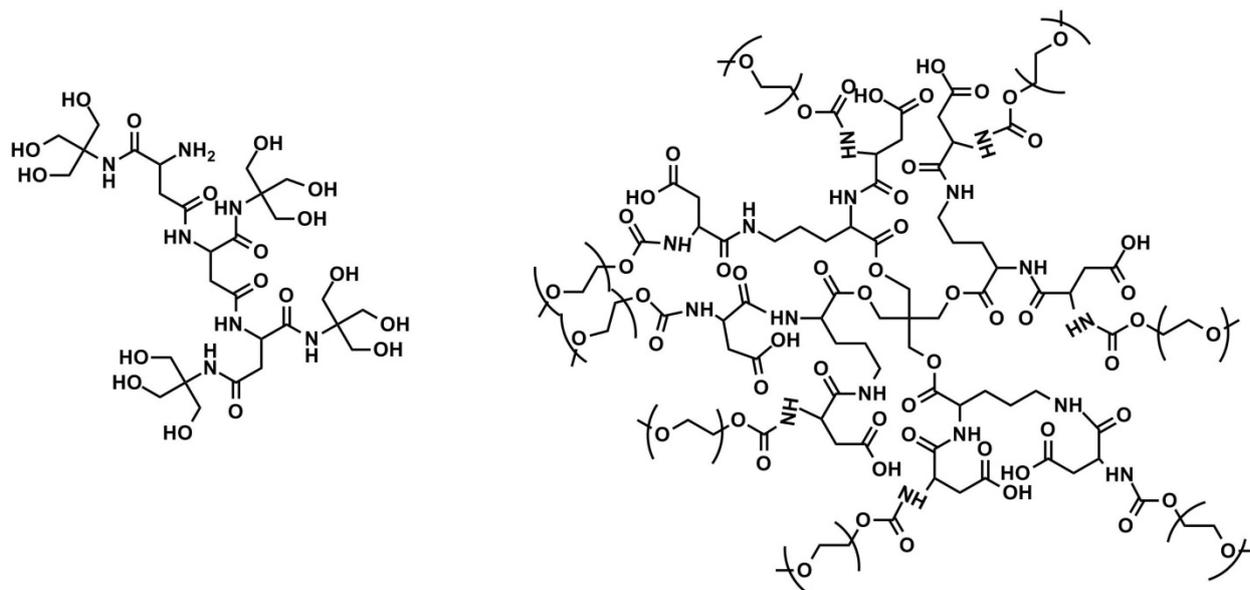
aspartic acid based dendrimer Asp                    esteramide EA
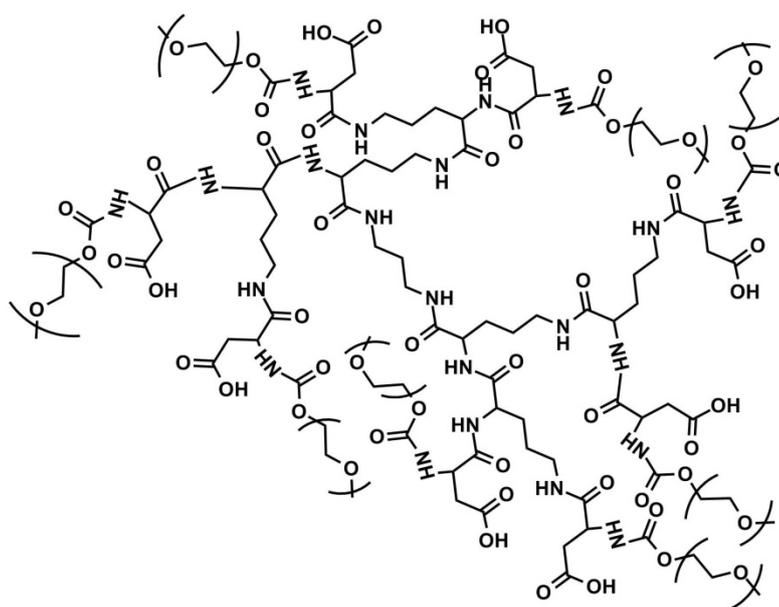


poly-L-lysine PLL

**Figure 13 Dendrimers utilized in HOPO synthesis**

In the next paper that dealt with HOPO CAs attached to dendrimers[86] two types of cargo molecules were investigated. 3,2-HOPO complex was attached to an esteramide (EA) and poly-L-lysine (PLL) (both Fig. 13). In both cases relaxivity

increased in comparison to the monomeric analogue and the EA platform showed higher $r_1$ values. It was proposed that the difference occurred due to hydrogen bonding between amide groups of the PLL dendrimer and metal centre of the complex resulting in decreased access of water molecules to the $Gd^{3+}$. Another advantage of the EA dendrimer was also its higher biodegradability in comparison with PLL. The same conjugate was also investigated with different lanthanide ions to test its potential applications in near-infrared (NIR) imaging.[87]

A next report about HOPO conjugates with dendrimers[80] involved the EA platform mentioned earlier but the attached Gd-HOPO complex contained a cyclic TACN scaffold instead of a flexible TREN. Attachment of a complex exhibiting already 3 water molecules and high relaxivity to a cargo molecule increased $r_1$ to 31 $mM^{-1}s^{-1}$ (60 MHz, 37 °C). In the same study a complex with an aromatic scaffold was attached to the aspartic acid dendrimer and compared with the identical complex with a pending PEG chain. The more rigid branched dendrimer ensured higher $r_1$ in comparison to the linear and more flexible ether chain although both conjugates have similar molecular weight. The same complex was also attached to the EA dendrimer and showed twice as high relaxivity. The increase in solubility was dramatic – from 10 µM to over 50 mM in water.

### 1.4.4.2 HOPO and biomolecules

As became evident from the previous paragraph, synthetic dendrimers showed great potential as cargo molecules but proteins or virus capsids are even bigger and have higher biocompatibility than synthetic dendrimers. Their large size slows down the tumbling rate of the agent and decelerates its circulation time in blood. The obvious application of such agents would be the imaging of blood vessels and vasculature.

Human serum albumin, HSA,[88] was the first investigated biomolecule adduct with HOPO CAs.[82] The study showed that a balance between relaxivity and binding affinity exists. The stronger binding between HOPO CA and HSA is obtained at a cost of decreased q and therefore reduced relaxivity. The highest $r_1$, 74 $mM^{-1}s^{-1}$, occurs with the weakest binding ($K_A$=186 $M^{-1}$) while the strongest connection ($K_A$=8640 $M^{-1}$) gives $r_1$ only 15 $mM^{-1}s^{-1}$. Much lower to the excepted value.[6]

A next step to improve $r_1$ via attachment to a macromolecule was an attempt with a virus capsid.[89,90] Two conjugation sites were compared: one placed on the exterior and the other on the interior of the capsid.[89] Relaxivity studies and NMRD profiles showed 25% higher $r_1$ and 30% higher $\tau_r$ value in case of the internal conjugate. The obtained results were attributed to the more rigid structure of the internal attachment.

Following this lead, another study examined a conjugate with a rigid cyclohexane linker between HOPO CA and the virus capsid.[90] Both RR and SS stereoisomers of the linker were investigated and additionally compared with a linear connection without a stereocentre. The results showed a 35% higher $r_1$ for the SS-isomer in comparison to *RR*-isomer, with 38 and 25 mM$^{-1}$s$^{-1}$ (60 MHz, 37 °C), respectively. This result was explained with the help of modelled structures, suggesting that the *RR*-isomer was flipping the HOPO CA towards the surface of the capsid obstructing the access of water molecules to the metal centre of the CA which resulted in lower relaxivity. The *SS*-isomer was orienting the complex above the capsid surface. The linear linker showed $r_1$ values right in the middle between both stereoisomers due to its flexibility. It is noteworthy that the reported relaxivities are one of the highest up to date.

## 1.4.5. Interactions with endogenous ions

Interactions of HOPO CAs with endogenous ions were already briefly mentioned in the previous sections. In this paragraph all studies considering transmetallation of $Gd^{3+}$ with cations and coordination of anions to the metal centre are described.

One of the most important parameters a CA should fulfil is thermodynamic stability, a feature which determines how easily toxic $Gd^{3+}$ in the CA can be displaced by endogenous cations. Due to their structure HOPO CA show high thermodynamic stability. The 5-membered ring formed between chelators and the metal centre favours larger cations to smaller ones like $Zn^{2+}$ or $Cu^{2+}$. Even $Ca^{2+}$, which is similar in size to $Gd^{3+}$, shows lower thermodynamic stability constant in comparison to the identical $Gd^{3+}$ complex. Furthermore, HOPO CAs show higher

affinity towards $Gd^{3+}$ than $Zn^{2+}$ or $Ca^{2+}$ in comparison to the commercially available agents like DOTA or DTPA-BMA (Fig. 14).[70,77,83,91]
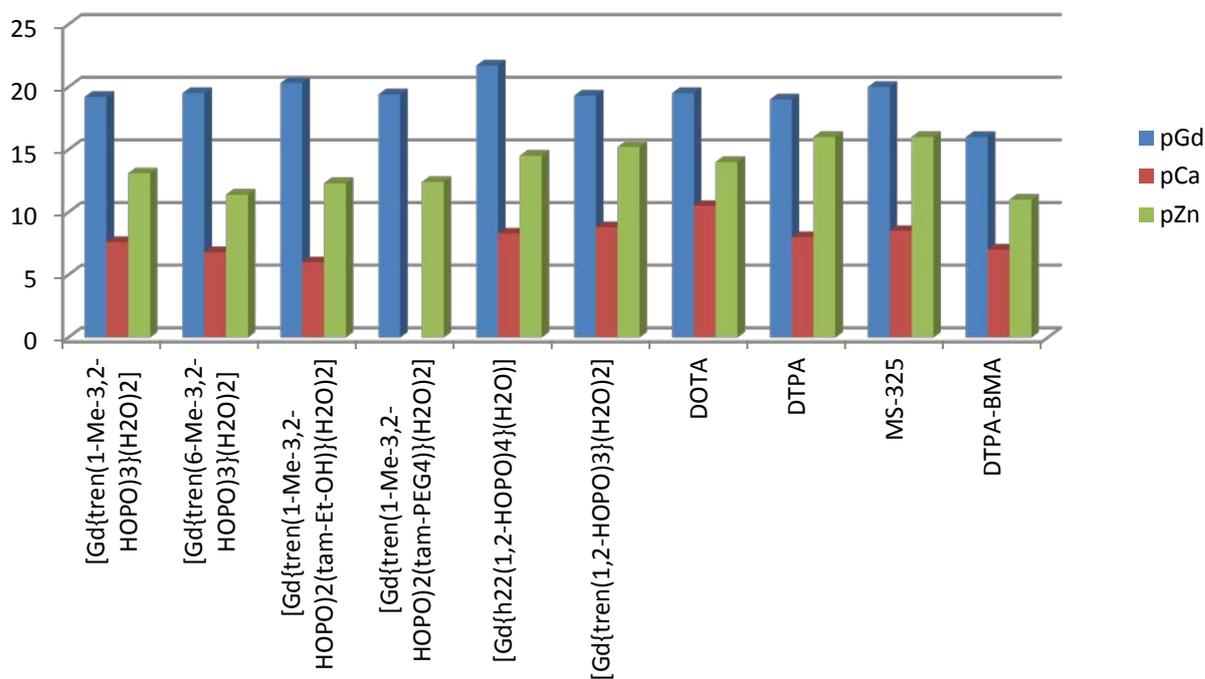


**Figure 14 Comparison of pM values between HOPO and commercial CAs in respect to $Gd^{3+}$, $Ca^{2+}$ and $Zn^{2+}$**

Anions do not have an impact on the stability of HOPO CAs, but they can significantly decrease relaxivity by displacing one or both water molecules.[83] However, there are only two anions which cause a considerable drop of $r_1$. Oxalate can reduce q to 0 and relaxivity by 80%, but interactions of HOPO CAs with oxalates are a minor problem as the endogenous concentration of the anion is within the range of 0.8-2.5 µM.[92] Biphosphates are much more abundant in plasma, 0.38 mM,[7] but displace only one water molecule bound to the $Gd^{3+}$ and leave relaxivity in the range of DOTA type agents upon binding to HOPO CA. Interestingly, no interactions with biphosphates were observed for 1,2-HOPO CA.[70] The presented results for HOPO CAs show a clear improvement in comparison to DO3A type ligands which suffer from relaxivity decrease in the presence of bicarbonates, biphosphates and citrates.[7,64]

# Chapter 2

# Ca$^{2+}$-responsive

# HOPO-SCAs

## 2.1 Aim of the project

3,2-Hydroxypyridinone (HOPO)-based $Gd^{3+}$ complexes exhibit great potential as MRI contrast agents (CAs). HOPO CAs show higher longitudinal relaxivity than cyclen based agents and show no interactions with endogenous ions. Despite the advantages, no "smart" probe which would incorporate this system was reported up to date. To explore the capability of HOPO to create a responsive agent, the aim of this thesis was to develop HOPO-based $Ca^{2+}$-responsive MRI CAs and evaluate their performance by means of NMR and MRI spectroscopy.

As mentioned in section 1.3.1.1., $Ca^{2+}$ transfers electrical charges between brain cells and works as a second messenger in release of neurotransmitters.[93] In addition, it was recently shown that the ions work also as a first messenger mediating axon and dendrite growth.[94] I chose calcium as the analyte due to its relatively high concentration changes (from 1.2 to 0.8 mM) in extracellular space during neuronal activity in the brain.[95] Such high concentrations make $Ca^{2+}$ a suitable target for MRI investigations, since milimolar concentrations of a CA are required to obtain a contrast enhancement in MR image.

The current and the following chapter focus on two issues: a) a synthesis of $Ca^{2+}$-responsive HOPO-based CAs with a newly established synthetic pathway (Chapter 2) and b) their relaxometric evaluation (Chapter 3).

## 2.2 Background

In the resting state of the brain the concentration of $Ca^{2+}$ in extracellular space is higher than during neuronal activity when the ions are transported through the cell membrane inside the cells.[93] In the course of this research two $Ca^{2+}$-responsive agents based on 3,2-hydroxypyridinone (HOPO) were designed and synthesized. The proposed mechanism of their activation involves changes in the number of coordinated water molecules to the $Gd^{3+}$ centre (q), as already presented in section 1.3 (Fig. 5a). Considering HOPO CAs, there are two possible mechanisms of response to $Ca^{2+}$ involving q changes.

A first system ensures access of water molecules to the $Gd^{3+}$ in presence of $Ca^{2+}$ providing an enhanced contrast of the MR image in the resting state of the brain. During brain activity when the concentration of $Ca^{2+}$ is decreasing, the calcium chelator is displacing water molecules on the metal centre decreasing the relaxivity. This phenomenon results in decrease of the contrast of the MR image. A graphical representation of this mechanism in presented in Fig. 15.
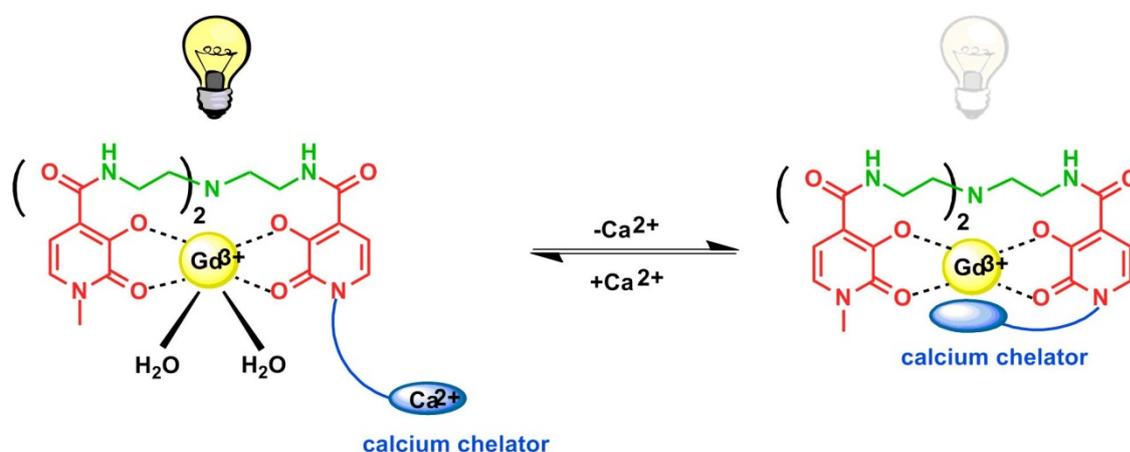


**Figure 15 A cartoon depicting the "flipping" mechanism including HOPO moieties**

A second mechanism is based on the possibility to coordinate three water molecules to the $Gd^{3+}$ as reported by Raymond *et al.*[83] The third water molecule was stabilized by hydrogen bonding provided by additional acidic pendants present on one of the chelating moieties (Fig. 16).
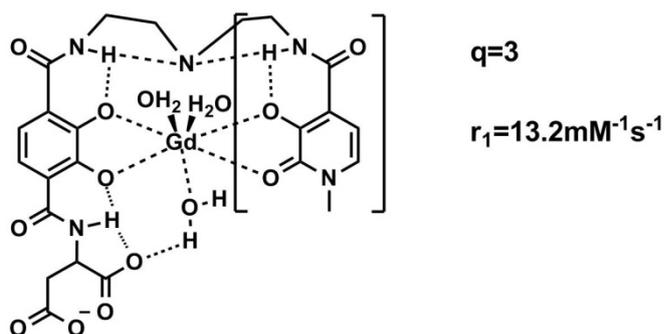
**Figure 16 A HOPO CA synthesized by Raymond *et al.*[83] containing additional acid moieties and their influence on hydration state of the agent**

In this case, due to higher q a higher $r_1$ value would be observed during neuronal activation when $Ca^{2+}$ concentration is decreased. As a result, an enhanced contrast of an MR image would be observed. Yet, increase in $Ca^{2+}$ concentration during resting state of the brain would decrease the q and, hence, the longitudinal relaxivity. An effect would be a diminished contrast in an MR image. The alternative "flipping" mechanism with respect to the third coordinated water molecule stabilized by the carboxyl groups of the $Ca^{2+}$-chelator is presented in Fig. 17.
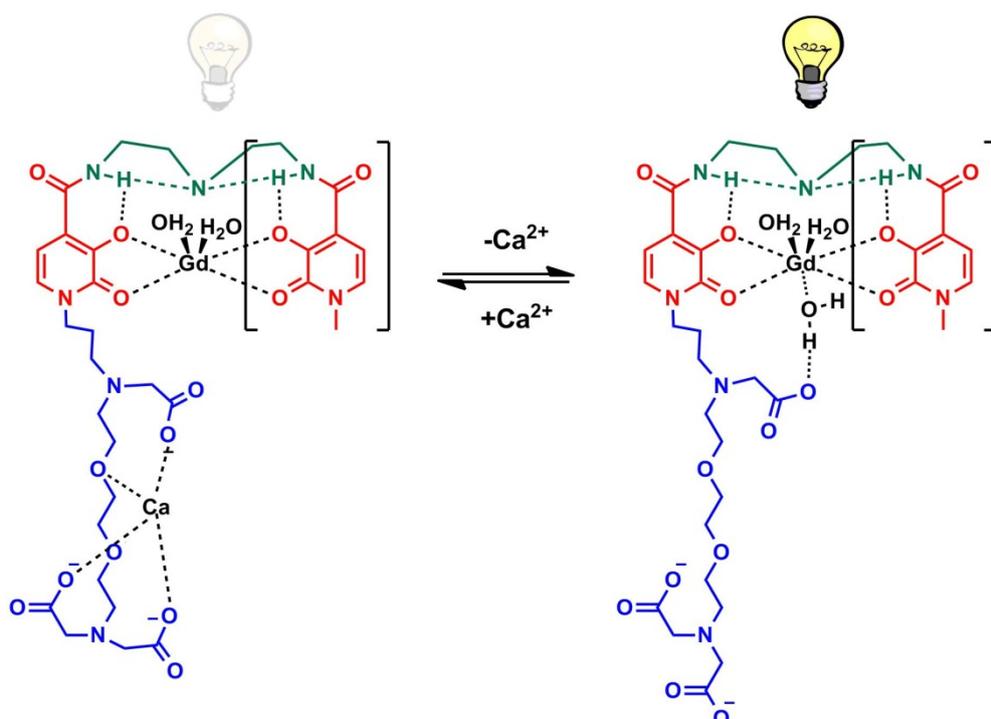


**Figure 17 Assumed mechanism of response towards $Ca^{2+}$ based on Raymonds' report[83]**

Based on the presented mechanisms, the connection between HOPO MR-reporter and the $Ca^{2+}$-chelator should be flexible. Accordingly, two $Ca^{2+}$-responsive HOPO-based agents were designed and synthesized. The difference between the two prepared probes lies in the type of the link between the $Ca^{2+}$-chelator and the HOPO ring.

## 2.3 Synthesis of Gd-L1 and Gd-L2

The synthesis of Gd-**L1** and Gd-**L2** started with preparation of ligands **L1** and **L2** containing an MR-reporter and a $Ca^{2+}$-responsive moiety. A new synthetic pathway for the synthesis of HOPO MR-reporter was established to obtain the two ligands.

In the targeted structures of **L1** and **L2** (Fig. 18) the HOPO moiety was modified compared to the archetype in order to incorporate a $Ca^{2+}$-chelator into its skeleton. In detail, in place of a methyl group on the nitrogen atom of one of the HOPO rings a $Ca^{2+}$-responsive moiety was installed. Unlike **L1**, **L2** contains an amide bond between the $Ca^{2+}$-chelator and a HOPO ring to sustain as far as possible the original structure of ethylene glycol-bis(2-aminoethylether)-*N,N,N',N'*-tetraacetic acid (EGTA), which was chosen as a model $Ca^{2+}$-chelator (Fig. 18 and 19). The synthesis involved preparation of two building blocks: the N-Me-HOPO and the EGTA-HOPO.

Additionally, as a reference probe the Raymonds' archetype, tren(1-Me-3,2-HOPO)$_3$ (Fig.19) was synthesized to determine to what degree the applied structure modifications influence the favourable characteristics of the HOPO-based agents.
In summary, different approaches were explored to accomplish the synthesis of Gd-**L1** and Gd-**L2** and they will be discussed in detail in the following sections.
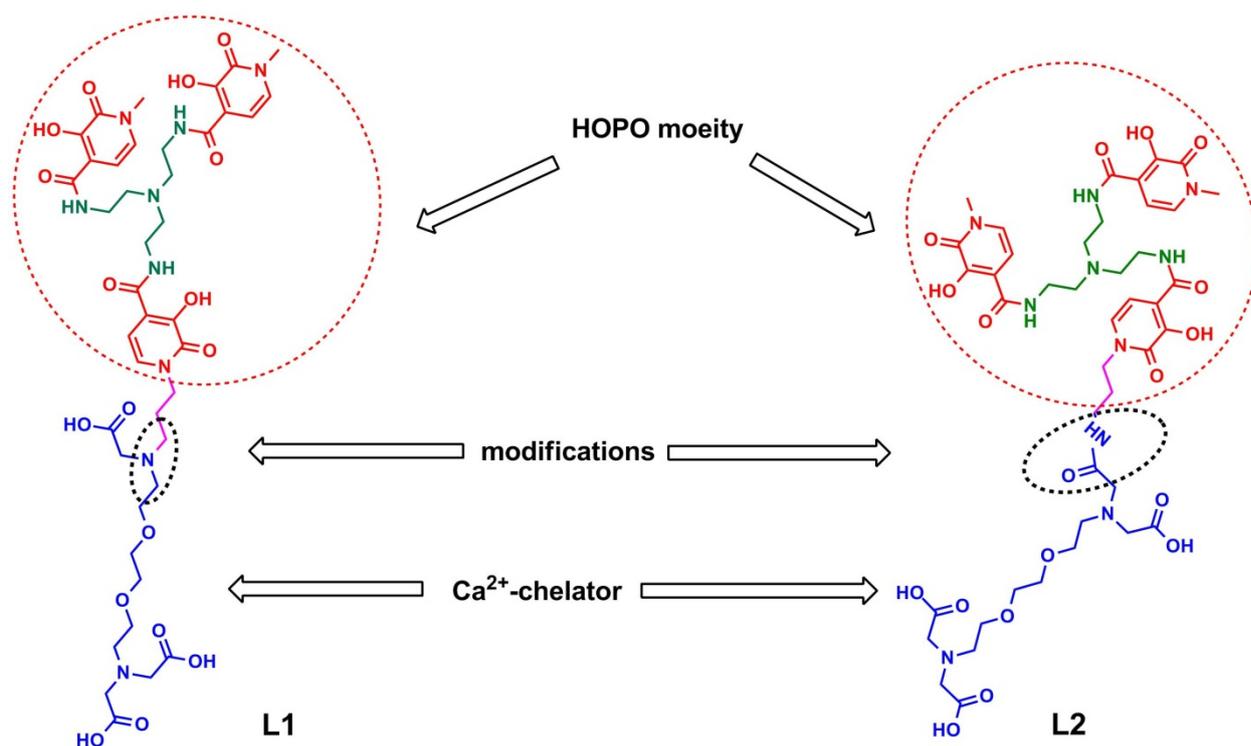
Figure 18 Building blocks of Ca2+-responsive HOPO-based CAs with marked modifications.
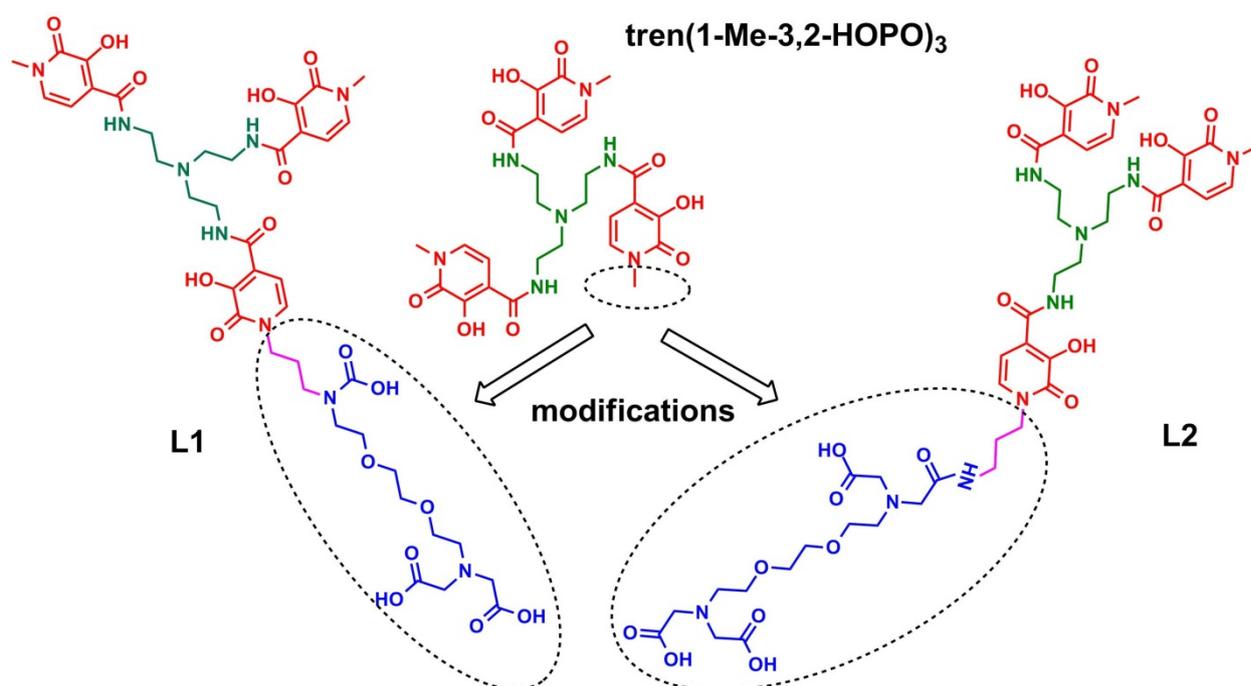


Figure 19 Comparison of both L1 and L2 with original archetype. In ellipses are marked additionally introduced modifications.

## 2.3.1 Synthesis of the core structure

I established a new synthetic pathway for the HOPO MR-reporter within this work. The novel route, in contrary to the published procedures, does not require autoclaves[65] and safety measures that usually apply to published methods involving gaseous ammonia.[96]

The synthesis of N-Me-HOPO began with introduction of a carboxylic group on the HOPO ring. To achieve this goal several strategies were explored.

The first approach involved preparation of a model compound **B** (Fig. 20). The compound **B** could additionally be utilized to optimize its attachment to the $Ca^{2+}$-chelator. The preparation of compound **B** according to a published procedure[97] started with the alkylation of **1** at the nitrogen atom with ethyl bromoacetate to give compound **2** with good yield. However, the following ring alkylation in the *para* position of **2** gave the Mannich product **3** only in a moderate yield (21%) in contrary to the reported result.
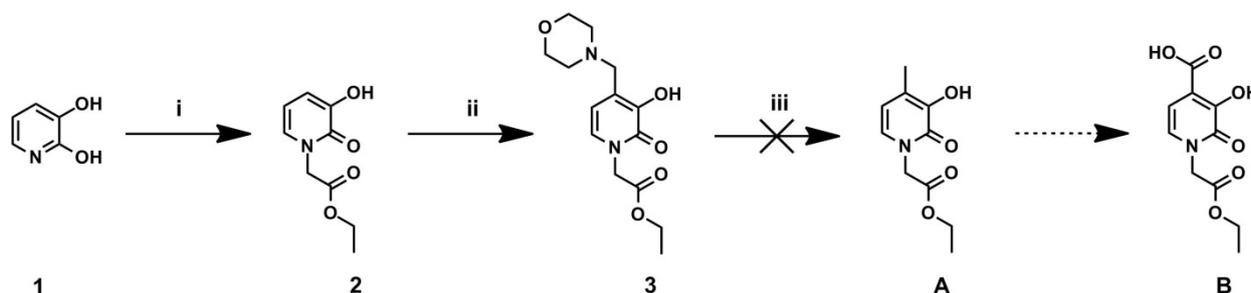


**Figure 20 First attempt to insert a fuctional group on the HOPO ring. Reactions conditions: i) Ethyl bromoacetate, 48 h, 200 °C, 64% ii) Morpholine, HCHO, 2 h, r.t, 21%; iii) Pd/C, cyclohexane, EtOH, reflux 24 h, no product**

Although the authors report on efficient cleavage of morpholine with Pd/C, this reaction could not be reproduced (Fig. 20). Therefore the model compound was abandoned and the efforts focused on developing a new synthetic pathway to obtain the HOPO MR-reporter.

Another synthetic approach that was exploited focused on a direct attachment of a carboxyl moiety to the HOPO ring. This was approached with use of the Fries rearrangement[98] on compound **4**. The Fries rearrangement allows migration of the

acyl group from a phenolic –OH group to the neighbouring position. The compound **4** was synthesized to obtain a molecule suitable for the Fries rearrangement. Two alkylating agents were screened for this purpose: ethyl chloroformate and diethyl pyrocarbonate. Both gave comparable results as summarised in Table 1. The best yields (up to 50%) were obtained for solvent and base free conditions (Fig. 21).
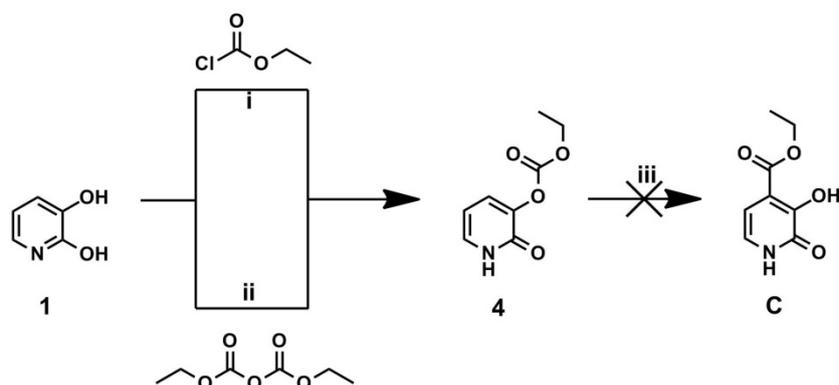


**Figure 21 Attempted Fries rearrangenmt and preparation of suitable educts for it. Reaction conditions: i) & ii) conditions given in Table 1; iii) DIPEA, $^{n}$BuLi**

**Table 1 Alkylation conditions of the HOPO –OH group**

| Acylating agent | Base | Solvent | Temperature [˚C] | Yield [%] |
|---|---|---|---|---|
|  1.0 eq | NaH | DMF | 55 | 12 |
| | | | 93 | 25 |
| | no base | no solvent | 93 | 40 |
|  1.2 eq | no base | no solvent | 40 | 30 |
| | | | 90 | 50 |
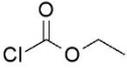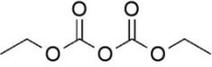
However, the rearrangement of the carbonate derivative **4** in the next step turned out to be unsuccessful as $^{n}$BuLi with DIPEA were not able to trigger the Fries reaction.

Further efforts focused on an introduction of a carboxyl group onto the HOPO ring while retaining the protecting group of the phenol. Two protecting groups for the hydroxyl group in *meta* position were primarily chosen: methyl and methoxy-methyl (MOM).

Methyl and MOM were chosen as protecting groups due to their ability to direct metallation towards the neighbouring carbon atom in the aromatic ring.[99] Additionally, their small size would not inhibit the carboxylation step. Methylation of

the –OH group in *meta* position was performed with good yields as reported by Hanessian *et al.*[100] It was found that the ratio of reagents is crucial for achieving high yields. The reaction proceeded most efficiently with 80% isolated yield of **6** (Fig. 22), when an equimolar ratio of substrates was used. The use of excess of sodium hydroxide or dimethyl sulphate led to additional alkylation on the nitrogen atom.

In parallel, a protection with the MOM ether was investigated. MOM chloride was used as alkylating agent with sodium hydride NaH or potassium tert-butoxide (KO$^t$Bu) as base. The MOM protected pyridinone **5** was obtained in 20 to 25% yield using NaH and in 1% using KO$^t$Bu. Protection with MOM was less efficient than reaction to obtain the methyl ether **6**. Therefore, the derivative **6** was further used for the insertion of carboxyl group via ester intermediate. However, the conditions required to obtain **7** had to be carefully optimised. In presence of diisopropylamine (DIPEA) or 1,1',2,2'-tetra-methylethylenediamine (TMEDA) the desired ester **7** was not formed. When 2.5 equivalents of $^n$BuLi and 2.5 equivalents of ethyl chloroformate were used in absence of additional base the ester **7** was obtained with a yield of 50%. Also time had an important role in this reaction as complete metalation of **6** in *para* position required approximately 15 hours. Addition of ethyl chlorofomate before the lapse of that period resulted only in recovering of the starting material.

The subsequent protection of the nitrogen atom in **7** with MeI, was screened with two different bases: potassium carbonate and caesium carbonate. Initially the reaction was approached with $Cs_2CO_3$ and $Bu_4NI$ as a phase transfer catalyst; however the removal of the ammonium salt proved to be difficult despite the good yield. Therefore, $K_2CO_3$ was used and N-methyl pyridinone **8** was formed with 90% yield avoiding impurities from the phase transfer catalyst. Cleavage of the ethyl ester with sodium hydroxide and subsequent acidification with a concentrated solution of HCl gave the desired acid **9** (Fig. 22).
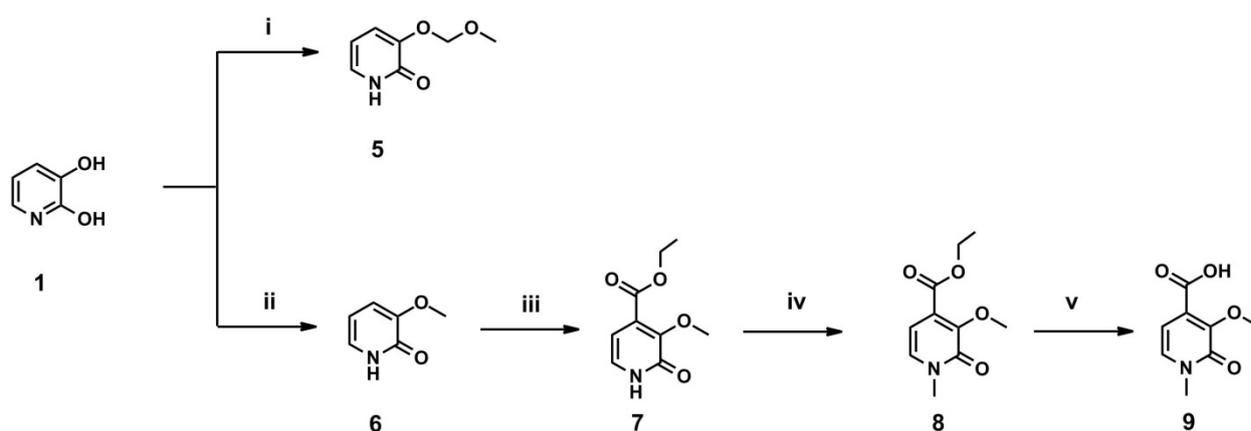
**Figure 22 Synthesis of 3,2-HOPO derived carboxylic acid. Reaction conditions: i) MOMCl, KO$^t$Bu or NaH, 1-25%; ii) Me$_2$SO$_4$, NaOH, 3 h, r.t, 80%; iii) $^n$BuLi, ethyl chloroformate, -78-0 °C, 50%; iv) MeI, K$_2$CO$_3$, r.t. 24 h, 90%; v) NaOH, reflux, overnight, 70%.**

Having obtained the acid **9**, further efforts focused on coupling it to the amine scaffold **10**. The amide formation of **9** with mono-Boc-protected TREN **10**[101] (Fig. 24) required extensive optimization of the reaction conditions. The activation of the acid **9** with 2-mercapto-2-thiazoline was approached according to a procedure published by Raymond *et al.*[66] Although the authors reported that the activated form of **9** should be stable enough to be purified by column chromatography, this reaction failed for acid **9**.

Also *in situ* transition of acid **9** to an acid chloride with oxalic chloride or thionyl chloride with subsequent addition of amine did not yield the desired **11**. Several consecutive coupling agents were examined (Fig. 23) but only using perfluorophenyl 2,2,2-trifluoroactetate (PFP TFA) the amide **11** was obtained with 50% yield. After successful coupling of the acid **9** to the protected amine **10** (50% yield), the Boc group was removed to give the primary amine **12** in quantitative yield (Fig. 24).
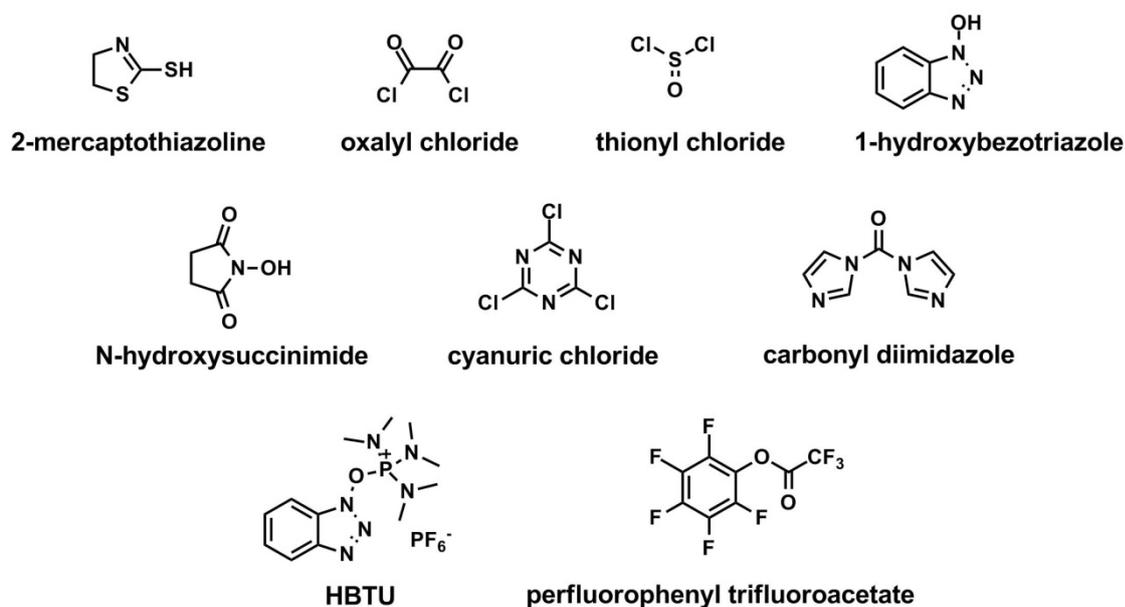
Figure 23 Screened coupling agents for attachment of acid 9 to an polyamine scaffold

In summary, in this section synthesis of the acid **9** was accomplished along with its successful coupling to the scaffold **10**. The obtained compound **12** was ready to be coupled to the last HOPO ring with an attached $Ca^{2+}$-chelator.

The further efforts focused on synthesis of EGTA-HOPO and its subsequent attachment to amine **12**. In parallel, the exact copy of the Raymonds' archetype, tren(1-Me-3,2-HOPO)$_3$ (Fig. 19) was synthesized using the synthetic strategy presented above.



**9**  **10**  **11**  **12**
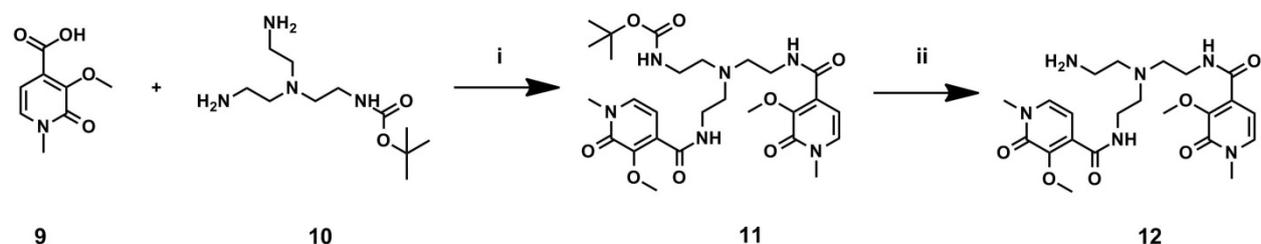
Figure 24 Coupling of 3,2-HOPO derived carboxylic acid 9 to an aliphatic scaffold 10. Reaction conditions: i) a) py, overnight, r.t., b) PFP TFA, DIPEA, overnight, r.t. 50%; ii) TFA, overnight, r.t, quant.

## 2.3.2 The synthesis of the archetype

To have a reference agent to compare with $Ca^{2+}$-responsive probes, [Gd{tren(1-Me-3,2-HOPO)$_3$}(H$_2$O)$_2$] was synthesized. The synthesis started with preparation of the ligand tren(1-Me-3,2-HOPO)$_3$ (Fig. 25).

The acid **9** was coupled to the TREN amine **13** with the help of PFP TFA as an activating agent to give the tris-amide **14** in 30% yield. The removal of the phenolic methyl groups was attempted with the use of boron tribromide and boron trichloride, but both reagents yielded no product. The eventually successful removal of methyl groups was accomplished with sodium ethanethiolate in DMSO at 140 $^0$C as published by Kiessling et al.[102] The obtained ligand (50% yield) was submitted for complexation reaction with GdCl$_3$ (Fig. 25) to give [Gd{tren(1-Me-3,2-HOPO)$_3$}(H$_2$O)$_2$]. The absence of free $Gd^{3+}$ was confirmed by a xylenol orange test and measurements of the longitudinal relaxation times $T_1$. The obtained results will be discussed in detail in further chapters.
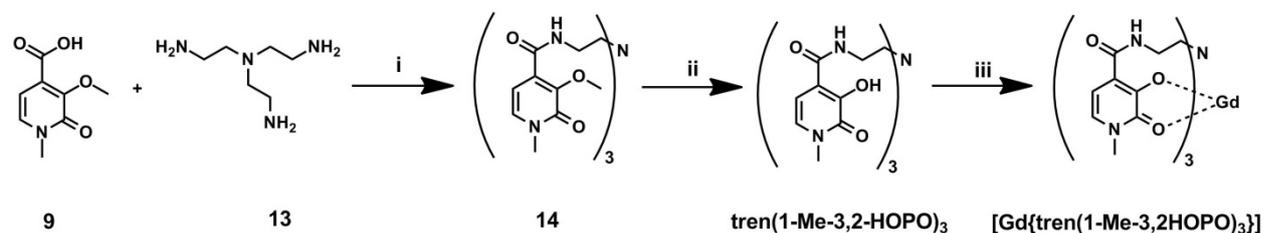


**Figure 25 Synthesis of the archetype of HOPO CA using new methodology. Reaction conditions: i) a) py, PFP TFA, overnight, r.t., b) DIPEA, overnight, r.t. 30%; ii) NaSEt, 2 h, 140 °C, 87%; iii) GdCl$_3$, overnight 40 °C.**

## 2.3.3 Attachment of a $Ca^{2+}$-chelator to a HOPO ring. Final steps towards L1

To synthesize a $Ca^{2+}$-responsive HOPO-based CA I needed two building blocks: N-Me-HOPO, synthesized and attached to the scaffold in section 2.3.2, and the EGTA-linked HOPO. The efforts to synthesize the latter moiety will be presented in detail in the following section.

At first, the $Ca^{2+}$-chelator precursor was synthesized in house as presented in Fig. 26. Compound **15** was synthesized as published by Liu et al.[103] In the next step the Boc protecting group was removed with TFA and a subsequent alkylation of both

terminal amines with excess of *tert*-butyl bromoacetate gave compound **16** in 77% yield after two steps. Removal of the benzyl group gave the Ca$^{2+}$-chelator precursor **17** in quantitative yield.
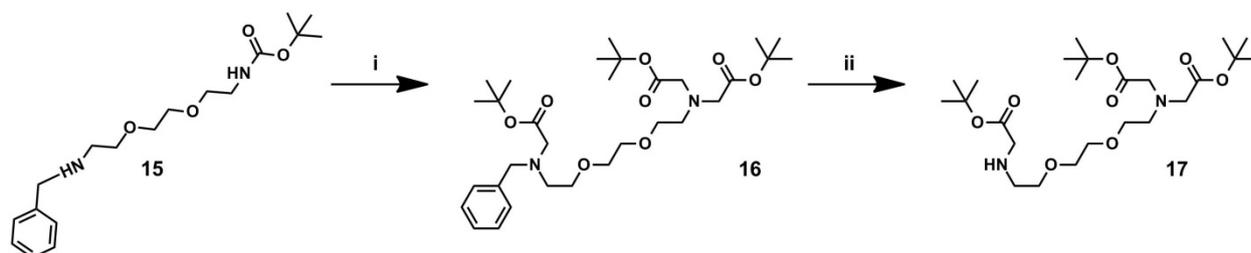


**Figure 26 The first Ca$^{2+}$-chelator precursor. Reaction condirtions: i) a) TFA, overnight, r.t.; b) K$_2$CO$_3$, *tert*-butyl bromoacetate, overnight, r.t., 77%; ii) H$_2$/Pd/C, overnight, r.t., 99%.**

Further efforts focused on attachment of **17** to a HOPO ring containing an aliphatic linker. Therefore synthesis of **F** (Fig. 27) was investigated, that involved alkylation of pyridinone **6** using three different dihalogenalkanes: 1,2-dichlorethane, 1,3-dibromopropane and 1-bromo-4-chlorobutane (Fig. 27).
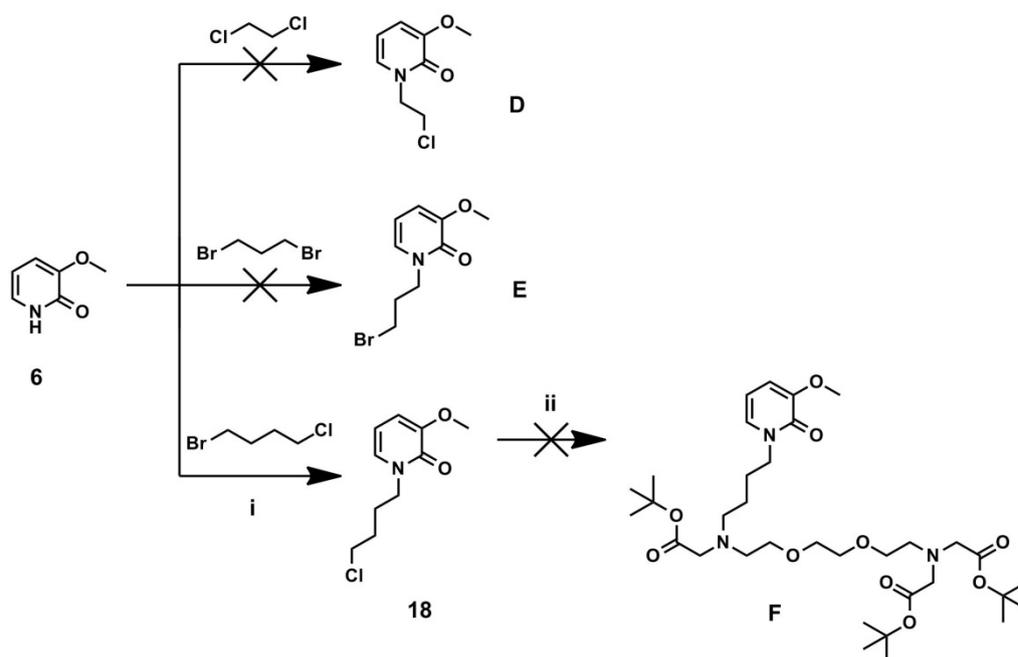


**Figure 27 Second try to attach the Ca$^{2+}$-chelator to a HOPO-moiety. Reaction conditions: i) K$_2$CO$_3$, KI, overnight, 100 °C, 36%; ii) K$_2$CO$_3$, KI, r.t..**

The linkers of different length were chosen to determine the optimal distance between the Ca$^{2+}$-chelator and the MR-reporter with regard to create the best SCA.

While 1,2-dichlorethane and 1,3-dibromopropane did not result in the desired products, the 1-bromo-4-chlorobutane gave the alkylation product **18** in 36% yield. However, the subsequent alkylation of the Ca$^{2+}$-chelator **17** with the obtained halogen derivative of HOPO failed (Fig 27).

The next investigated pathway to attach Ca$^{2+}$-chelator **17** to the compound **6** involved reductive amination. This approach required first alkylation of the heteroatom in **6** with a protected aldehyde. First trials focused on an attachment of a cyclic acetal to **6**. The cyclic acetal was considered to be more stable over its aliphatic analogue in harsh reaction conditions. Indeed, the desired acetal **19** was obtained in satisfying yields, but the following deprotection to aldehyde failed (Fig. 28). Pyridinium *p*-toluenesulfonate[104] was not able to deprotect the acetal.
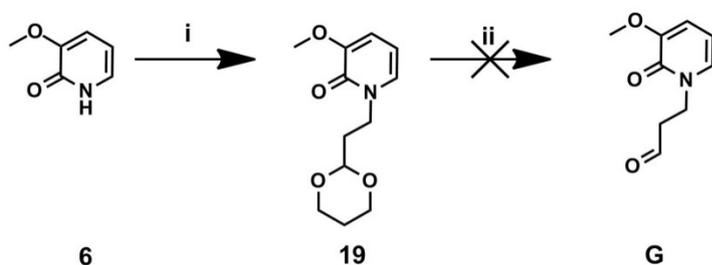


**Figure 28 The first attempt to attach an aldehyde function to HOPO-ring. Reaction conditions: i) Na$_2$CO$_3$, overnight, 100 °C, 60%; ii) pyridinium p-toluenesulfonate, 60 °C.**

Due to these problems the corresponding acyclic dimethyl acetal was used instead. An attachment of dimethyl acetal to **6** was examined with three different bases. The best result was obtained with sodium hydroxide (59%) while potassium carbonate gave the alkylation product **20** in only 8% yield. Caesium carbonate with addition of Bu$_4$NI gave **20** as well, but the accurate yield could not be determined due to the contamination with ammonium salts (Fig. 29).
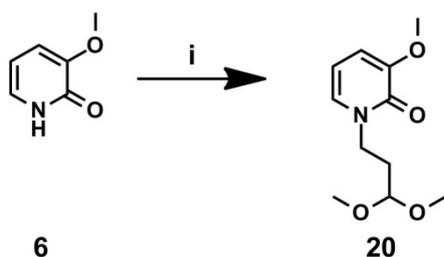


**Figure 29 Various bases screen for alkylation of HOPO. Reaction conditions: i)3-bromopropionylaldehyde dimethylacetal, base (Table 2), overnight, 100 °C**

**Table 2 Various bases screen for alkylation of HOPO with 3-bromopropionylaldehyde dimethylacetal**

| Base | Yield |
|---|---|
| $Na_2CO_3$ | 0% |
| $K_2CO_3$ | 8% |
| NaOH | 59% |
| $Cs_2CO_3/Bu_4NI$ | ? |

Typically for attachment of dimethyl acetal terminated linker sodium hydroxide should be used. However, this was not considered due to the presence of the ethyl ester on the HOPO ring **7** (Fig. 30). [i] Consequently, potassium and caesium carbonate were screened to give **21** in 60% yield in case of $K_2CO_3$ and from 18 to 84% yield for $Cs_2CO_3$. Therefore, potassium carbonate became the base of choice. Deprotection of the acetal with water/TFA failed, but mixture of sulphuric acid adsorbed on silica gel and water[105] provided the desired aldehyde **22** in quantitative yield (Fig. 30). The next step involved reductive amination of aldehyde **22** with the $Ca^{2+}$-chelator **17**. The reaction with sodium borohydride failed. Therefore, sodium trisacetoxyborohydride[106] was used as a reducing agent. No formation of **23** was observed at room temperature. However, increasing the temperature to 100 $^0$C for 15 hours gave **23** in 30% yield. Further extension of reaction time to 3 days gave the product **23** with even higher yield of 60%. Selective removal of the ethyl ester under mild basic conditions with sodium hydroxide at room temperature failed and only starting material was recovered (Fig. 30). Harsher conditions involving higher temperatures could not be applied because the *tert*-butyl esters would also be removed.

---

[i] From this point on all condition optimisation was performed on the HOPO ester **7** as its synthesis was already established.
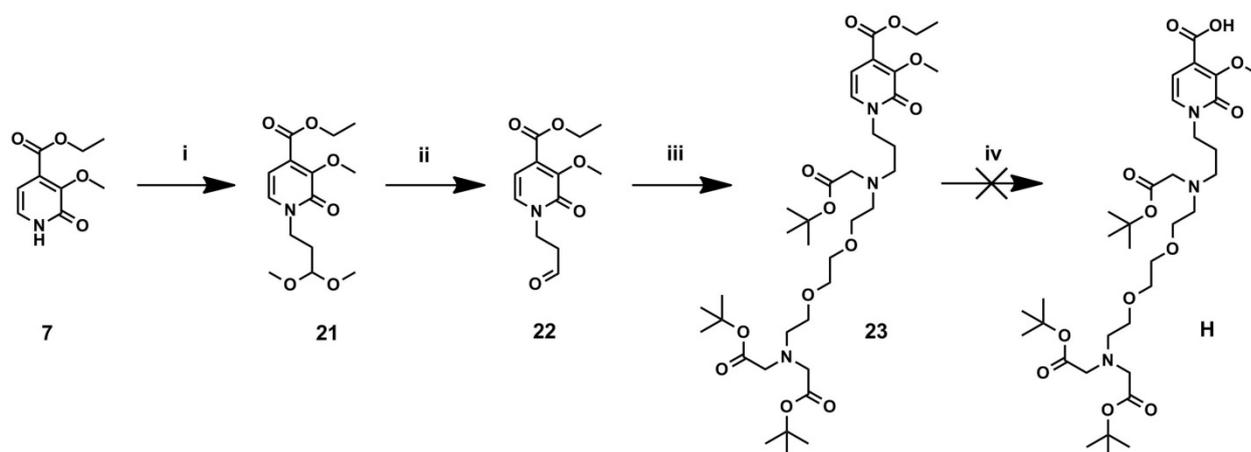
**Figure 30 First attempt to couple a Ca$^{2+}$-chelator to HOPO ring. Reaction conditions: i) base (Table 3), overnight, 100 °C; ii) acid/H$_2$O (Table 3), overnight, r.t.; iii) reducing agent (Table 3); iv) NaOH, r.t, overnight**

**Table 3 Screened conditions for reactions presented in Fig. 30**

| Base | Yield | Acid | Yield | Reducing agent | Yield |
|------|-------|------|-------|----------------|-------|
| K$_2$CO$_3$ | 60% | TFA | 0% | NaBH$_4$ | 0% |
| Cs$_2$CO$_3$/Bu$_4$NI | 18-84% | H$_2$SO$_4$/SiO$_2$ | Quant. | NaBH(OAc)$_3$ | 60% |

Consequently, another Ca$^{2+}$-chelator precursor with a different protecting group was developed. Compound **24** was synthesized according to a procedure reported by Gatto *et al.*[107] Further monoalkylation with benzyl bromide at low temperature gave tris-benzyl amine **25** with 60% yield (Fig. 31).
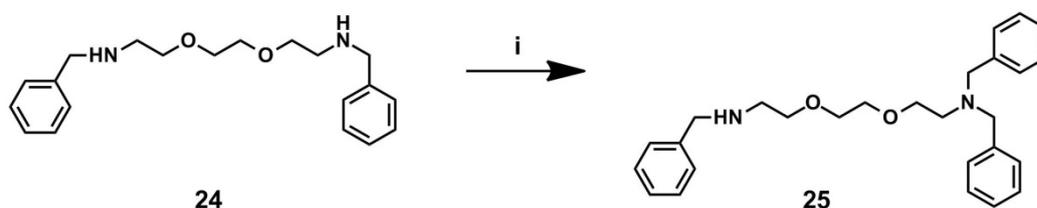


**Figure 31 The new Ca$^{2+}$-chelator precursor. Reaction conditions: i) BnBr, K$_2$CO$_3$, -40 °C-r.t., 60%**

The Ca$^{2+}$-chelator precursor **25** was then submitted to the reductive amination reaction with aldehyde **22** to give compound **26** in 50% yield. The next step involved basic hydrolysis of the ethyl ester resulting in acid **27**. Subsequent attachment to

amine **12** gave **28** containing three HOPO rings in 50% yield after two steps (Fig. 32).
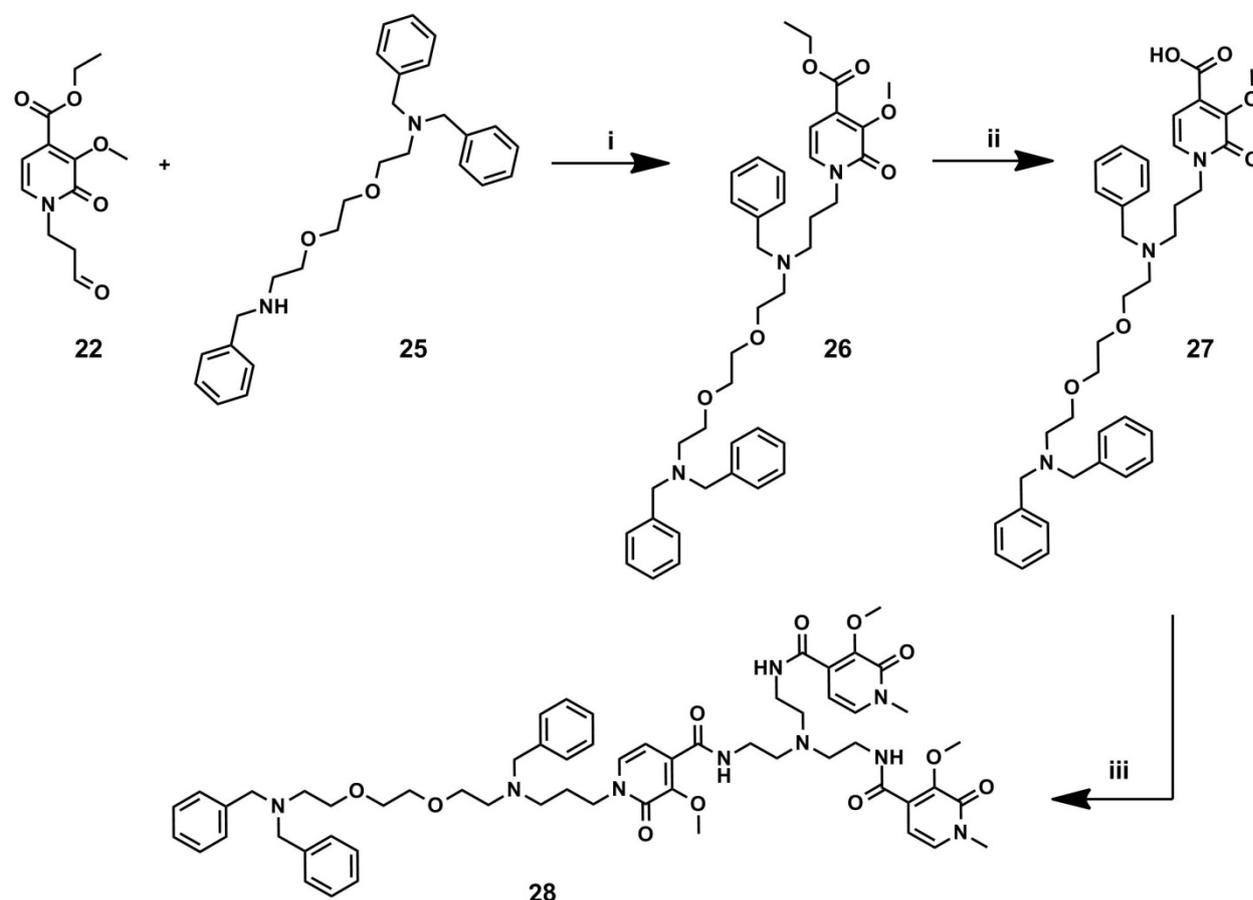


**Figure 32 Synthesis and attachment of the responsive HOPO moiety to the scaffold. Reaction conditions: i) NaB(OAc)₃H, 3d, 100 °C, 50%; ii) NaOH, overnight, reflux; iii) a) Py, overnight, r.t.; b) PFP TFA, DIPEA, 12, overnight, r.t., 50% after 2 steps.**

Catalytic hydrogenolysis of the benzyl amine groups using 3.5 bars of hydrogen pressure and 10% Pd/C as catalyst to remove the benzyl protecting groups could not be accomplished. Even high temperature and atmospheric pressure of hydrogen also did not yield the desired product **29** (Fig. 33). Nevertheless, ammonium formate used as a source of hydrogen and 10% Pd/C as catalyst proved to be an efficient method to obtain amine **29**, which was then alkylated with excess of *tert*-butyl bromoacetate to give triester **30** with 76% yield. After deprotection of the *tert*-butyl esters with TFA, the phenolic methyl groups from HOPO MR-reporter were removed using sodium ethanethiolate (procedure previously described for tren(1-Me-3,2-

HOPO)$_3$ in section 2.3.2). HPLC purification of the crude product gave the desired ligand **L1** (Fig. 33) However, due to poor solubility of **L1** in methanol or DMSO, no reliable NMR data could be obtained. Complexation of **L1** with GdCl$_3$ (0.1 eq.) was performed using GdCl$_3$ (0.1 eq.) in order to avoid an excess of metal. The reason for this ratio was that the Gd$^{3+}$ trapped inside the Ca$^{2+}$-chelator would occupy the cavity designated for Ca$^{2+}$.



**30**

**31**

ii

**32**

i
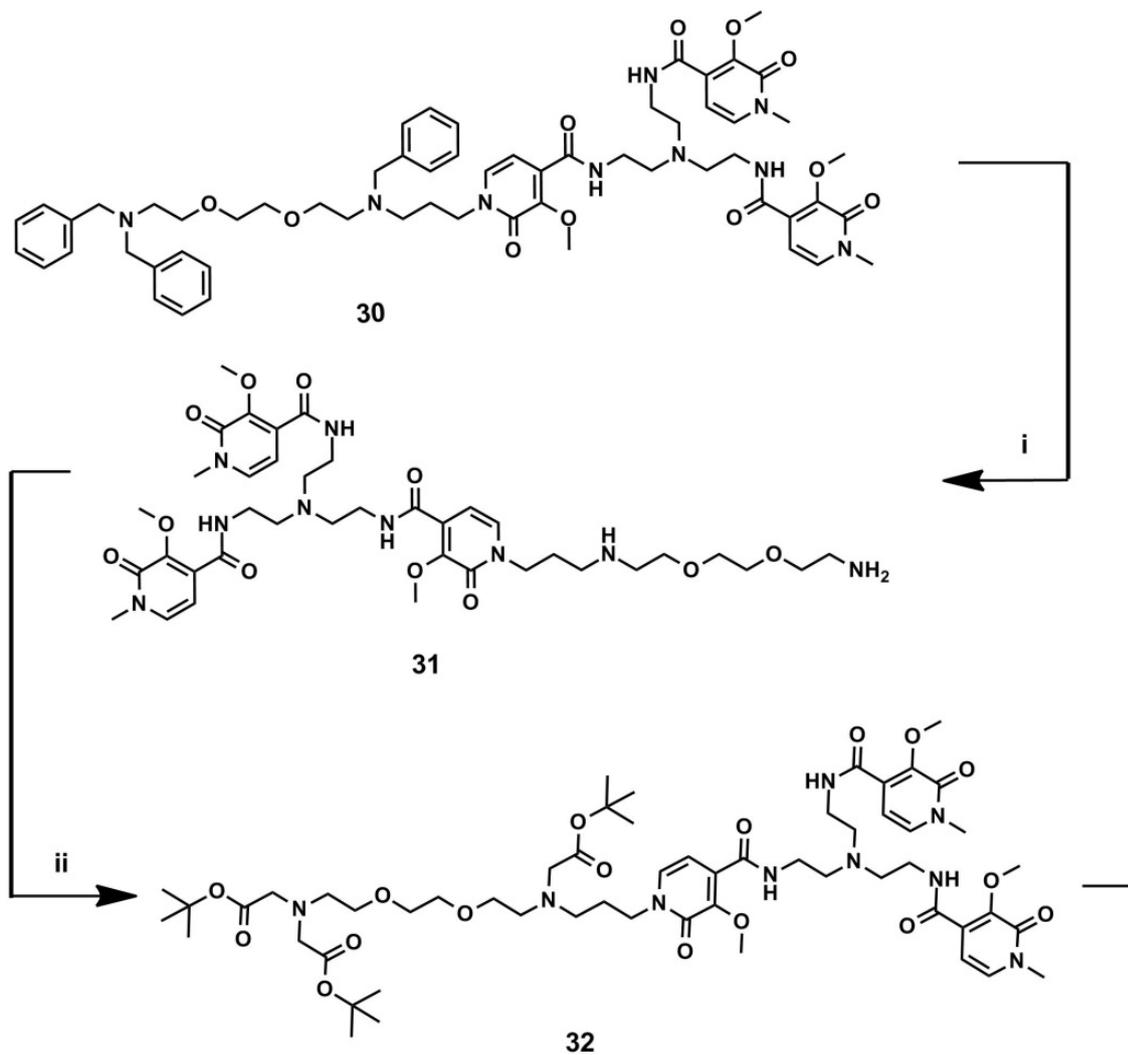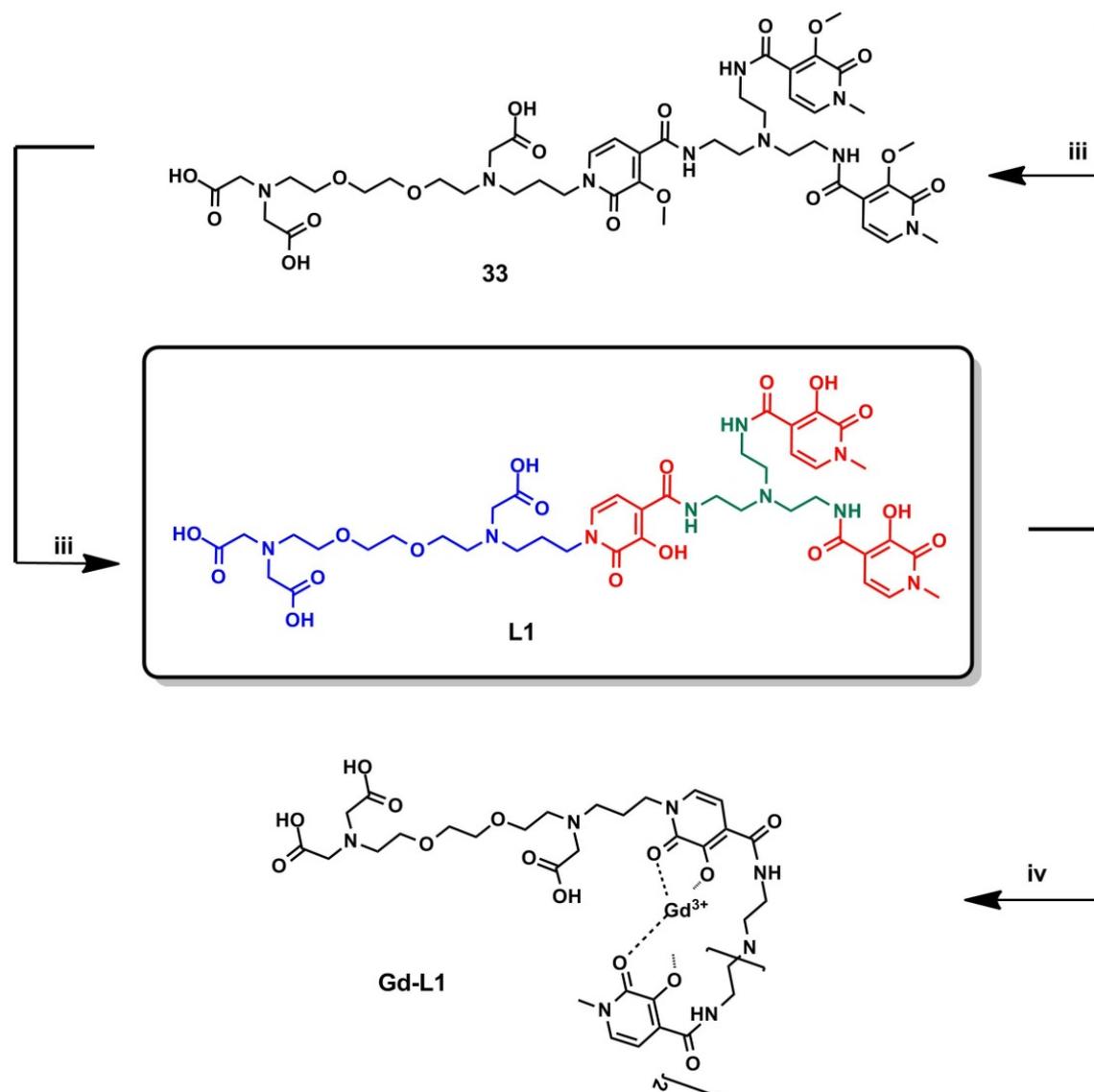
**Figure 33 Final synthetic steps to Gd-L1. Reaction conditions: i) NH$_4$CO$_2$, 10% Pd/C, overnight, reflux, quant; ii) BrCH$_2$CO$_2^t$Bu, K$_2$CO$_3$, 3 days, r.t. 76%; iii) TFA, overnight, r.t., quant; iv) NaSEt, 2 h, 140 °C; v) GdCl$_3$, pH=7, overnight 40 °C.**

## 2.3.4 Synthesis of Gd-L2

The synthesis of Gd-**L2** started with preparation of ligand **L2**. In contrast to the already obtained **L1**, **L2** contain an amide bond between the Ca$^{2+}$-chelator and the MR-reporter. I chose the amide connection to preserve as far as possible the original structure of EGTA.

In order to synthesize **L2**, further modifications of the newly established synthetic pathway needed to be implemented. Firstly, a linker with terminal amine had to be introduced into the HOPO MR-reporter. Three potential synthetic routes (Fig. 34) were investigated to obtain this aim.
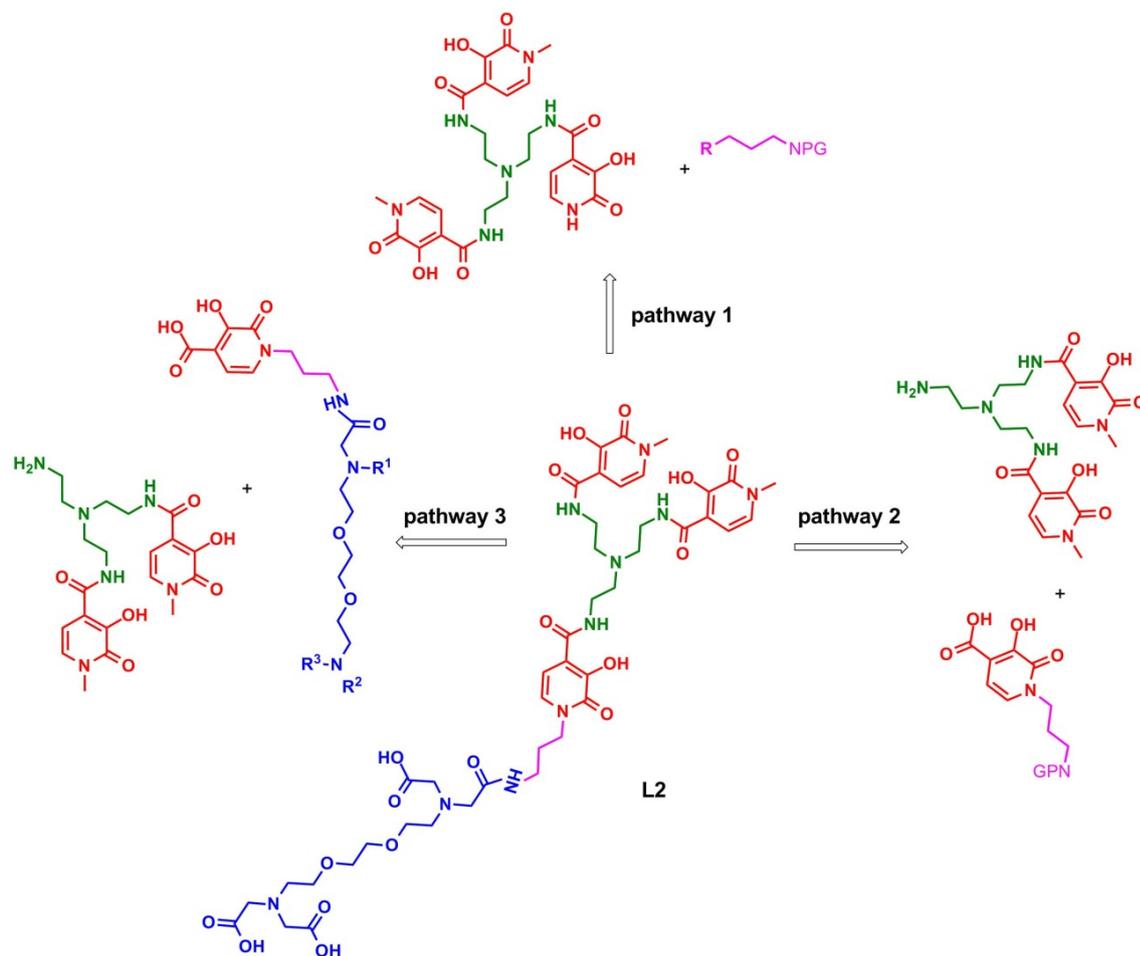


**Figure 34 Three possible pathways to construct L2**

Pathway 1, which was investigated first, was based on attachment of a HOPO acid with free nitrogen atom **32** to the scaffold **12**. Although the amide formation proceeded with good yield of 56%, the following alkylation of **33** with Boc-protected bromoamine was futile (Fig. 35).
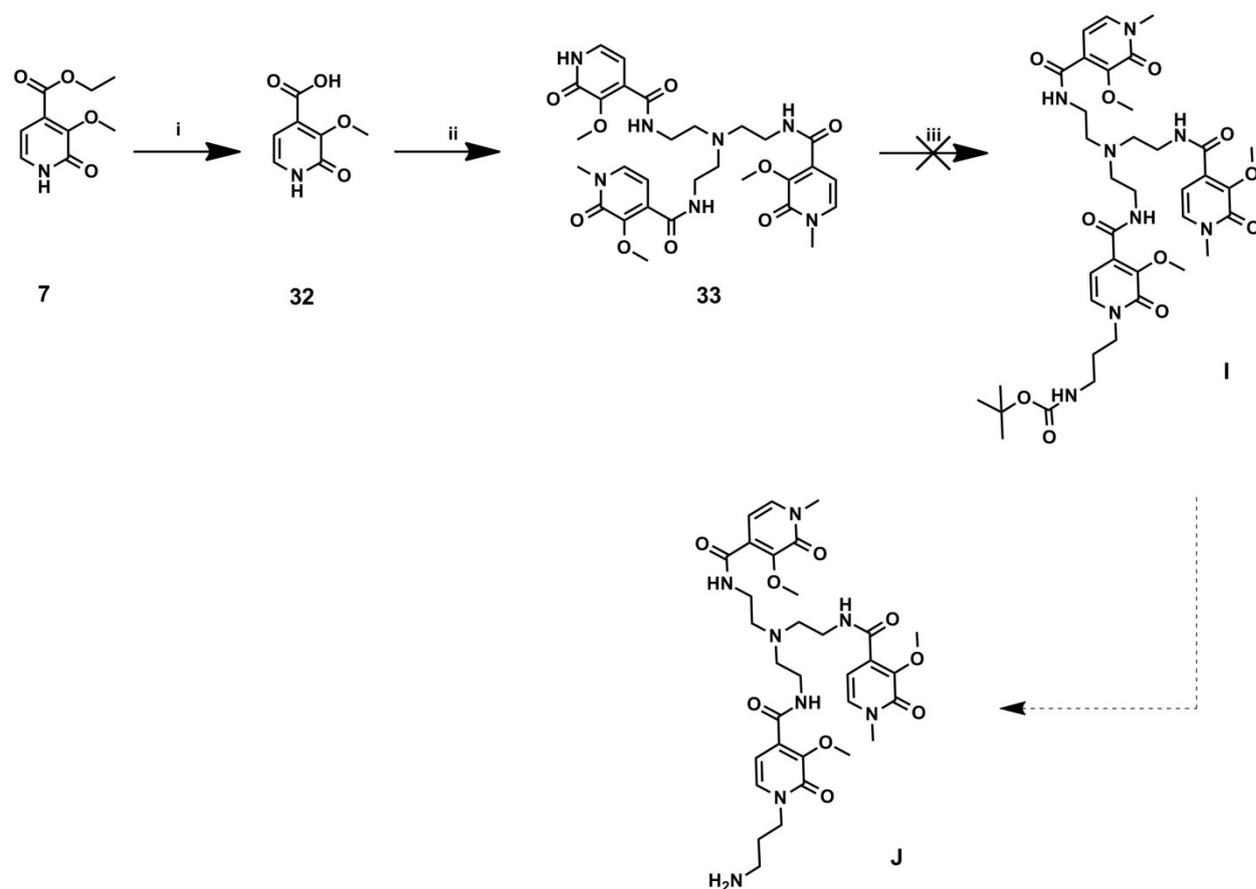
**Figure 35 Attachment of HOPO acid with free nitrogen atom to the scaffold 12. Reaction conditions: i) NaOH, overnight, reflux, 50%; ii) a) PFP TFA, Py, overnight, r.t., b) 12, DIPEA, overnight, r.t., 56%; iii) Boc-bromopropylamine, KI, K₂CO₃, 100 °C.**

Due to the encountered difficulties during nitrogen alkylation, the synthetic strategy was changed to pathway 2 (Fig. 34). In order to introduce Ca$^{2+}$-chelator into the HOPO MR-reporter, the linker with the terminal amine group had to be incorporated at first into pyridinone **7**. Basic hydrolysis of ester **34** and following coupling of the resulting acid **35** to the scaffold **12** gave the HOPO MR-reporter in 30% yield after two steps (Fig. 36). The removal of the benzyl groups from **36** was not possible even though several catalysts and reaction conditions were screened.
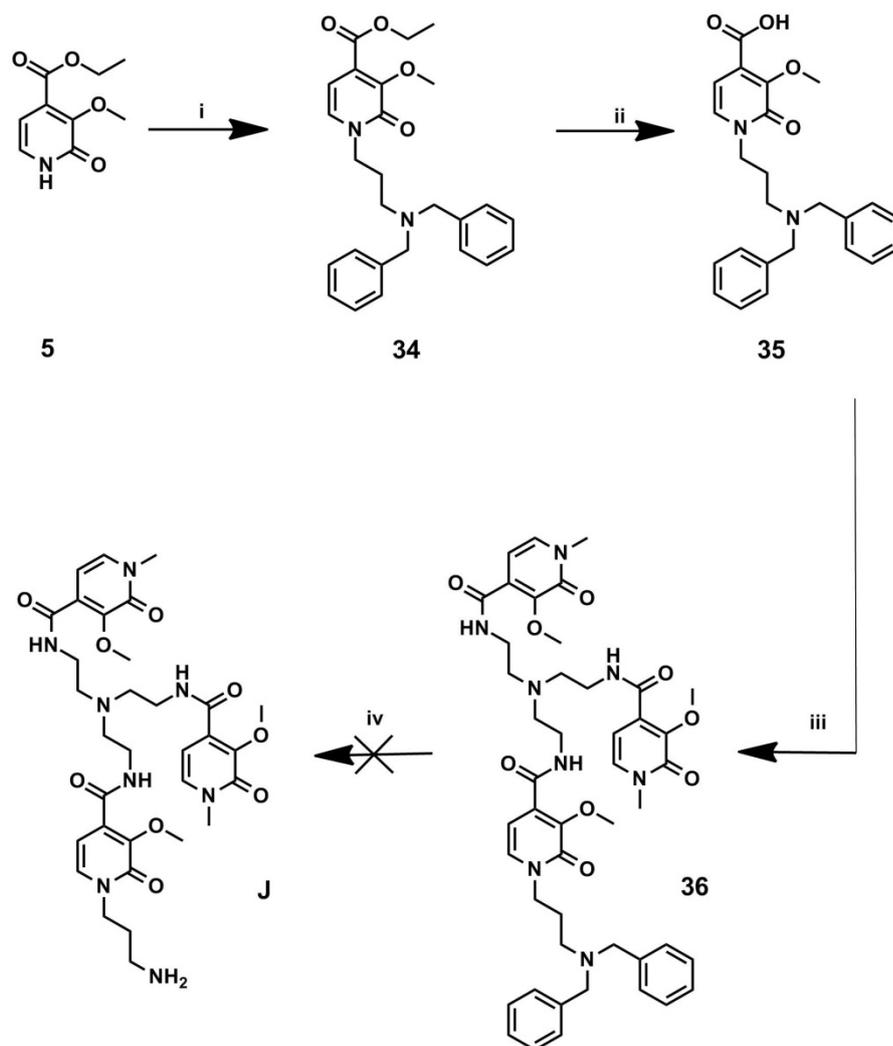
**Figure 36 Bis-benzyl protection of amine group turned out to be resistant for cleavage due to steric hindrance of three HOPO rings. Reaction conditions: i) bis-benzyl-bromopropylamine, KI, K$_2$CO$_3$, overnight, 100 °C, 45%; ii) NaOH, overnight, reflux, 50%; iii) a) PFP TFA, Py, overnight, r.t, b) 12, DIPEA, overnight, r.t., 29%; iv) H$_2$ or HCO$_2$NH$_4$, Pd/C, r.t or 60°C.**

At this stage I decided to change the synthetic pathway and pursue the concept already established for the synthesis of Gd-**L1** which involved at first the attachment of the Ca$^{2+}$-chelator precursor to a HOPO ring followed by subsequent attachment of this construct to scaffold **12**. In order to obtain **39** (Fig. 37), intended to be used further for attachment of the Ca$^{2+}$-chelator, its synthesis was first approached by debenzylation of dibenzylamine **34** using 3.5 bars of hydrogen at room temperature for 24 hours or 1 bar of hydrogen pressure at 60 °C for 15 hours. However, this reaction could not be accomplished like in the case of compound **36** (Fig. 36), despite lower steric hindrance in **34** compared to **36**.

Therefore a range of different synthetic strategies was investigated (Fig. 37). Bromopropionitrile was used to insert a nitrile group, but this did not give the alkylation product. The use of phthalimide protected amine resulted in 50% yield of **37** but deprotection occurred to be problematic due to its low efficiency. No product **39** was observed when sodium borohydride was used. When hydrazine hydrate was used its association to the amine group inhibited further alkylation with chloroacetic anhydride and bromoacetic acid (Fig. 37). Cbz-protected amine gave **38** in 46% yield but the further cleavage of Cbz group resulted only in 18% of **39** and a large amount of the starting material was recovered.
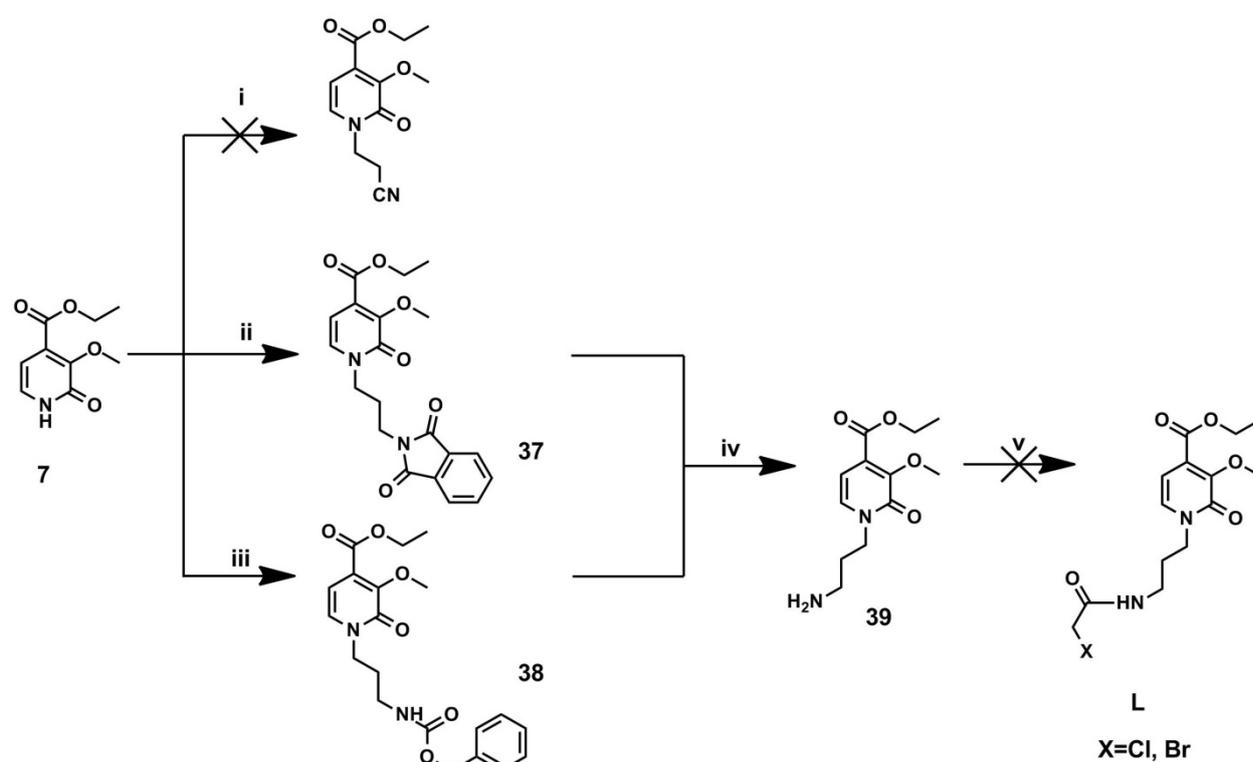


**Figure 37 Functionalization of HOPO ring with a protected amine and its further processing. Reaction conditions: i) 3-bromopropionitrile, KI, K₂CO₃, overnight, 100 °C; ii) N-(3-bromopropyl)phthalimide, KI, K₂CO₃, overnight, 100 °C, 50%; iii) N-Cbz-3-bromopropylamine, KI, K₂CO₃, overnight, 100 °C, 46%; iv) reducing agent, conditions in Table 4; v) alkylating agent, conditions in Table 5.**

**Table 4 Screened reducing agents for deprotection of amine group (Fig. 37)**

| Reducing agent | Conversion |
| --- | --- |
| NaBH$_4$, r.t, overnight | 0% |
| N$_2$H$_4$, reflux, 3 h | quant. |
| 3.5 bar H$_2$, K$_2$CO$_3$, r.t, 24 h | 18% |

**Table 5 Screened acylating agents for acylation of primary amine 41 Fig. 37**

| Acylating agent |
| --- |
| bromoacetyl chloride, K$_2$CO$_3$, 3 h, r.t |
| bromoacetic acid, CDI, 48 h, reflux |
| bromoacetic acid, DCC, DMAP, overnight, r.t |
| bromoacetic acid, EDC, overnight, r.t |
| chloroacetic anhydride, Et$_3$N, overnight, r.t |

The use of Boc-protected bromoamine proved to be optimal for formation of desired **40** in 56% yield. Two pathways were investigated. In the first approach acid **41** was obtained by basic ester hydrolysis of **40**, as the Boc group is considered to be stable under highly basic conditions.[108] Although the following coupling of acid **41** to the scaffold **12** gave product **42** in 22% yield after two steps, the synthetic pathway had to be further optimized as higher yields were required due to the time consuming and highly challenging preparation of the substrates (Fig. 38).

As consequence an alternative approach was used, where attachment of the Ca$^{2+}$-chelator precursor precedes the deprotection of ethyl ester. To obtain **39** initially the deprotection of Boc group was approached with use of HCl solution in isopropanol. No formation of the deprotected product was observed although reaction time was extended to 15 hours.
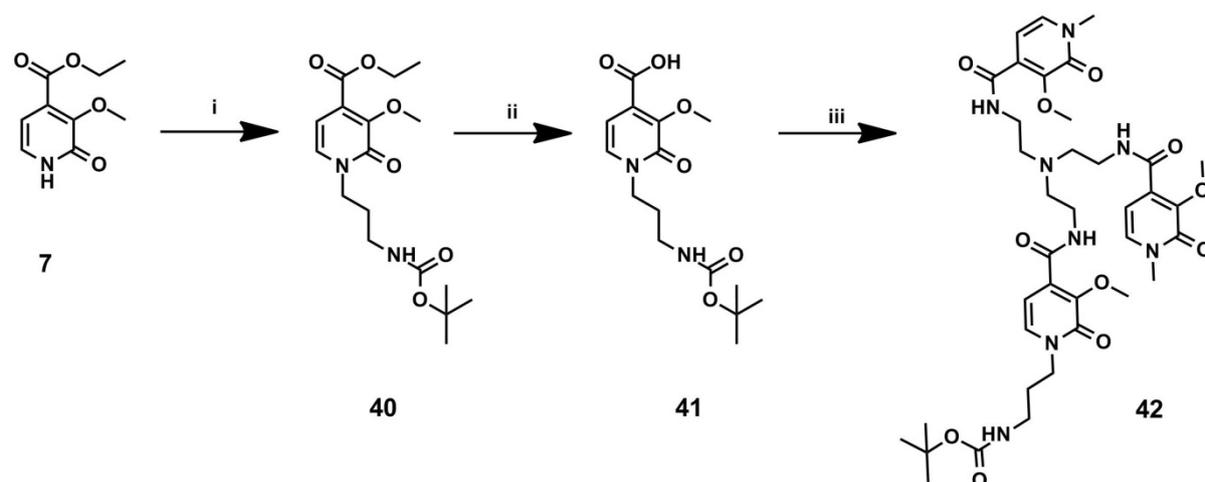
**Figure 38 Boc-group turned out to be not as stable in highly basic conditions as published[108] Reaction conditions: i) 3-(Boc-amino)propyl bromide, KI, $K_2CO_3$, overnight, 100 °C, 56%; ii) NaOH, overnight, reflux, 25%; iii) a) PFP TFA, Py, overnight, r.t., b) 10, DIPEA, overnight, r.t., 22%**

On the contrary, when diluted TFA was used the removal of Boc group was quantitative. The following reaction of amine **39** with chloroacetic anhydride failed. However, with the use of bromoacetic bromide under careful pH control amide **43** (Fig. 39) was obtained in 60% yield. The subsequent alkylation of amine **26** (Fig. 31) with the obtained bromoacetamide **43** gave **44** in 80% yield. At this point the ethyl ester was hydrolysed and the obtained acid **45** was coupled to the scaffold **12** to give tris-HOPO derivative **46** in 30% yield after 2 steps. Removal of benzyl groups was accomplished with ammonium formate as hydrogen source and 10% Pd/C as catalyst. The obtained intermediate **47** was submitted to alkylation with excess of *tert*-butyl bromoacetate resulting in 56% of **48**. Cleavage of the *tert*-butyl esters in **48** with TFA and methyl groups with NaSEt in **49** yielded the desired **L2** (Fig. 39) that was purified by HPLC. Yet, no reliable NMR data was obtained due to poor solubility of **L2** in methanol or even DMSO. Nevertheless, **L2** was submitted for complexation with $GdCl_3$. The presence of free $Gd^{3+}$ was excluded by xylenol orange test and measurements of the longitudinal relaxation times $T_1$. The obtained results are presented in following chapters.
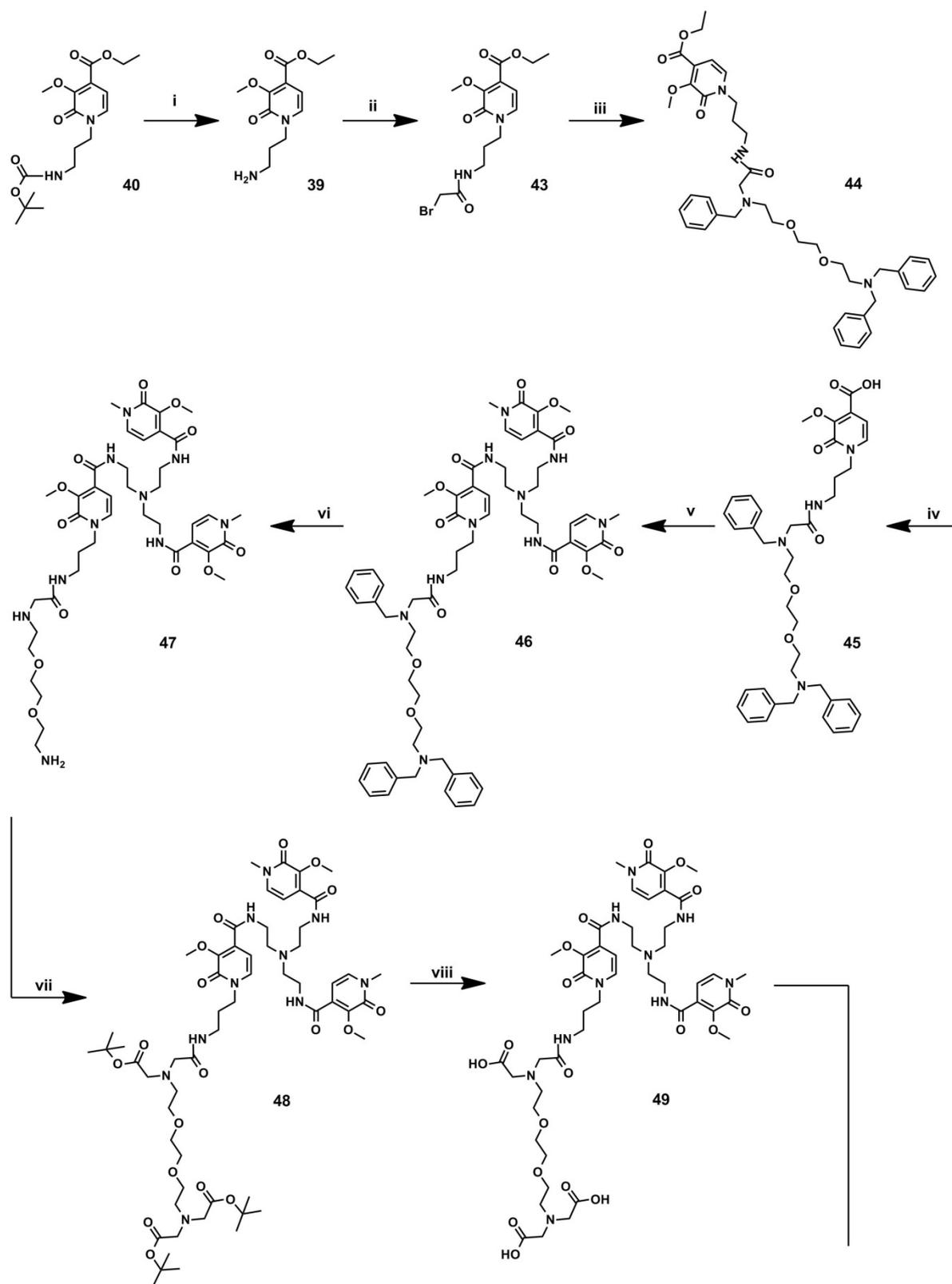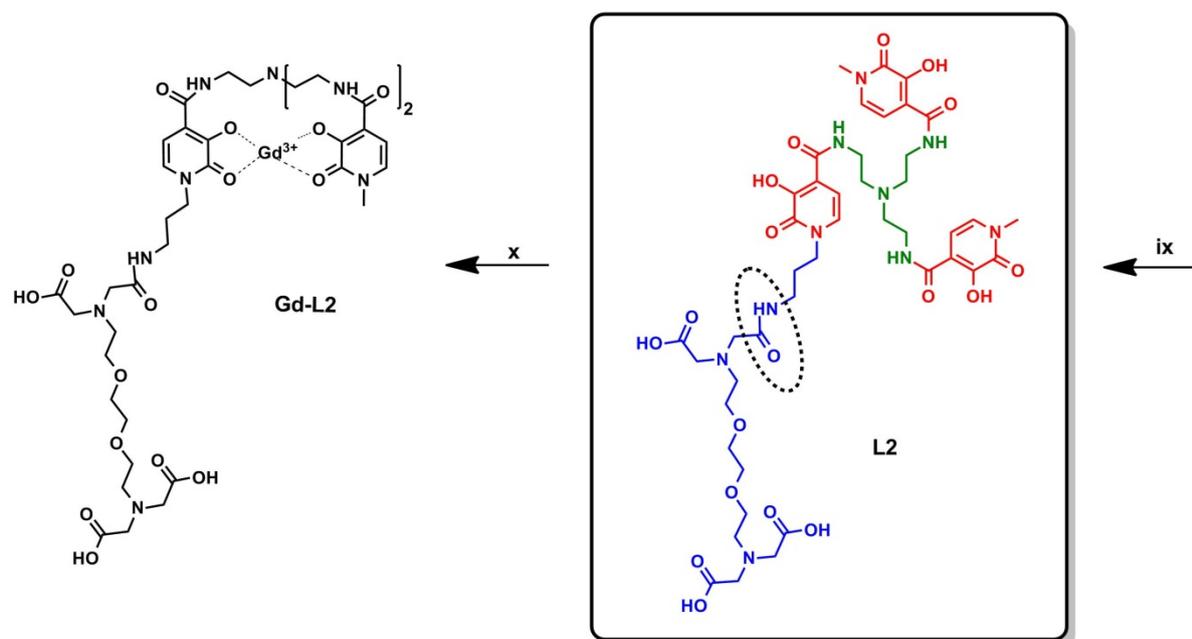
**Figure 39 The final synthesis of L2. In the dotted ellipse the amide connection is marked. Reaction conditions: i) TFA, overnight, r.t, quant.; ii) bromoacetyl bromide, K₂CO₃, 5 h, r.t., 61%; iii) 26, K₂CO₃, overnight, r.t., 53%; iv) NaOH, overnight, reflux, 99%; v) PFP TFA, py, overnight, r.t., b) 12, DIPEA, overnight, r.t., 47%; vi) HCO₂NH₄, Pd/C, overnight, reflux; vii) tert-butyl bromoacetate, K₂CO₃, 4 days, r.t., 56%; viii) TFA, overnight, r.t., quant; ix) NaSEt, 2 h, 140 °C; x) GdCl₃, pH=7, overnight, 40 °C.**

## 2.4 Conclusions

Although the synthesis of both Gd-**L1** and Gd-**L2** appeared to be straightforward, it occurred to be very challenging. Despite the problems faced, I synthesized two HOPO-based CAs containing a chelating moiety designed to detect Ca$^{2+}$. The newly established synthetic route allows an unlimited incorporation of functional moieties into HOPO CAs without the use of expensive and hazardous autoclaves system.

# Chapter 3

# Relaxometric evaluation of ion responsive HOPO SCAs

## 3.1 Targeting Ca$^{2+}$

As mentioned earlier, changes in Ca$^{2+}$ concentration can be used to follow the neural activity in the real time course. Moreover, its concentration in the brain (0.8-1.2 mM)[95] is optimal for detection by magnetic resonance imaging (MRI) which requires milimolar concentrations of a contrast agent (CA) to detect a signal change.

## 3.2 Relaxometric titration of Gd-L1 and Gd-L2 with Ca$^{2+}$

The starting longitudinal relaxivity $r_1$ of Gd-**L1** was found to be 9.4 mM$^{-1}$s$^{-1}$ while Gd-**L2** exhibited a value of 4.8 mM$^{-1}$s$^{-1}$ at 7T magnetic field in solution of HEPES buffer (pH=7.4) at 25 °C. In comparison, the archetype Gd[tren(1-Me-3,2-HOPO)$_3$] shows $r_1$ of 8.8 mM$^{-1}$s$^{-1}$ under the same conditions. In contrast to Gd[tren(1-Me-3,2-HOPO)$_3$], Gd-**L1** and Gd-**L2** contain a Ca$^{2+}$-chelator connected to the HOPO MR-reporter via aliphatic linker (Fig. 18 and 19).

To investigate the sensitivity of Gd-**L1** and Gd-**L2** towards Ca$^{2+}$, I measured the longitudinal relaxation times, $T_1$, of water protons in presence of different Ca$^{2+}$ concentrations. The relaxivity $r_1$ was then calculated using equation (4) (section 1.1). The relaxation curves were prepared by plotting the $r_1$ values as a function of molar ratio of the ion to the contrast agent (Fig. 40 and 41)

After the first addition of 0.5 equivalents of Ca$^{2+}$ to Gd-**L1,** a 16% increase in relaxivity was observed, 10.9 mM$^{-1}$s$^{-1}$ vs. 9.4 mM$^{-1}$s$^{-1}$. However, no further changes in $r_1$ were observed until addition of up to 5 equivalents of Ca$^{2+}$. When 11 equivalents of Ca$^{2+}$ were accumulated a 42% increase was observed as the relaxivity rose to 13.4 mM$^{-1}$s$^{-1}$. The $r_1$ changes reached a plateau at approximately 20 equivalents of Ca$^{2+}$. At this point of the titration curve the $r_1$ exceeded 14 mM$^{-1}$s$^{-1}$, which corresponds to a 60% increase in comparison to the starting value (Fig. 40).
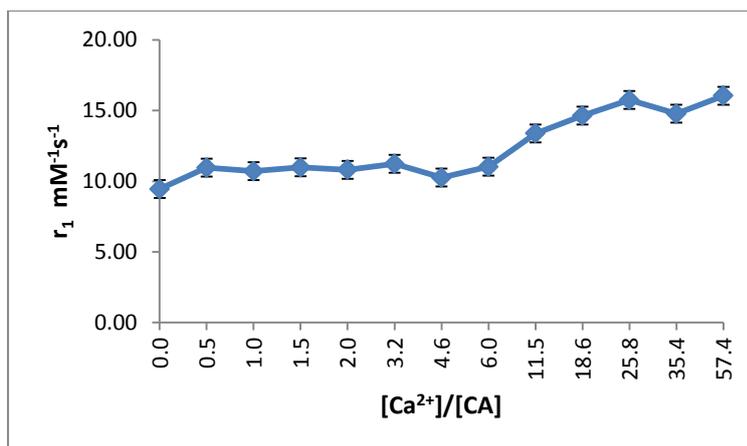
**Figure 40 Relaxometric response of Gd-L1 to increasing concentration of Ca^{2+}. Measurements were performed at pH=7.4 in a 7T NMR spectrometer at 25 °C.**

Similar investigations were performed for Gd-**L2.** Unlike Gd-**L1**, Gd-**L2** showed no significant changes in $r_1$ when 0.5 equivalent of $Ca^{2+}$ was accumulated. The fluctuations presented in Fig. 41 seem to show no pattern until 1 equivalent of $Ca^{2+}$ was amassed.
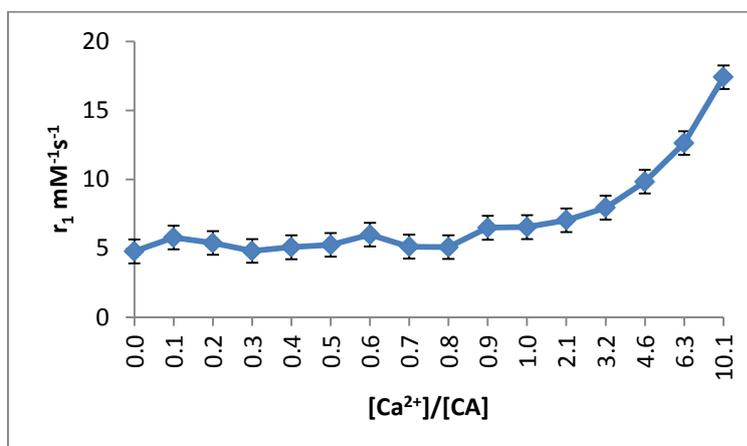


**Figure 41 Relaxometric response of Gd-L2 to increasing concentration of Ca^{2+}. Measurements were performed at pH=7.4 in a 7T NMR spectrometer at 25 °C.**

However, a 47% increase in relaxivity was observed upon addition of 2 equivalents of $Ca^{2+}$, 7.0 $mM^{-1}s^{-1}$ vs. starting 4.8 $mM^{-1}s^{-1}$. The increasing trend was sustained until the end point of titrations at 10 equivalents of $Ca^{2+}$, where $r_1$ equalled 17.4 $mM^{-1}s^{-1}$. This value is 364% higher than the starting relaxivity.

For both Gd-**L1** and Gd-**L2** a significant increase in relaxivity was observed in presence of a large excess of the analysed ion. To confirm those results, $T_1$ weighted images were obtained in a 3T MR scanner[ii] in HEPES buffer (pH=7.4) at 25 °C.

The experiments performed in the MR scanner allowed to exclude the time variable between trials. Hence, it ensured the same starting point in time for all samples in contrary to the measurements carried out at 7T, where every sample had at least a 10 minutes delay in respect to the previous one. This way I could verify if the observed $r_1$ changes are occurring due to increasing concentration of $Ca^{2+}$ or if the agents are changing their properties over time.

The $T_1$ weighted images acquired for Gd-**L1** in presence of varying concentrations of $Ca^{2+}$ are presented in Fig. 42.
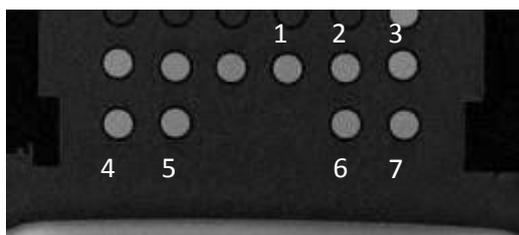


**Figure 42 3T MR images of solutions containing Gd-L1 with different concentrations of $Ca^{2+}$. Numbering of samples is consistent with Table 2. [Gd-L1]=20 µM, HEPES buffer (pH=7.4), 25 °C.**

The longitudinal relaxivity $r_1$ of Gd-**L1** at 3T magnetic field was calculated to be 12.7 $mM^{-1}s^{-1}$. However, no changes in $r_1$ values were observed for any concentration of $Ca^{2+}$ (Table 6). This may potentially originate from the lack of coordination between the metal centre and the $Ca^{2+}$-chelator (Fig. 15). Moreover, absence of any effect of $Ca^{2+}$ concentration on $r_1$ at 3T suggests that the increase in $r_1$ values observed for higher amounts $Ca^{2+}$ at 7T may be due to dissociation of the CA over time and that the presence or amount of additional ion seem not to influence the decomposition of Gd-**L1**.

---

[ii] All phantom experiments in 3T whole body scanner were conducted in collaboration with Dr. Jörn Engelmann, Department of High-Field Magnetic Resonance, MPI for Biological Cybernetics, Tübingen.

| No of sample | $Ca^{2+}$/CA | $T_1$ [ms] | $r_1$ [mM$^{-1}$s$^{-1}$] |
|:---:|:---:|:---:|:---:|
| **1** | 0 | 1390.6 | 12.7 |
| **2** | 1 | 1385.8 | 12.8 |
| **3** | 2 | 1362.9 | 13.4 |
| **4** | 4 | 1376.0 | 13.1 |
| **5** | 10 | 1407.4 | 12.3 |
| **6** | 20 | 1381.8 | 12.9 |
| **7** | 50 | 1406.1 | 12.3 |

An identical experiment was performed for Gd-**L2**, where the starting $r_1$ value was calculated to be 12.4 mM$^{-1}$s$^{-1}$ (Fig. 43).
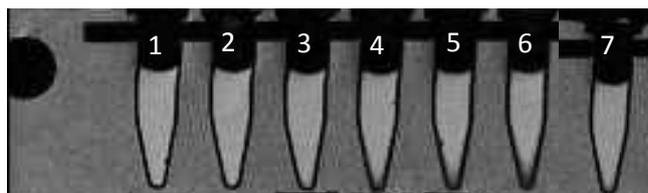


Figure 43 $T_1$ weighted MR images of solutions of Gd-L2 with different concentrations of $Ca^{2+}$. Numbering of samples is consistent with Table 2.

Similarly to Gd-**L1**, also in case of Gd-**L2** no changes in $T_1$ and $r_1$ were observed for solutions containing up to 20 equivalents of $Ca^{2+}$ as summarized in Table 7. The only exception was a decrease of $r_1$ value by 42% to reach 7.3 mM$^{-1}$s$^{-1}$ in solution containing 50 equivalents of $Ca^{2+}$.

Again, the results show no proof for the expected interaction of the $Ca^{2+}$-chelator with the $Gd^{3+}$ (Fig. 15). Additionally, like in the case of Gd-**L1** this demonstrated that the increase of $r_1$ values observed at 7T was rather time dependent, potentially due to the decomposition of Gd-**L2** and not influenced by presence of $Ca^{2+}$.

Table 7 Response of Gd-L2 to different concentrations of Ca$^{2+}$ measured in 3T MRI scanner at 25 °C. [Gd-L2]=10 μM in HEPES buffer at pH=7.4

| No. of sample | Ca$^{2+}$/CA | T$_1$[ms] | r$_1$[mM$^{-1}$s$^{-1}$] |
|---|---|---|---|
| 1 | 0 | 1663.9 | 12.4 |
| 2 | 1 | 1662.4 | 12.4 |
| 3 | 2 | 1670.4 | 12.2 |
| 4 | 4 | 1664.2 | 12.4 |
| 5 | 10 | 1678.0 | 11.9 |
| 6 | 20 | 1712.9 | 10.9 |
| 7 | 50 | 1824.9 | 7.5 |

The results obtained at both magnetic fields, 3T and 7T, were contradictory for large excess of Ca$^{2+}$ (above 4 equivalents). A possible explanation for the observed phenomenon can be potentially related to the kinetic stability of Gd-**L1** and Gd-**L2** in aqueous solutions. Despite the numerous reports in the literature on HOPO-based contrast agents, nothing is known about their kinetic stability. Also the assessment of their stability over time in presence or absence of additional ions was not published. Therefore, to confirm this hypothesis about Gd-**L1** and Gd-**L2**, further experiments determining their kinetic stability should be performed. However, the hypothesis can be justified by the fact that no differences in r$_1$ values were observed between solutions containing 4, 10 and 20 equivalents of Ca$^{2+}$ for the results obtained at 3T and 7T. Those two experiments differ from each other in the starting point of every measurement – in MRI all samples are measured at the same time, while in spectrometer a delay of at least 10 minutes was present between each trial.

While both measurements were performed at two different magnetic fields, it has been shown that both Gd-**L1** and Gd-**L2** do not respond to changing concentrations of Ca$^{2+}$. Increases in longitudinal relaxivity r$_1$ are observed only upon addition of large excess of analysed ion and were confirmed to be time dependent.

The absence of a response of Gd-**L1** to Ca$^{2+}$ may be associated with very weak or none at all interactions of the EGTA moiety responsible for chelating Ca$^{2+}$ and the Gd$^{3+}$ centre of the HOPO MR-reporter. To support this conclusion, the starting value of r$_1$ for Gd-**L1** and the archetype were compared and a difference of

6%, 9.4 mM$^{-1}$s$^{-1}$ vs. 8.8 mM$^{-1}$s$^{-1}$, was observed. The variance in r$_1$ values are within the measurement error and therefore a conclusion may be drawn that the structural modification has no influence on the metal centre of Gd-**L1**.

However such reasoning cannot be applied in case of Gd-**L2**. The starting value of longitudinal relaxivity r$_1$ for Gd-**L2** at 7T was observed to be 4.8 mM$^{-1}$s$^{-1}$ which is approximately 45% lower than the value for the archetype (8.8 mM$^{-1}$s$^{-1}$). This may indicate two things: a) an interaction between the EGTA moiety and the MR-reporter or b) slower water exchange rate k$_{ex}$ due to steric hindrance introduced by the rigid amide link.

The first possibility is ruled out by the T$_1$ weighted images obtained at 3T. The longitudinal relaxivity was determined to be 12.4 mM$^{-1}$s$^{-1}$ which is comparable to the value of Gd-**L1** where no interactions between Ca$^{2+}$-chelator and the MR-reporter were suspected. Therefore, the probable explanation of the differences in longitudinal relaxivity may originate from the disturbed water exchange between the bulk solvent and the water molecules coordinated directly to Gd$^{3+}$. It is known that the amide bond tends to slow down the water exchange rate k$_{ex}$ in comparison to amine or acid. A good example was published by Sherry et al.[109] Additionally, a more rigid structure may influence the rotational correlation time τ$_r$.[25] Therefore, the slower internal motion of the agent in solution influences the relaxivity at 3T in comparison to 7T and hence the increased relaxivity at lower magnetic field.

## 3.3 Zn$^{2+}$ as target

Having observed no response of Gd-**L1** or Gd-**L2** to Ca$^{2+}$, I decided to investigate their sensitivity to another ion. I focused on zinc, because of its abundance in the human body and affinity towards ethylene glycol bis(2-aminoethyl ether)-N,N,N′,N′-tetraacetic acid (EGTA). Zn$^{2+}$ is the most profuse ion in the human blood. Yet, its highest concentrations are present in the brain where it is responsible for modulating receptors and release of transporters.[38] Moreover, it is known that Zn$^{2+}$ binds to EGTA chelator 3 orders of magnitude stronger than Ca$^{2+}$,[110] making zinc a noteworthy target for the two newly developed SCAs.

## 3.4 Relaxometric titrations of Gd-L1 and Gd-L2 with Zn$^{2+}$

To examine the sensitivity of Gd-**L1** and Gd-**L2** to different amounts of Zn$^{2+}$, I measured the longitudinal relaxation times $T_1$ for samples containing 0 to 10 equivalents of Zn$^{2+}$. The longitudinal relaxivity $r_1$ was then calculated using equation (4) (section 1.1). The starting $r_1$ of Gd-**L1** was calculated to be 10.1 mM$^{-1}$s$^{-1}$ at 7T in HEPES buffer (pH=7.4) at 25°C, while the $r_1$ of Gd-**L2** remained at 4.4 mM$^{-1}$s$^{-1}$ in identical conditions. The titration curves were drawn by plotting $r_1$ as a function of molar ratio of Zn$^{2+}$ to CA as presented in figures 44 and 45.

Upon addition of 0.1 equivalent of Zn$^{2+}$ the relaxivity of Gd-**L1** decreased 15% to the value of 8.6 mM$^{-1}$s$^{-1}$. No significant changes were further observed as the curve reached plateau already after addition of 0.3 equivalents of Zn$^{2+}$ with $r_1$ of 8.1 mM$^{-1}$s$^{-1}$, an approximately 20% reduction. The end point $r_1$ equal 8.0 mM$^{-1}$s$^{-1}$ corresponds to a 21% decrease in comparison to the starting value (Fig. 44).
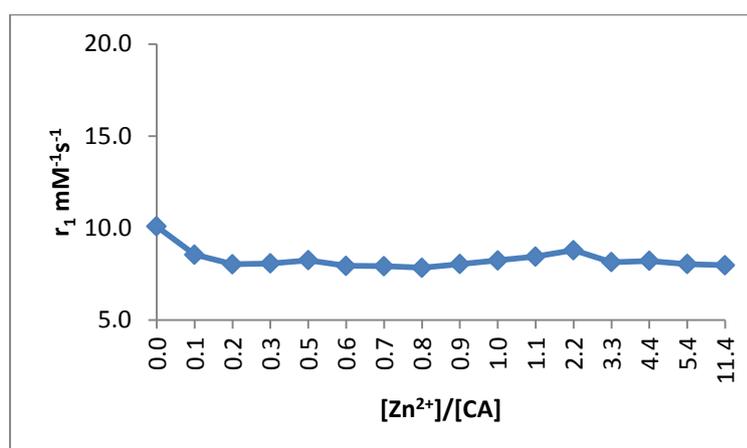


**Figure 44 Relaxometric response of Gd-L1 to increasing concentration of Zn2+. Measurements were performed in HEPES buffer (pH=7.4) at 7T NMR spectrometer at 25 °C.**

A similar experiment was performed for Gd-**L2** in presence of Zn$^{2+}$. A 20% increase in longitudinal relaxivity, $r_1$, from 4.4 to 5.2 mM$^{-1}$s$^{-1}$, was observed upon addition of approximately 0.2 equivalents of Zn$^{2+}$. From this point until 3 equivalents of Zn$^{2+}$ were accumulated, the $r_1$ value oscillated around a value of 5.1 mM$^{-1}$s$^{-1}$. Another increase in relaxivity was observed upon addition of 4.5 equivalents of Zn$^{2+}$. The $r_1$ increased by 50% in comparison to the starting value, 6.6 vs. 4.4 mM$^{-1}$s$^{-1}$,

respectively. The growth continued until the end point of the titration curve, where the relaxivity reached a value of 13.7 mM$^{-1}$s$^{-1}$ at approximately 13 equivalents of Zn$^{2+}$ (Fig. 45).
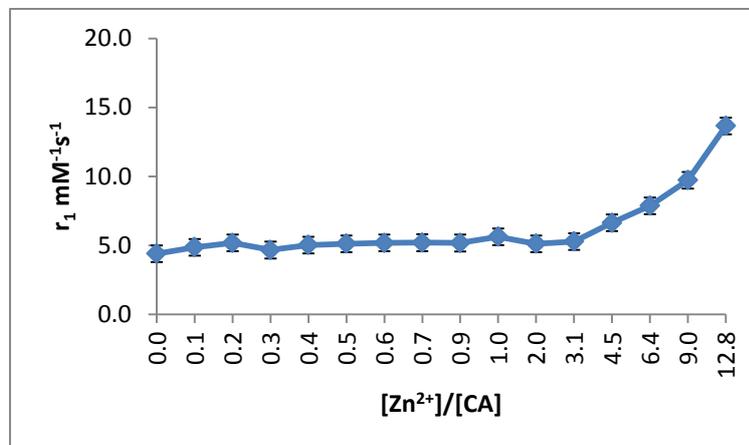


**Figure 45 Relaxometric response of Gd-L2 to increasing concentration of Zn$^{2+}$. Measurements were performed at pH=7.4 at 7T and 25 °C.**

Gd-**L1** and Gd-**L2** gave different response to different amounts of Zn$^{2+}$. While Gd-**L1** showed decrease of longitudinal relaxivity $r_1$ upon addition of small amount of Zn$^{2+}$, Gd-**L2** exhibited an increase in $r_1$ in presence of large excess of ion. To investigate whether the changes in relaxivity in both cases were related to the varying concentrations of Zn$^{2+}$ or if the observed phenomenon has a different origin, phantom measurement at 3T MR scanner were performed. The experiments allowed measurements of multiple samples containing different concentrations of Zn$^{2+}$ starting from the same time point. In comparison, during trials at 7T there was a delay of approximately 10 minutes between every measurement. Therefore, the tests at 3T allowed excluding the time variable.

The T$_1$ weighted MR images of Gd-**L1** in HEPES buffer (pH=7.4) containing different concentrations of Zn$^{2+}$ are presented in Fig 46.
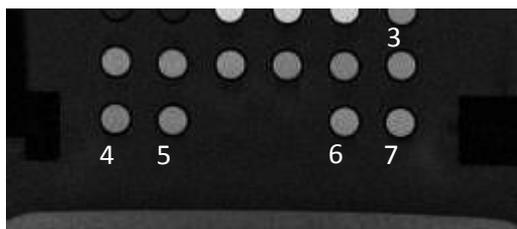
**Figure 46 T$_1$ weighted MR images obtained at 3T MR scanner. Measurements were performed at 25 °C in HEPES buffer at pH=7.4. [Gd-L1]=20 µM. Tubes are numbered according to Table 3.**

The starting longitudinal relaxivity of Gd-**L1** was found to be 10.8 mM$^{-1}$s$^{-1}$. Yet, no changes in relaxivity values were observed in solutions containing equimolar amount up to 4 equivalents of Zn$^{2+}$ in comparison to the sample with pure Gd-**L1** (Table 8). However, a 20% increase, up to 12.9 mM$^{-1}$s$^{-1}$, in longitudinal relaxivity was observed in samples containing 10 equivalents of Zn$^{2+}$. The values increased up to 13.9 mM$^{-1}$s$^{-1}$, which corresponds to a 29% increase, in presence of 20 and 50 equivalents of Zn$^{2+}$.

**Table 8 Longitudinal relaxation times T$_1$ and calculated longitudinal relaxivity values r$_1$ of Gd-L1 measured at 3T in presence and absence of Zn$^{2+}$. [Gd-L1]=20 µM in HEPES buffer, pH=7.4, 25 °C**

| No. of sample | Zn$^{2+}$/CA | T$_1$ [ms] | r$_1$[mM$^{-1}$s$^{-1}$] |
|---|---|---|---|
| **1** | 0 | 1469.8 | 10.8 |
| **2** | 1 | 1456.7 | 11.1 |
| **3** | 2 | 1429.1 | 11.8 |
| **4** | 4 | 1425.4 | 11.9 |
| **5** | 10 | 1381.2 | 12.9 |
| **6** | 20 | 1345.7 | 13.9 |
| **7** | 50 | 1346.2 | 13.9 |

A similar experiment was performed for Gd-**L2**. T$_1$ weighted images at 3T magnetic field were obtained of the agents' solutions in HEPES buffer (pH=7.4) containing different concentrations of Zn$^{2+}$ (Fig. 47).
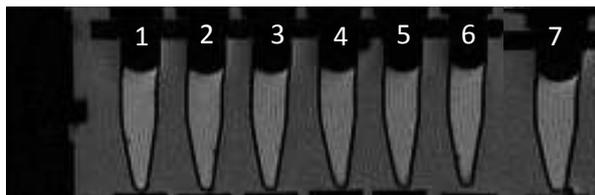
**Figure 47 T1 weighted images obtained at 3T MR scanner. Tubes contain from 0 to 50 equivalents of Zn²⁺ according to Table 4. Measurements were performed in 3T MRI whole body scanner at 25 °C. [Gd-L2]=10 µM in HEPES buffer at pH=7.4**

The starting longitudinal relaxivity $r_1$ was calculated to be 11.7 $mM^{-1}s^{-1}$. Yet, no contrast changes in the images were observed but data summarized in Table 9, show that $r_1$ values were oscillating around 10 $mM^{-1}s^{-1}$. However no significant pattern could be detected.

**Table 9 Longitudinal relaxation times $T_1$ and longitudinal relaxivity $r_1$ values obtained for Gd-L2 in presence of variable concentrations of Zn²⁺ at 3T MRI scanner at 25 °C. [Gd-L2]=10µM in HEPES buffer at pH=7.4**

| No. of sample | [Zn²⁺]/[CA] | $T_1$ [ms] | $r_1$ [$mM^{-1}s^{-1}$] |
|---|---|---|---|
| 1 | 0 | 1685.7 | 11.7 |
| 2 | 1 | 1778.6 | 8.8 |
| 3 | 2 | 1683.6 | 11.7 |
| 4 | 4 | 1792.2 | 8.4 |
| 5 | 10 | 1821.5 | 7.6 |
| 6 | 20 | 1772.5 | 9.0 |
| 7 | 50 | 1839.5 | 7.1 |

In summary, longitudinal relaxation time $T_1$ measurements at 7T and 3T magnetic fields gave contradictory results for Gd-**L1** and Gd-**L2** in presence of Zn²⁺. In case of Gd-**L1** a 20% decrease in $r_1$ at 7T was observed for 0.1 equivalent of Zn²⁺ but no such behaviour was detected for the 3 T field. Gd-**L2** exhibited at 7T a substantial increase upon addition of approximately 5 equivalents of Zn²⁺, yet at 3T only random fluctuations of the longitudinal relaxivity $r_1$ were detected. The variations in behaviour may be attributed to the decomposition of the agents with time. As mentioned in section 3.2, there are no available data in respect to the kinetic stability

of the HOPO-based non-responsive agents over time (neither in presence nor in absence of additional ions). Therefore, further experiments to determine the kinetic stability should be conducted.

No response to changing concentrations of $Zn^{2+}$ was observed for both probes, Gd-**L1** and Gd-**L2** due to lack or very weak interactions between the $Ca^{2+}$-chelator and the HOPO MR-moiety. As mentioned in section 3.2 differences in $r_1$ between probes at 7T may be potentially based on the alterations in the structure.

An amide bond is known to decrease the water exchange rate in comparison to an amine or carboxyl group.[109] This may be a possible explanation of the lower $r_1$ value of Gd-**L2** at 7T. Additionally, the same rigid amide bond may be a potential cause to slow down the tumbling rate of the agent in solution and, hence, the increased $r_1$ at lower magnetic field.[25]

## 3.4 Conclusions

Two CAs designed to detect changes in $Ca^{2+}$ concentrations were evaluated in respect to their performance in presence of $Ca^{2+}$ and $Zn^{2+}$. The presented results for Gd-**L1** and Gd-**L2**, obtained at a 7T NMR spectrometer and at a 3T MRI whole body scanner are in conflict with each other for both probes. At a magnetic field of 7T an increase in the longitudinal relaxivity $r_1$ of both Gd-**L1** and Gd-**L2** was observed in excess of $Ca^{2+}$. Yet, no changes in respect to increasing $Ca^{2+}$ concentrations were observed in $T_1$ weighted images obtained at 3T. Noteworthy, the $r_1$ changes are observed during experiments with a time delay between the single measurements and no differences are detected when all samples are measured at once. Therefore, whatever changes in the $r_1$ values were observed at 7T may be potentially attributed to the decomposition of the Gd-**L1** and Gd-**L2** over time. Whether the hypothetical decomposition of probes is induced by presence of ions needs to be investigated.

However, while the same pattern is observed for Gd-**L2** at 7T in presence of $Zn^{2+}$, Gd-**L1** behaved opposite in identical conditions. An $r_1$ decrease upon addition of 0.1 equivalent of $Zn^{2+}$, present at 7T was not detected at the lower magnetic field. This phenomenon may be potentially connected with the observed precipitate

forming after adding the first portion of $Zn^{2+}$. Still, further studies to confirm that relation need to be implemented.

The lack of response to both investigated ions in case of Gd-**L1** may be attributed to the fact that the $Ca^{2+}$-chelator does not interact or interacts very weakly with the $Gd^{3+}$ in the HOPO cavity. The initial longitudinal relaxivity $r_1$ value of 9.4 $mM^{-1}s^{-1}$, very similar to the obtained for the archetype of HOPO agents, 8.8 $mM^{-1}s^{-1}$, may support this conclusion.

Yet, this hypothesis cannot be applied in case of Gd-**L2**, as this SCA shows a starting relaxivity of 4.7 $mM^{-1}s^{-1}$ which is almost half lower than the parent HOPO CA. Considering the obtained starting $r_1$ and introduced structural modification in form of an amide bond, two explanations for the behaviour of Gd-**L2** in solution are possible. Firstly, a coordination of $Ca^{2+}$-chelator to the $Gd^{3+}$-centre of the MR-reporter may occur and a decrease in hydration number q would be observed. CAs exhibiting $r_1$ of         4 $mM^{-1}s^{-1}$ due to q=1 are reported, e.g. Gd-DOTA.[2] However, this reasoning was not sustained by the MR measurements at lower magnetic field. Therefore, a second option connected with the presence of the rigid amide bond was considered. It was reported that an amide bond, being more rigid in comparison to an acid or amine group, has an impact on the $r_1$ of a CA at both low and high magnetic fields. At higher magnetic fields, above 100 MHz, the water exchange rate $k_{ex}$ plays a significant role in modulating longitudinal relaxivity $r_1$.[6] An introduction of the amide bond into a CA slows down the $k_{ex}$ and leads to a decrease of the $r_1$.[109] However, at lower magnetic fields an important parameter influencing $r_1$ is rotational correlation time $\tau_r$.[111] It is known that rigid amide bond slows down the tumbling of a CA in solution.[25] A feature not presented by linkage containing a flexible amine group. The combined arguments present a potential explanation how the amide connection between the EGTA-moiety and the HOPO MR-reporter may be manipulating behaviour of Gd-**L2** at two different magnetic fields.

# Chapter 4

# Towards targeted HOPO CAs

## 4.1 Aim of the project

Published reports in the topic of potentially targeting HOPO-based CAs required sophisticated bioengineering performed on virus capsids.[89,90] The detailed description of the published results was presented in section 1.4.4.2. Yet, even a very specific target can be reached by a small targeting vector.

Therefore, the aim of this project was to establish a novel synthetic route towards targeted HOPO-based CAs. I decided to modify the scaffold itself this time instead of one of the HOPO rings. The new scaffold should contain of four arms, three of which would be designated to hold HOPO rings. The fourth arm, not necessarily symmetrical with the other three, would provide an additional binding site to introduce a targeting vector (Fig. 48). Such approach would allow a) further modifications and b) to by-pass the demanding synthesis of an asymmetric HOPO CA.

## 4.2 Synthesis of the new agents

The intended modifications to the scaffold in comparison with the archetype tren(1-Me-3,2-HOPO)$_3$ are presented in Fig. 48.

The detailed synthesis of the HOPO acid **9** was described in section 2.3.1. A suitable scaffold was published by Zhao *et al.*[112] The reported method featured an efficient two-step synthesis. Moreover, it permitted co-existence of NO$_2$ and NH$_2$ groups, which greatly simplified the selective protection of the primary amines.
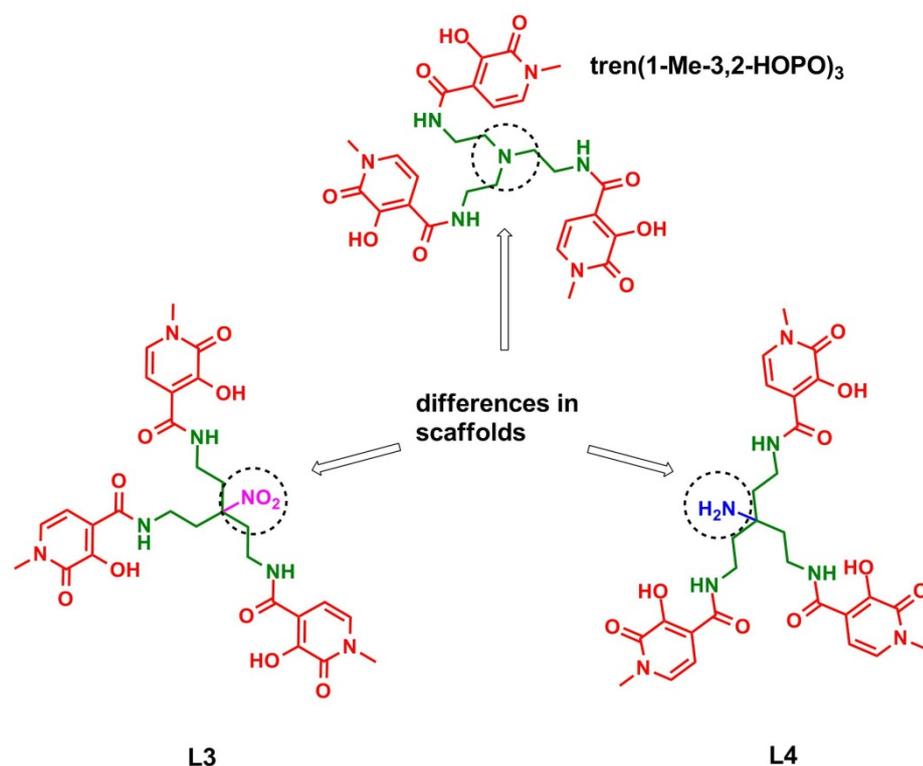


**Figure 48 Comparison of novel synthesized ligands L3 and L4 with the HOPO archetype.**

Therefore, I prepared the scaffold containing a NO$_2$ group according to the procedure of Zhao. The key steps in the preparation of amine **53** involve formation of a triple acyl chloride from carboxylic acid followed by triple Curtius rearrangement. Attachment of **9** gave **51** in 45% yield (Fig. 49). The next step involving reduction of the nitro group to an amine, did not give the desired product **56** neither at 3.5 bars of H$_2$ pressure and 80 °C nor at 10 bars of H$_2$ pressure at the same temperature. This occurred probably due to the steric hindrance of the reacting nitro group created by

the pyridinone rings, which obstructed access of the molecule to the catalysts' surface.
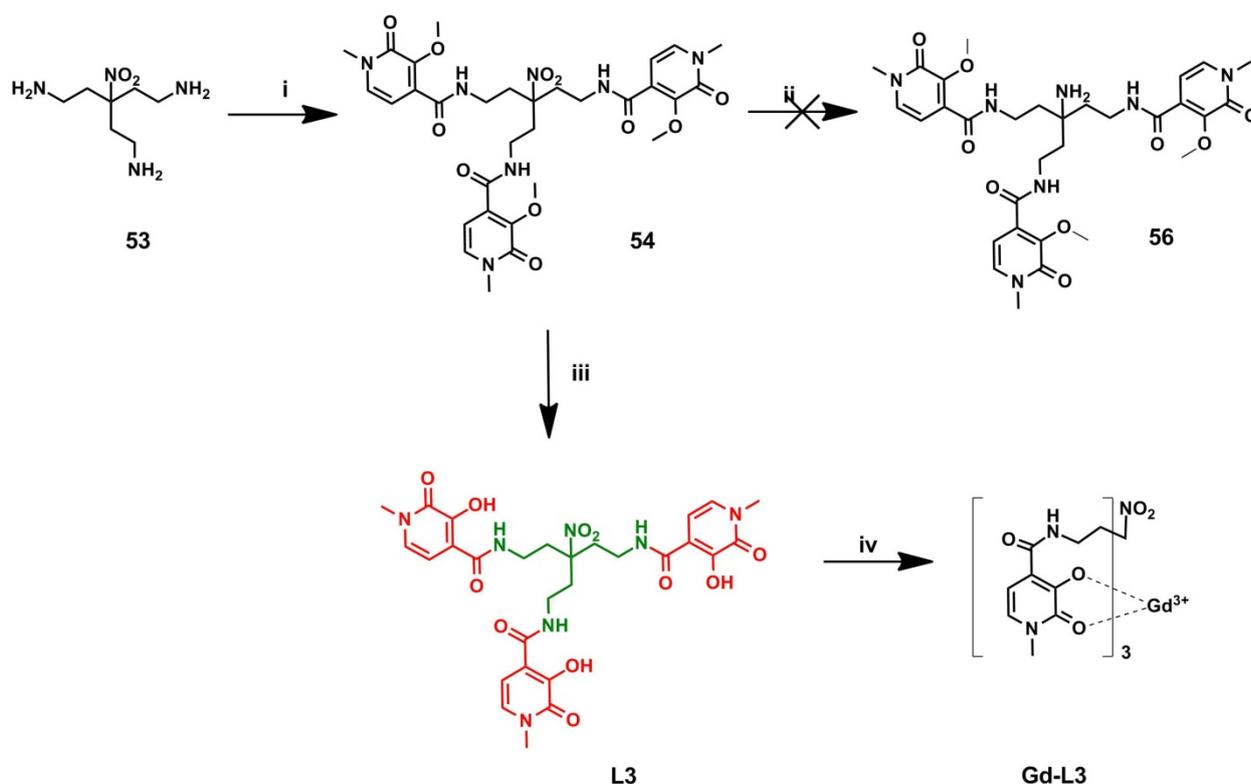


**Figure 49 Synthetic scheme to obtain ligand L3. Reaction conditions: i) a) 7, PFP TFA, Py, overnight, r.t., b) DIPEA, overnight, r.t, 45 %; ii) Ra-Ni, 3.5 or 10 bar $H_2$, 80 °C; iii) NaSEt, 2 h, 140 °C, 54%; iv) $GdCl_3$, pH=7, overnight, 40 °C.**

Methyl groups were cleaved from compound **51** with NaSEt to give the final ligand **L3**. No NMR or mass spectra could be obtained for this molecule due to its very limited solubility in solvents generally used for HOPO-based ligands, e.g methanol, DMSO and water.

This phenomenon is widely occurring in nature and its most extreme example is the family of pteridines.[113] These heterocycles, containing fused rings of pyrimidine and pyrazine, are known to decrease their solubility upon introduction of hydroxyl groups into their structure. This occurrence is taking place due to formation of multiple intermolecular hydrogen bonds.[114] Nevertheless, **L3** was submitted for complexation with $GdCl_3$ to give Gd-**L3** (Fig. 49).

The problem of reduction of the $NO_2$ group to $NH_2$ was easily overcome by switching the order of steps. In the new pathway the obtained three amine groups were protected with Boc to give compound **52** and then the $NO_2$ group was successfully reduced to amine using Raney-Nickel and low pressure of hydrogen.[112] Protection of the free amine group with CbzCl gave the carbamate **53** in almost quantitative yield (Fig. 50).
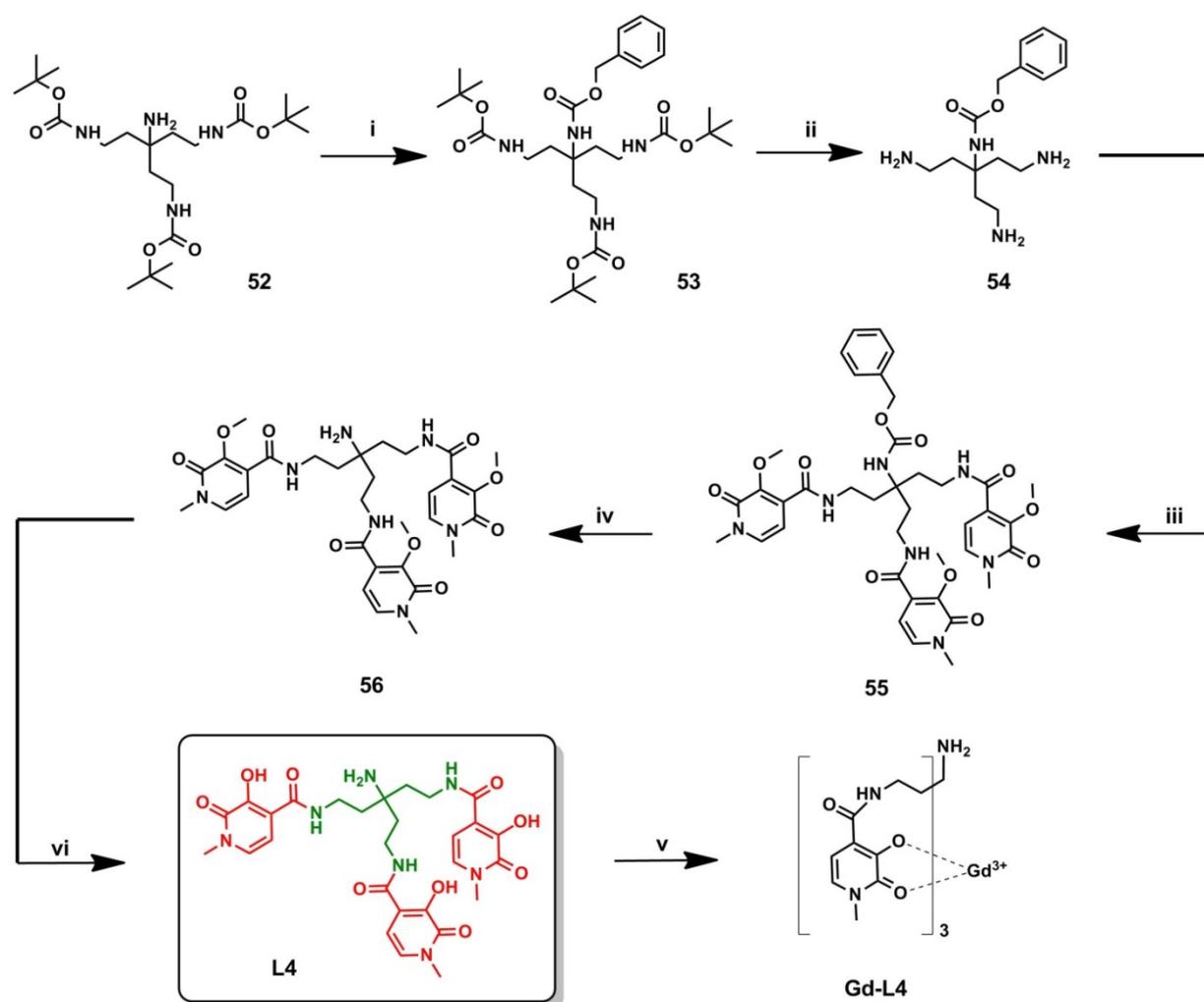


**Figure 50 Synthesis of Gd-L4. Reaction conditions: i) CbzCl, NaHCO₃, overnight, r.t., 99%; ii) TFA, 72 h, r.t., quant.; iii) a) 7, Py, PFP TFA, overnight, r.t., b) DIPEA, overnight, r.t, 20%; iv) HCO₂NH₄, Pd/C, overnight, 60 °C, quant.; v) NaSEt, 2 h, 140 °C, 58%; vi) GdCl₃, pH=7, overnight, 40 °C.**

Subsequent cleavage of the Boc groups and the following coupling with acid **9** gave **55** in 20% yield. The Cbz group was quantitatively removed with ammonium formate. The following cleavage of the methyl groups protecting the phenols with NaSEt gave the crude ligand, which was purified by HPLC. Due to poor solubility of **L4** both in

DMSO and methanol, the obtained $^1$H NMR spectrum was not conclusive. The residual peaks of solvents were overlapping with signals from the scaffold making any reliable integration impossible. Only $^{13}$C NMR spectrum provided reliable information about the structure of **L4** and is reported in Chapter 6. The final ligand **L4** was submitted for complexation with GdCl$_3$ to give Gd-**L4** (Fig. 50).

## 4.3 Purity determination[iii]

The purity determination is a necessary measurement before attempting to define the thermodynamic stability of Gd-**L3** and Gd-**L4**. Additionally, purity of tren(1-Me-3,2-HOPO)$_3$ and a commercial DTPA-BMA was also determined. All four ligands will be later utilized in experiments leading to determination of thermodynamic stability of the novel agents.

The purity measurements were performed according to a method published by Berge *et al.*[115] Firstly, a calibration curve was constructed from the measured absorption spectra of xylenol orange solution containing known amounts of free Gd$^{3+}$ in acetate buffer. The absorption spectrum of xylenol orange in acetate buffer shows two absorbance maxima at 433 and 563 nm (Fig 51).

The absorbance ratio of those two peaks is known to be linearly dependent on the amount of free Gd$^{3+}$,[115] e.g. an increase in Gd$^{3+}$ concentration causes a decrease of the band intensity at 433 nm and a consequent increase of the band at 563 nm. Exactly this behaviour is presented in Fig. 51. A calibration curve based on this dependence is presented in Fig. 52.
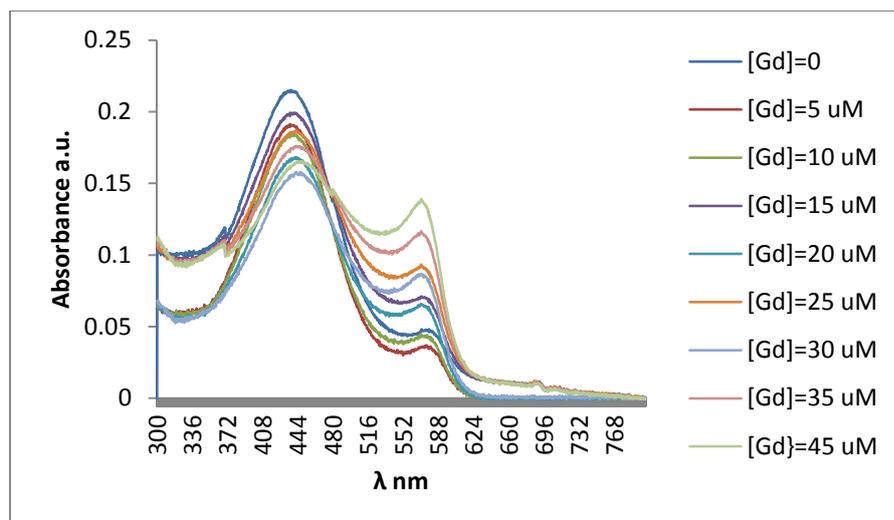
**Figure 51 UV-VIS absorbance spectrum of xylenol orange in acetate buffer (pH=5.8) in presence of different concentrations of free Gd$^{3+}$. Measurements were performed at 25 °C**
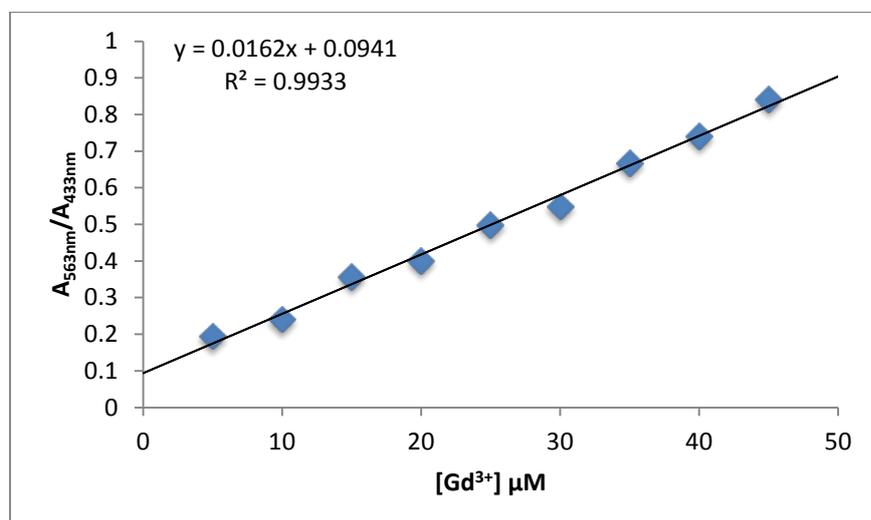


**Figure 52 Calibration curve used to determine the purity of investigated ligands. Additionally the fitting curve equation and the linear relationship are presented in the inset.**

Secondly, complexes of both ligands with Gd$^{3+}$ were prepared in an assumed 1:1 stoichiometric ratio of both reagents according to a published procedure.[102] The UV-VIS absorption spectra of their mixtures with xylenol orange and acetate buffer in range of 300 to 800 nm were recorded and the ratios of absorbance maxima were calculated. The amount of free Gd$^{3+}$ was determined based on the above described calibration curve and summarized in Table 10.

Knowing the amount of unreacted Gd$^{3+}$ in an analysed sample, and assuming that the complexes were formed in 100% yield, the amount of complexed metal can

be determined. From here amount of reacted ligands can be verified and the purity of the ligands calculated. As summarized in Table 11, purity of all ligands exceeded 95%.

**Table 10 Spectrophotometric data obtained during purity determination of L3 and L4 with calculated amount of free Gd$^{3+}$. Absorption spectra were recorded in acetate buffer (pH=5.8) at 25 °C.**

|  | 433nm | 565 nm | ratio | [Gd]$_{free}$ [µM] |
|---|---|---|---|---|
| **L3** | 0.1958 | 0.0381 | 0.19 | |
| | 0.1945 | 0.0312 | 0.16 | |
| | 0.1940 | 0.0386 | 0.20 | |
| | | average | **0.18** | 5.6 |
| **L4** | 0.1766 | 0.0610 | 0.35 | |
| | 0.1987 | 0.0758 | 0.38 | |
| | 0.1997 | 0.0759 | 0.38 | |
| | | average | **0.37** | 17.0 |
| **tren(1-Me-3,2-HOPO)$_3$** | 0.1852 | 0.0501 | 0.27 | |
| | 0.2088 | 0.0692 | 0.33 | |
| | 0.2098 | 0.0656 | 0.31 | |
| | | average | **0.30** | 13.0 |
| **DTPA-BMA** | 0.2230 | 0.0532 | 0.24 | |
| | 0.1971 | 0.0314 | 0.16 | |
| | 0.2019 | 0.0326 | 0.16 | |
| | | average | **0.19** | 5.7 |

**Table 11 Determined purity for three HOPO-based ligands and a commercial DTPA-BMA**

| Ligand | [Gd]$_{free}$ [µM] | Total vol [µL] | $n_{Gdfree}$ in total vol | $n_{Gdtotal}$ | $n_{GdL}$ | purity [%] |
|---|---|---|---|---|---|---|
| L3 | 5.6 | 810 | 2.26E-08 | 1.40E-06 | 1.38E-06 | 98.4 |
| L4 | 17.0 | 810 | 6.34E-08 | 1.47E-06 | 1.41E-06 | 95.3 |
| tren(1-Me-3,2-HOPO)$_3$ | 13.0 | 1000 | 6.51E-08 | 1.50E-06 | 1.43E-06 | 95.7 |
| DTPA-BMA | 5.7 | 810 | 2.31E-08 | 2.37E-06 | 2.35E-06 | 99.0 |

## 4.4 Relaxivity and solubility

Since the longitudinal relaxivity $r_1$ is one of the main characteristics for a $T_1$ CA it was also the first determined value in case of the novel HOPO CAs with the modified scaffold. Complexes of **L3** and **L4** with $Gd^{3+}$ were prepared according to published procedure.[102] During complexation **L3** gave a clear solution at 5 mM concentration in water suggesting that the Gd-**L3** may also exhibit improved solubility. Bulk magnetic susceptibility (BMS) measurements, confirmed by ICP-MS, showed that Gd-**L3** is almost 7 times better soluble than the parent (Gd{tren(1-Me-3,2-HOPO)$_3$}) (Fig. 48), 0.68 mM vs. 0.1 mM. Also Gd-**L4** exhibited better solubility, 0.36 mM, in comparison to the archetype. The longitudinal relaxation times $T_1$ were measured at 7T and 25 °C and longitudinal relaxivities $r_1$ were calculated for both complexes. Gd-**L3** containing the scaffold with the $NO_2$ group showed $r_1=8.5$ mM$^{-1}$s$^{-1}$ while the Gd-**L4** containing the scaffold with free primary amine exhibited $r_1=5.5$ mM$^{-1}$s$^{-1}$.

## 4.5 Thermodynamic stability[iv]

Thermodynamic stability is one of the most important requirements that a potential contrast agent has to fulfil. The original HOPO family is known for the high thermodynamic stability of its members.[6] Yet, the novel scaffold may potentially jeopardize this favourable feature. Therefore, to ensure that the novel CAs are still safe, the thermodynamic stability of Gd-**L3**, Gd-**L4** and Gd{tren(1-Me-3,2-HOPO)$_3$} as a reference compound was determined via spectrophotometric methods as published by Raymond *et al*.[83] A series of solutions was prepared containing one of HOPO-based ligands, $Gd^{3+}$ and varying concentration of DTPA-BMA as a competing ligand. A 0.1 M solution of NaCl maintained the constant ionic strength. After equilibrating the reaction mixtures overnight at 40 °C, absorption spectra in the range of 240 nm to 600 nm were obtained. An absorbance maximum was observed at 330 nm which is specific for the free **L3**, **L4** or tren(1-Me-3,2-HOPO)$_3$. The increasing

---

amount of DTPA-BMA allowed release of the novel ligands and, hence, increase in absorbance at 330 nm (Fig. 53).

Having measured absorbance, concentrations of free ligands and their complexes with $Gd^{3+}$ can be calculated for wavelengths 335-365 nm using equations 9-14.

$$A_{tot} = A_{GdL} + A_L + A_{GdC} + A_C + A_{Gd} \qquad (9)$$

Where

A $_{tot}$ – total observed absorbance

A $_{GdL}$ – absorbance of Gd-HOPO

A $_L$ – absorbance of HOPO

A $_{GdC}$ – absorbance of Gd-DTPA-BMA

A $_C$ – absorbance of DTPA-BMA

If:

$A_{GdC} \rightarrow 0$

$A_C \rightarrow 0$

$A_{Gd} \rightarrow 0$

Then:

$$A_{tot} = \varepsilon_{GdL} c_{GdL} + \varepsilon_L c_L$$
$$(10)$$

Where

$\varepsilon_{GdL}$ - molar absorptivity of Gd-HOPO

$c_{GdL}$ – concentration of Gd-HOPO

$\varepsilon_L$ - molar absorptivity of HOPO

$c_L$ – concentration of HOPO
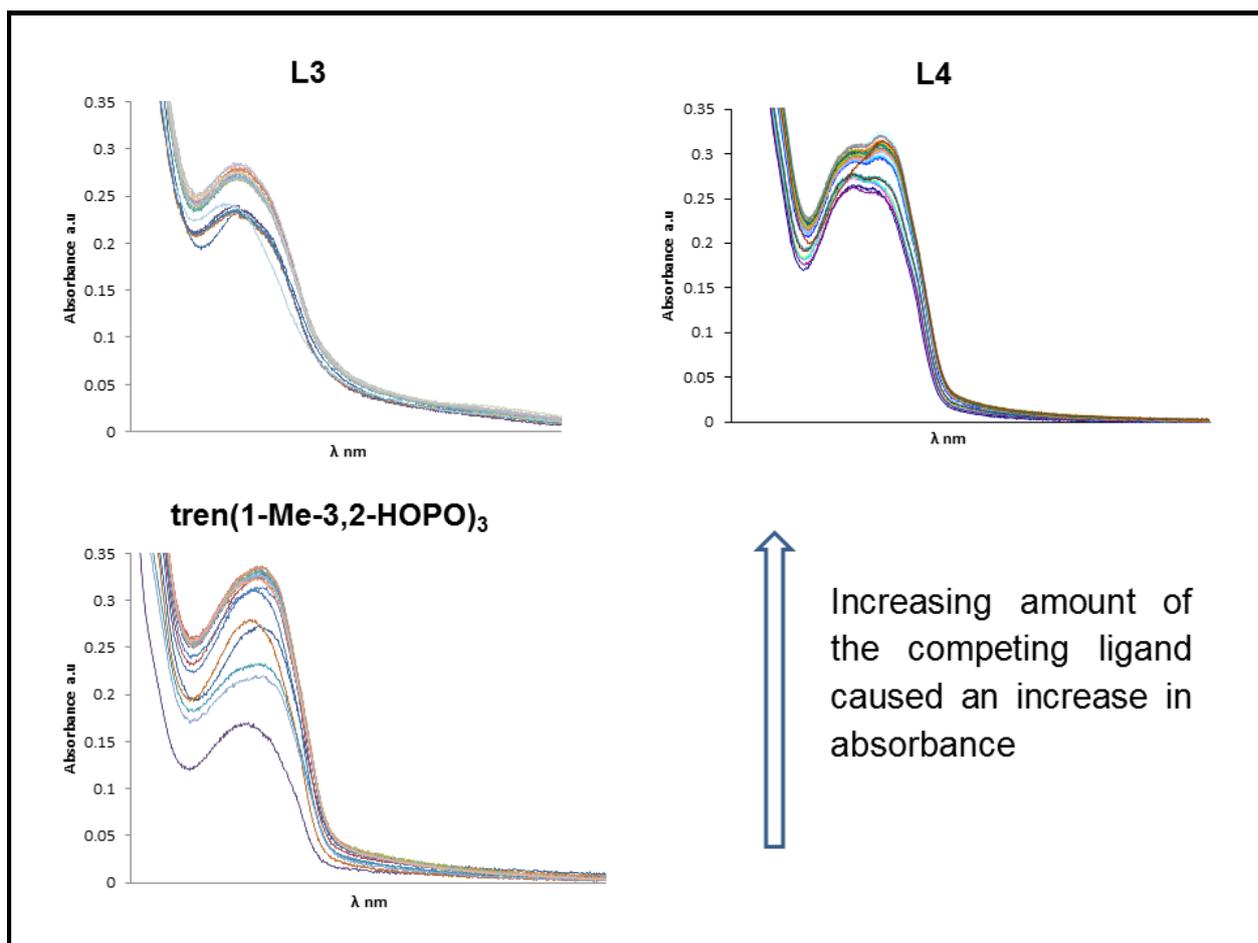
**Figure 53 Absorption spectra recorded for series of solutions used for determination of thermodynamic stability.**

Transforming eq. 10 allows calculation of $c_{GdL}$

$$c_{GdL} = \frac{A_{tot} - \varepsilon_L c_L}{\varepsilon_{GdL} - \varepsilon_L} \tag{11}$$

Knowing the $c_{GdL}$, concentrations of Gd-DTPA-BMA and free HOPO were calculated:

$$c_L = c_{L_{tot}} - c_{GdL} \tag{12}$$

$$c_{GdC} = c_{Gd_{tot}} - c_{GdL} \tag{13}$$

$$c_C = c_{C_{tot}} - c_{GdC} \tag{14}$$

The x intercept of the plot of $\log\frac{c_{GdC}}{c_{GdL}}$ as a function of $\log\frac{c_C}{c_L}$ gives the ΔpGd value which is defined by eq. 15

$$\Delta pGd = pGd_{GdL} - pGd_{GdC} \tag{15}$$

Where

pGd$_{GdC}$ - stability of Gd-DTPA-BMA

pGd$_{GdL}$ - stability of analyzed complex.

As shown in Fig. 53 all three HOPO-based ligands, **L3**, **L4** and tren(1-Me-3,2-HOPO)$_3$ show comparable behavior in presence of competing DTPA-BMA. Therefore it may imply that stabilities of Gd-**L3** and Gd-**L4** are comparable with the stability of Gd{tren(1-Me-3,2-HOPO)$_3$}(H$_2$O)$_2$ (Fig. 48).[96]

## 4.6 Conclusions

Two new HOPO-based contrast agents, Gd-**L3** and Gd-**L4**, were successfully synthesized. Their relaxivity, solubility and purity were determined.

The longitudinal relaxivity r$_1$ of both Gd-**L3** and Gd-**L4** was calculated based on measured longitudinal relaxation times T$_1$ and occurs to be slightly below the values observed for main branch of HOPO CAs, 8.5 mM$^{-1}$s$^{-1}$ and 5.5 mM$^{-1}$s$^{-1}$ vs. 8.8 mM$^{-1}$s$^{-1}$ for the original HOPO agent, respectively. Bulk magnetic susceptibility (BMS) and inductively coupled plasma mass spectrometry (ICP-MS) showed that both of the complexes are 4 to 6 times more soluble in water in comparison to Gd[tren(1-Me-3,2-HOPO)$_3$].[67,81]

The purity of all analysed ligands exceeded 95%. The preliminary spectrophotometric studies show similar behaviour of Gd-**L3** and Gd-**L4** in presence of DTPA-BMA in comparison to the archetype of the HOPO family. This may potentially imply comparable thermodynamic stability. The obtained UV-VIS absorption spectra for the Gd-**L3** and Gd-**L4** show identical absorbance maximum at

300 nm as the well identified archetype Gd[tren(1-Me-3,2-HOPO)$_3$]. This confirms the existence and similar coordination behaviour of ligands **L3** and **L4**.

Observed difficulties in hydrogenation of the NO$_2$ group in presence of HOPO rings may imply further problems with attachment to any biological target. Biomolecules have fixed and rigid structures to ensure selectivity for a particular target or receptor and HOPO rings present a significant steric hindrance. Therefore, to overcome potential problems with coupling to any targeting vector a flexible linker should be introduced.

The amount of potential applications of novel HOPO-based agents with a new scaffold is enormous. Hypothetical attachment to a dendrimer would create a perfect blood pool agent.[116] Coupling of folic acid to the novel CA would allow tumour detection.[117] Novel medical materials for chemodialysis could also be obtained.[118] All those possibilities are now open for investigation thanks to the facile synthesis presented in this chapter.

# Chapter 5

# Final conclusions and outlook

## 5.1 Conclusions

The research described in this thesis was divided into three parts.

The first part focused on synthesis of two novel CAs based on 3,2-HOPO that are capable to detect changes in concentrations of ions during brain activity. Two "smart" probes, Gd-**L1** and Gd-**L2** (Fig. 54), were synthesized using a novel synthetic route established from the very beginning without using autoclaves or toxic and corrosive gases.
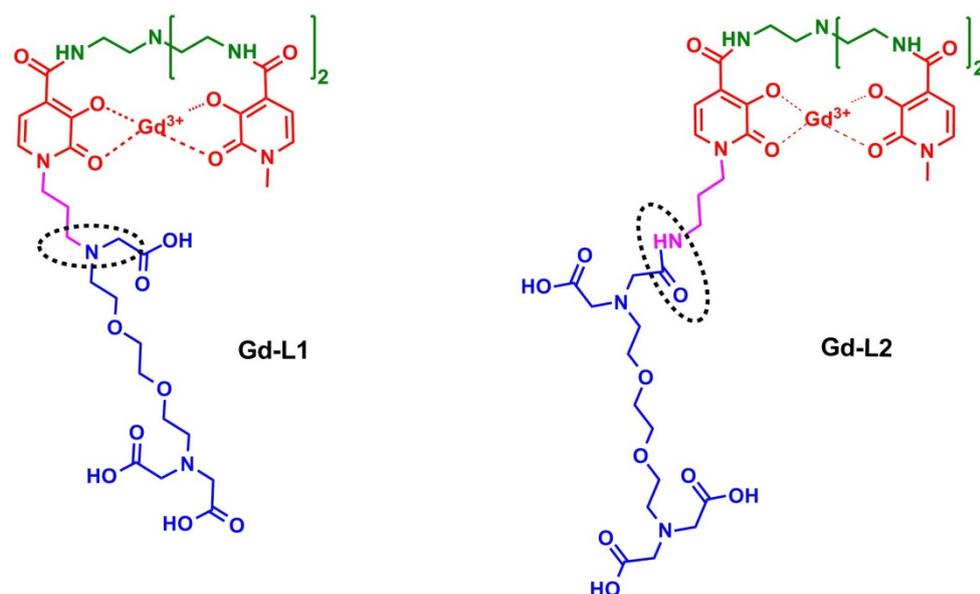


**Figure 54 HOPO-based CAs modified with a Ca²⁺-chelator. Specific building blocks are marked in different colours: scaffold (green), 3,2-HOPO chelating Gd³⁺ (red), linker (pink) and Ca²⁺-chelator (blue)**

Additionally, the exact copy of the first 3,2-HOPO CA, Gd[tren(1-Me-3,2-HOPO)$_3$] (Fig. 55), was synthesized using the newly established route. This compound allowed comparison of relaxivity values with the responsive probes at 300 MHz magnetic field as no such data was published.
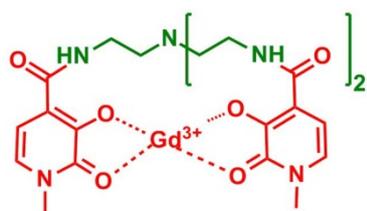
Gd[tren(1-Me-3,2-HOPO)₃]

**Figure 55 The archetype of HOPO-family. Building blocks are in colours: 3,2-HOPO chelating Gd$^{3+}$ (red) and scaffold (green)**

The second part discussed the response of both Gd-**L1** and Gd-**L2** to Ca$^{2+}$ and Zn$^{2+}$. None of the compounds showed relaxivity changes in presence of any of the investigated ions. The lack of response may be attributed to the fact that the coordination between the Gd$^{3+}$ centre and the calcium chelator is very weak or does not occur at all.

The third part concentrated on synthesis of 3,2-HOPO based CAs containing a new type of scaffold. Two molecules, Gd-**L3** and Gd-**L4** (Fig. 56), were obtained.
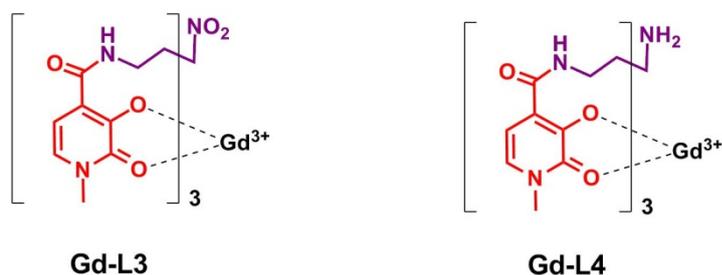


**Figure 56 Two new 3,2-HOPO (red) agents bearing a novel scaffold (violet)**

Their relaxometric and spectrophotometric characteristics were examined. The relaxivity values were lower in comparison to the original HOPO CA. BMS and ICP-MS measurements showed that the solubility of both agents exceeds that of the archetype. Spectrophotometric measurements show similar behaviour of Gd-**L3** and Gd-**L4** in presence of DTPA-BMA in comparison to the archetype of the HOPO family Gd[tren(1-Me-3,2-HOPO)₃][96] (Fig. 53), implicating similar thermodynamic stability.

## 5.2 Outlook

Further research can potentially focus on two directions: a) physico-chemical investigations of already prepared agents and b) introduction of further structural modifications.

In addition, the number of water molecules coordinated to the $Gd^{3+}$ centre, q, along with water exchange rate $k_{ex}$ and rotational correlation time $\tau_r$ of Gd-**L1** and Gd-**L2** should be measured to explain the differences in starting $r_1$ values. The same parameters should be determined for Gd-**L3** and Gd-**L4** to find a reason for lower $r_1$ values in comparison with the main branch of HOPO agents.

Structural modifications into skeletons of Gd-**L1**, Gd-**L2** and Gd-**L4** should be introduced. The structures of **L1** and/or **L2** need to be altered in order to obtain response to biologically relevant ions. Based on obtained results, change in distance between the HOPO moiety and the $Ca^{2+}$-chelator could potentially trigger the desired sensitivity to endogenous ions.

Problems with conversion of **L3** straight to **L4** during hydrogenation may indicate problems with further coupling to a targeting vector. Therefore an introduction of a flexible linker would be advised before coupling to any targeting vector. Furthermore, the targeting ability and general behaviour of Gd-**L4** *in vivo* should be examined.

# Chapter 6

# Experimental section

# 6.1 General methods

All chemicals were purchased from commercial sources and used as delivered with the exception of THF which was distilled over sodium prior to use.

*Column chromatography*
Column chromatography was performed on silica gel 60 (70-230 Mesh) from Merck (Germany).

*Reversed phase High performance liquid chromatography RP-HPLC*
Reversed phase high-performance liquid chromatography (RP-HPLC) was performed on a Varian PrepStar Instrument (Australia), equipped with PrepStar SD-1 pump heads. Preparative RP-HPLC was performed on an Atlantis C18 column 19mm x 150mm, particle size 5µm, Waters Corp. (USA) using method given in Table 6.

**Table 6 Elution conditions for preparative HPLC**

| Time (min) | % $H_2O$ | % MeOH |
|---|---|---|
| 00:00 | 90 | 10 |
| 10:00 | 90 | 10 |
| 15:00 | 10 | 90 |
| 35:00 | 10 | 90 |

*NMR*
^{1}H, ^{13}C NMR spectra and all relaxometric experiments were recorded on a Bruker Avance III 300 MHz Microbay spectrometer from Bruker (Germany) at 25 °C.

*Mass spectra*
ESI-LRMS spectra were performed on an ion trap SL 1100 system Agilent (Germany).

FAB-MS spectra (3-nitrobenzyl alcohol (NBA) as matrix) were performed in Institute of Organic Chemistry, Faculty of Science, University of Tübingen, Germany on a Finnigan MAT TSQ 70 spectrometer.

HR-MS spectra were obtained, at a Bruker FT-ICR Apex II spectrometer (Bruker, Germany)., and in the Insitituet of Analytical Chemistry, University of Leipzig, Germany, at a MAT Sektorfeld mass spectrometer (Finnigan, Germany).

*$T_1$ measurements*

The relaxivities of the complexes are an average of two measurements at concentrations ranging from 0.1 mM to 0.5 mM in HEPES buffered solution (0.2 M, pH=7.4). Measurements were performed at Bruker Avance III 300 MHz Microbay spectrometer from Bruker (Germany) at 25 °C.

The $Gd^{3+}$ content was primarily determined by bulk magnetic susceptibility measurements (BMS) as published[119] and by ICP measurement performed by Currenta GmbH & Co. OHG, Leverkusen, Germany.

*MR measurements*

MR imaging of the samples was performed at 3T (123 MHz, 21 °C) on a clinical human MR scanner (MAGNETOM Tim Trio, Siemens Healthcare, Germany) in Department of High-Field Magnetic Resonance, MPI for Biological Cybernetics, Tübingen.

Stock solutions of Gd-**L1** and Gd-**L2** (0.4 and 0.16 mM, respectively) were prepared in HEPES buffer (25 mM, pH 7.4). The concentration of Gd-**L1** and Gd-**L2** was kept constant (0.02 and 0.01 mM, respectively) while the concentration of $Zn^{2+}$ and $Ca^{2+}$ varied up to a ratio of 50 $Zn^{2+}$/$Ca^{2+}$– Gd-**L1**/Gd-**L2**. The obtained results are mean ± SEM of two independent experiments.

Longitudinal relaxation times ($T_1$) were measured using an inversion recovery sequence to obtain images from an axial slice of 1 mm thickness through the samples. The inversion time ($T_i$) was varied from 23 ms to 3000 ms in 12 steps. Images were read out with a turbo spin echo technique, acquiring 5 echoes per scan. The repetition time (TR) was 10 000 ms to ensure complete relaxation. Six averages per $T_i$ were possible within 18 min. Diffusion sensitivity was reduced by

minimizing the crusher gradients surrounding the refocusing pulse. A matrix of 256 × 256 voxels was used over a field-of-view of 110 × 110 mm$^2$ resulting in a voxel volume of 0.43 × 0.43 × 1 mm$^3$. Data analysis was performed by fitting of relaxation curves with self-written routines under MATLAB 7.1 R14 (The Mathworks Inc., United States). The series of $T_1$ (with varying t = TI) relaxation data were fitted to the eqn (16).

$$S = S_0 \left( 1 - exp \left( -\frac{t}{T_1} \right) \right) + S_{(TI=0)} \exp \left( -\frac{t}{T_1} \right) \tag{16}$$

Nonlinear least-squares fitting of three parameters $S_0$, $S_{(TI=0)}$, and $T_1$ was done for manually selected regions of interest with the Trust-Region Reflective Newton algorithm implemented in MATLAB. The quality of the fit was controlled by visual inspection and by calculating the mean errors and residuals. The obtained $T_1$ values of the samples were converted to $R_1$ (= $1/T_1$).

$$r_1 = \left( R_{1,obs} - R_{1,dia} \right) / [SCA] \tag{17}$$

Relaxivities $r_1$ were calculated by using eqn (17), where $R_{1,obs}$ – observed relaxation rate, $R_{1,dia}$ – diamagnetic contribution to the relaxation rate and [SCA] – applied concentration of SCA.

*UV-VIS measurements*
Spectrophotometric measuremens were performed at CBM-CNRS Orleans, France, on a Uvikon XL UV-VIS spectrophotometer from Secomam (France) in 1-cm quartz cuvettes at 25 °C.

## 6.2 Syntheses of compounds

Compounds **2**, **3**,[120] **6**[100], **10**[101], **15**[121], **16**[103] and **50**[112] were prepared as published.

## Carbonic acid ethyl ester 2-oxo-1,2-dihydro-pyridin-3-yl ester (4)
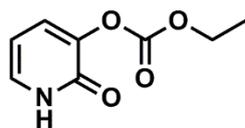
Pyridine-2,3-diol (1.0 g, 9.00 mmol) and diethyl dicarbonate (1.59 mL, 10.80 mmol) were placed in a flask under inert atmosphere. The mixture was heated at 90 $^0$C overnight. The next day the reaction mixture was diluted with ethyl acetate and washed with water. The organic phase was dried over sodium sulfate, concentrated under reduced pressure and purified by column chromatography (DCM:acetone; 3:1) to give carbonate **4** (0.84 g, 50 % yield) as grey crystals.

**$^1$H NMR:** (acetone-d$_6$) δ(ppm): 7.30-7.27 (m, 2H, NHC*H*CHC*H*), 6.18 (t, 1H, *J*=7.0 Hz, NHCH*CH*CH), 4.13 (q, 2H, *J*=7.2 Hz, C*H$_2$*CH$_3$), 1.19 (m, 3H, CH$_2$C*H$_3$*).

**$^{13}$C NMR:** (acetone-d$_6$) δ(ppm): 158.9 (*C*ONH), 153.2 (O*C*(O)O), 142.6 (*C*HCO), 133.4 (NH*C*H), 130.7 (*C*HCO), 105.1 (NH*C*HCH), 65.5 (*C*H$_2$CH$_3$), 14.4 (CH$_2$*C*H$_3$).

## 3-Methoxymethoxy-1*H*-pyridin-2-one (5)
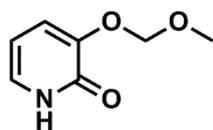
Chloro(methoxy)methane (0.68 mL, 9.00 mmol) was added portionwise to a solution of pyridine-2,3-diol (1.0 g, 9.00 mmol) in dry DMF (20 mL). The mixture was stirred at r.t. for 30 min. Then sodium hydride (0.21 g, 9.00 mmol) was added with ice cooling. The cooling bath was removed and the reaction mixture was stirred at 50 $^0$C overnight. Water was carefully added to quench the remains of sodium hydride and the solution was evaporated to dryness. The residue was dissolved in DCM and washed with water. The organic phase was dried over sodium sulfate and concentrated under reduced pressure. Purification by column chromatography (DCM:acetone; 3:1) gave pyridinone **5** (0.36 g, 26 % yield) as a brown oil.

**$^1$H NMR:** (MeOH-d$_6$) δ(ppm): 7.14 (m, 1H, NHC*H*), 6.84 (m, 1H, CHC*H*CH), 6.26 (m, 1H, C*H*CO), 5.37 (s, 2H, OC*H$_2$*O), 3.37 (m, 3H, OC*H$_3$*).

**$^{13}$C NMR:** (acetone-d$_6$) δ(ppm): 159.8 (NH*C*O), 147.8 (CH*C*O), 128.0, 127.5 (NH*C*H), 114.7, 114.6 (*C*HCO), 106.77, 106.6 (CH*C*HCH), 96.2 (O*C*H$_2$O), 79.2, 75.7, 57.8, 55.7 (O*C*H$_3$).

### Ethyl 3-methoxy-2-oxo-1,2-dihydropyridine-4-carboxylate (7)
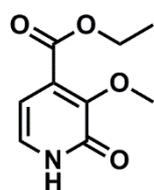
 3-Methoxypyridin-2(1H)-one[100] (1.0 g, 7.99 mmol) was dissolved in freshly distilled THF (10 mL) under inert atmosphere. After cooling the solution to -78 $^0$C, butyllithium (12.5 mL, 19.98 mmol) in hexanes was added dropwise. The reaction mixture was stirred for 15 h. The reaction mixture was cooled back to -78 $^0$C and ethyl chloroformate (1.9 mL, 19.98 mmol) was added drop wise. The reaction mixture was stirred for 72 h gradually returning to r.t. The crude product was extracted with DCM, the organic phase was washed with water, dried over sodium sulfate and concentrated under reduced pressure. The residue was purified by column chromatography (DCM:acetone; 3:1) to give ester **7** as a brown oil (0.64 g, 40%).

**$^1$H NMR** (CDCl$_3$): δ (ppm): 13.08 (broad s, 1H, N*H*), 7.2 (d, 1H, *J*=6.6 Hz, NHC*H*), 6.34 (d, 1H, *J*=6.8 Hz, CHC*H*), 4.25 (q, 2H, *J*=7.0 Hz, C*H$_2$*CH$_3$), 3.88 (s, 3H, OC*H$_3$*), 1.26 (t, 3H, *J*=7.2 Hz, CH$_2$C*H$_3$*).

**$^{13}$C NMR** (CDCl$_3$): δ (ppm): 164.2 (*C*(O)O), 161.7 (NH*C*O), 148.5 (*C*OCH$_3$), 132.2 (NH*C*H), 128.9 (*C*C(O)), 105.5 (CH*C*HCH), 61.5 (*C*H$_2$CH$_3$), 60.2 (O*C*H$_3$), 13.9 (CH$_2$*C*H$_3$).

**HR-MS**: calc. 220.058029 [M+Na]$^+$, found 220.057859 [M+Na]$^+$.

### 3-Methoxy-1-methyl-2-oxo-1,2-dihydro-pyridine-4-carboxylic acid ethyl ester (8)
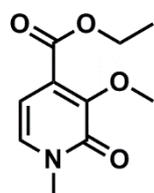
 Ethyl 3-methoxy-2-oxo-1,2-dihydropyridine-4-carboxylate (1.6 g, 8.11 mmol) and potassium carbonate (6.0 g, 43 mmol) were suspended in dry DMF (50 mL) under inert atmosphere. Then iodomethane (5 mL, 81 mmol) was added. The reaction mixture was stirred overnight at r.t. The solvent was evaporated under reduced pressure, the solid residue was dissolved in DCM and washed with water. The organic phase was dried over sodium sulfate and concentrated under reduced pressure to give pyridinone **8** as a brown oil (1.5 g, 86%).

**¹H NMR**: (CDCl₃) δ (ppm): 7.02 (d, 1H, $J$=7.0 Hz, CH₃NC$H$), 6.26 (d, 1H, $J$=7.2 Hz CHC$H$C), 4.29 (m, 2H, OC$H_2$CH₃), 3.94 (s, 3H, OC$H_3$), 3.5 (s, 3H, C$H_3$N), 1.31 (t, 3H, $J$=7.2 Hz, CH₂C$H_3$).

**¹³C NMR**: (CDCl₃) δ (ppm): 164.9 ($C$(O)O), 159.8 (CH₃N$C$O), 148.9 ($C$OCH₃), 135.8, 132.2 (CH₃N$C$H), 129.8, 128.3 ($C$C(O)O), 103.9 (CH$C$HC), 65.1 (O$C$H₂CH₃), 61.6, 60.2 (O$C$H₃), 37.5 (N$C$H₃), 14.0 (O$C$H₃).

**HR-MS**: calc. 234.07368 [M+Na]⁺, found 234.07374 [M+Na]⁺.

### 3-Methoxy-1-methyl-2-oxo-1,2-dihydro-pyridine-4-carboxylic acid (9)
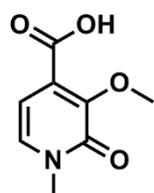
A suspension of ester **8** (0.45 g, 2.14 mmol) in 1.4M sodium hydroxide (76 mL) was heated under reflux overnight. The pH of the solution was adjusted to 1 with conc. HCl. The product was extracted with ethyl acetate. The organic phase was dried over sodium sulfate and concentrated under reduced pressure to give acid **9** as a brown oil (0.38 g, 97%).

**¹H NMR**: (acetone-d₆) δ(ppm): 7.35 (d, 1H, $J$=7.2 Hz, CH₃NC$H$), 6.25 (d, 1H, $J$=7.0 Hz, CHC$H$C), 3.85 (s, 3H, OC$H_3$), 3.44 (s, 3H, NC$H_3$).

**¹³C NMR**: (acetone-d₆) δ(ppm): 172.2 ($C$(O)OH), 166.0, 164.1, 160.1 (CH₃NH$C$(O)), 148.8 ($C$OCH₃), 134.5 (CH₃NH$C$H), 130.6, 120.0 ($C$C(O))H), 110.9, 104.1 (CH$C$HC), 60.4 (O$C$H₃), 37.6 ($C$H₃N).

**HR-MS**: calc. 206.04238 [M+Na]⁺, found 206.04232 [M+Na]⁺.

### [2-(Bis-{2-[(3-methoxy-1-methyl-2-oxo-1,2-dihydro-pyridine-4-carbonyl)-amino]-ethyl}amino)-ethyl]-carbamic acid *tert*-butyl ester (11)
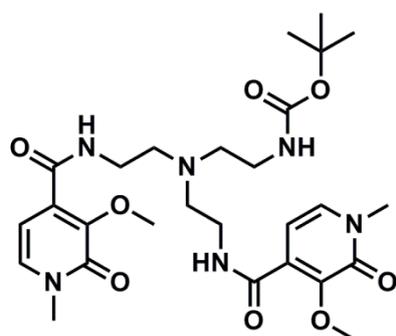
Pyridine (0.057 mL, 0.71 mmol) followed by perfluorophenyl 2,2,2-trifluoroacetate (0.104 mL, 0.60 mmol) was added to a vigorously stirred solution of **9** (0.1 g, 0.55 mmol) in dry DMF (5 mL). The reaction mixture was stirred overnight at r.t., diluted with EtOAc

and washed with water. The organic phase was dried over sodium sulfate and concentrated under reduced pressure. The crude product was used in the next step without further purification.

The activated ester in dry DMF (2 mL) was added dropwise over 30 min to a stirred solution of *tert*-butyl 2-(bis(2-aminoethyl)amino)ethylcarbamate[101] (0.034 g, 0.14 mmol) and DIPEA (0.19 mL, 1.09 mmol) in dry DMF (2 mL). The reaction mixture was stirred overnight at r.t., DMF was evaporated, the residue was dissolved in DCM and washed with water. The organic phase was dried over sodium sulfate, concentrated under reduced pressure and purified by column chromatography (DCM:MeOH=95:5) to give HOPO derivative **11** as a brown oil (0.039 g, 50% yield).

**$^1$H NMR:** (acetone-d$_6$) δ(ppm): 8.14 (m, 2H, amide N*H*), 7.05 (d, 2H, *J*=7.4 Hz, CH$_3$NC*H*C), 6.64 (d, 2H, *J*=7.2 Hz, CHC*H*C), 3.97 (s, 6H, C*H$_3$*N), 3.46 (m, 11H, OC*H$_3$*, C*H$_2$*NHC(O)), 3.15 (m, 2H, C*H$_2$*C(O)O), 2.68 (m, 6H, NC*H$_2$*), 1.32 (s, 9H, C(C*H$_3$*)$_3$).

**$^{13}$C NMR:** (acetone-d$_6$) δ(ppm): 164.4 (amide *C*(O)), 160.1 (CH$_3$N*C*(O)), 157.0 (carbamate *C*(O)), 147.7 (*C*OCH$_3$), 133.9, 131.7 (CH$_3$N*C*H), 104.6 (CH*C*HC), 78.8 (*C*(CH$_3$)$_3$), 60.3 (O*C*H$_3$), 54.4, 53.9 (N*C*H$_2$), 38.5, 37.6 (*C*H$_2$NH), 30.6 (*C*H$_3$N), 28.6 (C(*C*H$_3$)$_3$).

**ESI-MS:** calc. 576.3, found 577.1 [M+H]$^+$.

**HR-MS:** calc. 599.279983 [M+Na]$^+$, found 599.279491 [M+Na]$^+$.

## N-(2-(2-aminoethylamino)ethyl)-3-methoxy-1-methyl-2-oxo-1,2-dihydropyridine-4-carboxamide (12)
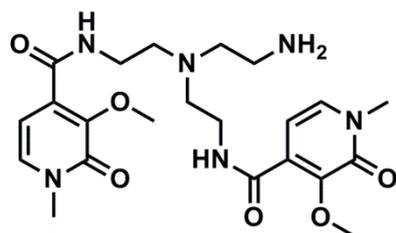


Carbamate **11** (0.6 g, 1.04 mmol) was dissolved in dry DCM (5 mL). Then 2,2,2-trifluoroacetic acid (0.64 mL, 8.32 mmol) was added and the solution was stirred at r.t. overnight. The next day the solvent was evaporated and the residue washed with methanol. Amine **12** (0.52 g, 85% yield) as a brown oil was dried under reduced pressure and used for the next step without further purification.

**¹H NMR:** (CDCl₃) δ(ppm): 8.12 (m, 2H, amide N*H*), 7.03 (d, 2H, *J*=7.2 Hz, CH₃NC*H*), 6.63 (d, 2H, *J*=7.0 Hz, CHC*H*C), 3.96 (s, 6H, OC*H₃*), 3.48 (m, 12H, C*H₃*N, C*H₂*NHC(O)), 2.76 (m, 6H, C*H₂*N).

**¹³C NMR:** (CDCl₃) δ(ppm): 163.6 (C*C*(O)NH), 159.3 (CH₃N*C*(O)), 147.4 (*C*OCH₃), 132.1 (CH₃N*C*H), 129.9 (*C*C(O)NH), 104.5 (CH*C*HC), 60.0 (O*C*H₃), 53.6, 53.1 (*C*H₂N), 37.8, 37.7, 37.5 (*C*H₂NH, *C*H₂NH₂).

**ESI-MS:** calc. 476.2, found: 477.1 [M+H]⁺, 499.1 [M+Na]⁺.

**HR-MS:** calc. 477.245609 [M+H]⁺, found 477.245986 [M+H]⁺.

**N,N',N''-(nitrilotris(ethane-2,1-diyl))tris(3-methoxy-1-methyl-2-oxo-1,2-dihydropyridine-4-carboxamide) (14)**
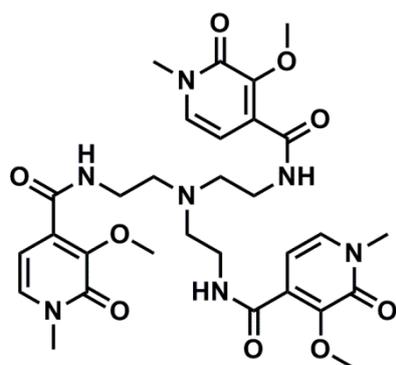


Carboxylic acid **9** (0.7 g, 3.82 mmol) and pyridine (0.927 mL, 11.47 mmol) were dissolved in dry DMF (5 mL). Perfluorophenyl 2,2,2-trifluoroacetate (0.856 mL, 4.97 mmol) was added dropwise. The reaction mixture was stirred overnight at r.t. The reaction mixture was diluted with ethyl acetate and washed with water. The organic phase was dried over sodium sulfate and concentrated under reduced pressure. The crude product was used without further purification in the next step.

N1,N1-bis(2-aminoethyl)ethane-1,2-diamine (0.093 mL, 0.620 mmol) and DIPEA (0.756 mL, 4.34 mmol) were dissolved in dry DMF (2 mL). Then the activated ester as a solution in DMF (2 mL) was added dropwise. The reaction mixture was stirred overnight at r.t. The next day the solvent was evaporated to dryness, the residue was dissolved in DCM and washed with water. The organic phase was dried over sodium sulfate, concentrated under reduced pressure and purified by column chromatography (DCM:MeOH; 95:5) to give **14** (0.119 g, 30 % yield) as a brown oil.

**¹H NMR:** (acetone-d₆) δ(ppm): 8.25 (m, 3H, amide N*H*), 7.33 (m, 3H, CH₃NC*H*), 6.47 (m, 3H, CHC*H*C), 3.97 (m, 9H, OC*H₃*), 3.48-3.55 (m, 17H, C*H₃*N, C*H₂*NH), 2.87 (m, 6H, C*H₂*N).

**$^{13}$C NMR:** (acetone-d$_6$) δ(ppm): 164.4 (amide $C$(O)), 159.9 (CH$_3$N$C$(O)), 147.6 ($C$OCH$_3$), 133.7 ($C$C(O)NH), 131.6 (CH$_3$N$C$H), 104.4 (CH$C$HC), 60.2 (O$C$H$_3$), 54.0 ($C$H$_2$N), 38.6 ($C$H$_2$NH), 37.4 ($C$H$_3$N).

**ESI-MS:** calc.641.3, found 642.3 [M+H]$^+$, 664.3 [M+Na]$^+$.

## N,N',N''-(nitrilotris(ethane-2,1-diyl))tris(3-hydroxy-1-methyl-2-oxo-1,2-dihydropyridine-4-carboxamide) (tren(1-Me-3,2-HOPO)$_3$)
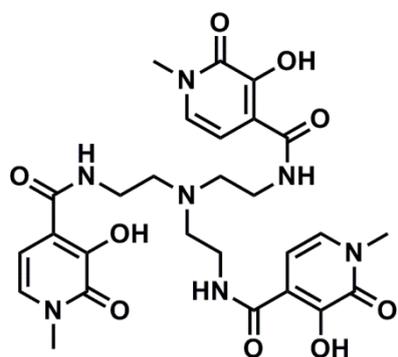


Methyl groups from phenols were removed as published by Kiessling et al.[102]

HOPO derivative **14** (0.046 g, 0.07 mmol) was dissolved in DMSO, so that the concentration was between 0.4 and 26 mM, under inert atmosphere and sodium ethanethiolate (0.045 g, 0.54 mmol) was added. The solution was heated at 140 °C for 3 h. After cooling to r.t 5 fold excess of water was added to quench the remaining sodium ethanethiolate. The water was evaporated and the DMSO was distilled of on a Kugelrohr apparatus. The crude product was purified by HPLC (RT 17.4 min) to give the tren(1-Me-3,2-HOPO)$_3$ as a brown oil (0.041 g, 87%).

**$^1$H NMR:** (MeOH-d4) δ(ppm): 6.73-6.35 (m, 6H, NC$H$), 3.52-3.46 (m, 9H, NC$H_3$), 2.92-2.76 (m, 7H, NHC$H_2$), 2.34-2.24 (m, 5H, NC$H_2$).

**$^{13}$C NMR:** (MeOH-d4) δ(ppm): 170.8 (amide $C$(O)), 166.7 (CH$_3$N$C$(O)), 163.3 ($C$OH), 118.7 ($C$C(O)NH), 115.0 (CH$_3$N$C$H), 108.6 (CH$C$HC), 55.9 ($C$H$_2$N), 42.5 ($C$H$_2$NH), 37.7 ($C$H$_3$N).

**ESI-MS:** calc. 599.2, found 688.2 [M-3H$^+$+4Na]$^+$.

## [Benzyl-(2-{2-[2-(bis-*tert*-butoxycarbonylmethyl-amino)-ethoxy]-ethoxy}-ethyl)-amino]-acetic acid *tert*-butyl ester (16)
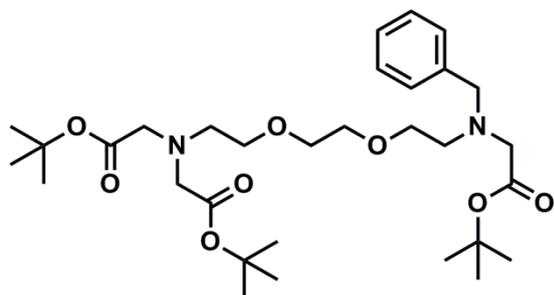
2-(2-(2-aminoethoxy)ethoxy)-N-benzylethanamine[103] (3.2 g, 13.43 mmol) was dissolved in dry DMF (20 mL). Potassium carbonate (13.0 g, 94 mmol) was added and the suspension was stirred at r.t. for 1 h. *tert*-Butyl bromoacetate (6.94 mL, 47 mmol) was added and the reaction mixture was stirred at r.t overnight. The solvent was evaporated under reduced pressure. The residue was dissolved in DCM and washed with water. The organic phase was dried over sodium sulfate, concentrated under reduced pressure and purified by column chromatography (DCM:MeOH; 95:5) to give **16** (6.0 g, 77 % yield) as a yellow oil.

**$^1$H NMR:** (CDCl$_3$) δ(ppm): 7.29-7.15 (m, 5H, Ph), 3.76 (s, 2H, C$H_2$Bn), 3.55-3.40 (m, 11H,C$H_2$OC$H_2$C$H_2$OC$H_2$, C$H_2$C(O)), 3.22 (s, 2H, C$H_2$C(O) at benzylamine), 2.88-2.79 (m, 4H, CH$_2$C$H_2$N), 1.42-1.37 (m, 27H, C(C$H_3$)$_3$).

**$^{13}$C NMR:** (CDCl$_3$) δ(ppm): 170.9, 170.7 (ester $C$(O)), 139.3, 128.9, 128.1, 126.1, 126.9 (aromatic ring), 80.7, 80.6 ($C$(CH$_3$)$_3$), 70.4, 70.3, 70.2, 70.1 (O$CH_2$$CH_2$O), 60.9 ($CH_2$Bn), 58.5 ($CH_2$C(O) at benzylamine), 56.6, 55.7 ($CH_2$C(O)), 53.3, 52.9 ($CH_2$N), 28.1, 28.0 (C($C$H$_3$)$_3$).

**ESI-MS:** calc. 580.4, found 619.2 [M+K]$^+$.

## (2-{2-[2-(Bis-*tert*-butoxycarbonylmethyl-amino)-ethoxy]-ethoxy}-ethylamino)-acetic acid *tert*-butyl ester (17)



Benzylamine derivative **16** (6.0 g, 10.33 mmol) was dissolved in MeOH (20 mL). Palladium on carbon (3.3 g, 31 mmol) and 5 drops of ammonia aqueous solution were added and the suspension was submitted to 3 bars of H$_2$ pressure for 24 h. The palladium on carbon was filtered off through a pad of celite and the solvent was evaporated under reduced pressure to give secondary amine **17** (5.0 g, 99 % yield) as a yellow oil.

**¹H NMR:** (CDCl₃) δ(ppm): 3.56-3.36 (m, 15H, C$H_2$NHCH₂C$H_2$OC$H_2$CH₂OC$H_2$, NC$H_2$C(O)), 3.25 (s, 2H), 2.87 (t, 2H, $J$=6.4, 5.9 Hz, NHC$H_2$CH₂), 2.72 (t, 2H, $J$=5.3 Hz, OCH₂C$H_2$N), 1.42-1.39 (m, 27H, C(C$H_3$)₃).

**¹³C NMR:** (CDCl₃) δ(ppm): 172.4, 171.4, 170.7 (ester $C$(O)), 81.0, 80.8 ($C$(CH₃)₃), 70.4, 70.1, 69.9 ($CH_2$O$CH_2$CH₂O$CH_2$), 60.8, 56.5 (N$CH_2$C(O)), 53.3 (O$CH_2$CH₂N), 51.4, 50.2 (NH$CH_2$C(O)), 48.6 (OCH₂$CH_2$NH), 28.0 (C($CH_3$)₃).

**ESI-MS:** calc. 490.3, found 491.2 [M+H]⁺, 513.2 [M+Na]⁺.

### 1-(4-Chloro-butyl)-3-methoxy-1*H*-pyridin-2-one (18)

To a solution of pyridinone **6** (0.5 g, 4.00 mmol) in DMF (10 mL) was added potassium carbonate (0.7 g, 4.80 mmol). The reaction mixture was stirred for 1 h at r.t. Then 1-bromo-4-chlorobutane (0.46 mL, 4.00 mmol) was added and the reaction was stirred at r.t. for 24 h. After that time DMF was evaporated and the residue was dissolved in DCM. The organic phase was washed with water, dried over sodium sulfate and concentrated under reduced pressure. The residue was purified by column chromatography (DCM:MeOH; 95:5) to give **18** as a brown oil (0.19 g, 22%).

**¹H NMR:** (MeOH-d₆) δ(ppm): 6.85 (m, 1H, NC$H$), 6.55 (m, 1H, CHC$H$CO), 6.05 (m, 1H, CHC$H$CH), 3.92 (m, 2H, NC$H_2$), 3.71 (s, 3H, OC$H_3$), 3.48 (m, 2H, C$H_2$Cl), 1.68-1.85 (m, 5H, NCH2C$H_2$C$H_2$CH₂Cl).

**¹³C NMR:** (CDCl₃) δ(ppm): 157.7 (N$C$(O)), 149.8 ($C$OCH₃), 128.0 (N$C$H), 112.1 (CHCH$C$H), 104.8 (CH$C$HCH), 55.6 (O$C$H₃), 48.4 (N$C$H₂), 44.3 ($C$H₂Cl), 29.2 (N$CH_2$CH₂), 26.4 ($C$H₂CH₂Cl).

### 1-(2-1,3-Dioxinan-2-yl-ethyl)-3-methoxy-1*H*-pyridin-2-one (19)

Sodium carbonate (0.06 g, 0.615 mmol), 2-(2-bromoethyl)-1,3-dioxane (0.07 mL, 0.513 mmol) and compound **6** (0.071 g, 0.564 mmol) were heated at reflux in dry acetonitrile (5 mL) under inert atmosphere for 48h. The inorganic salts were filtered off and the filtrate was evaporated under reduced pressure. The residue was purified by column chromatography (DCM:MeOH; 95:5) to give acetal **19** as a brwon oil (0.07 g, 56%).

**$^1$H NMR:** (MeOH-$d_6$) δ(ppm): 7.04 (dd, 1H, $J$=1.7 Hz, NC$H$), 6.77 (dd, 1H, $J$=1.7 Hz, C$H$CO), 6.17 (m, 1H, CHC$H$CH), 4.72 (s, 1H), 4.48 (m, 1H, OC$H$O), 3.99-3.89 (m, 5H, NC$H_2$, OC$H_2$), 3.69 (s, 3H, OC$H_3$), 1.80-1.96 (m, 4H, CH$_2$C$H_2$CH, OCH$_2$C$H_2$CH$_2$O).

**$^{13}$C NMR:** (acetone-$d_6$) δ(ppm): 162.8, 158.0 (N$C$(O)), 150.9 ($C$OCH$_3$), 130.3 (N$C$H), 113.6 (CH$C$HCH), 104.5 (CH$C$HCH), 100.5 (O$C$HO), 67.3 ($C$H$_2$CH$_2$$C$H$_2$), 56.0 (O$C$H$_3$), 45.8 (N$C$H$_2$), 36.2, 34.9 (N$C$H$_2$CH$_2$$C$H), 26.5 (OCH$_2$$C$H$_2$CH$_2$O).
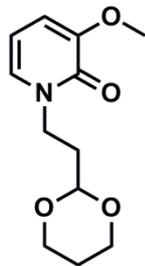
**ESI-MS:** calc. 239.1, found 262.1 [M+Na]$^+$, 278.1 [M+K]$^+$.

### 1-(3,3-Dimethoxy-propyl)-3-methoxy-1$H$-pyridin-2-one (20)
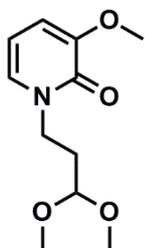
Pyridinone **6** (0.1 g, 0.8 mmol) and base (1.2-3 eq.) (see Table 2) were dissolved in dry DMF (10 mL). The reaction mixture was stirred for 1 h at r.t. Then 3-bromo-1,1-dimethoxypropane (0.13 mL, 0.96 mmol) was added. The reaction mixture was stirred for 20 h at 100 $^0$C. The solvent was evaporated and the residue dissolved in DCM. The organic phasewas washed with water, dried over sodium sulfate and concentrated under reduced pressure. Purification by column chromatography (DCM:MeOH; 90:10) gave acetal **20** as a brown oil.

**$^1$H NMR:** (CDCl$_3$) δ(ppm): 6.83 (dd, 1H, J=1.7, 7.0 Hz , NC$H$), 6.54 (dd, 1H, $J$=1.6, 7.5 Hz, CHCHC$H$), 6.02 (t, 1H, $J$=7.2 Hz, CHC$H$CH), 3.94 (t, 1H, $J$=5.8 Hz, ), 3.72 (s, 3H, OC$H_3$), 3.25-3.21 (m, 6H, OC$H_3$), 2.0 (m, 2H, CH$_2$C$H_2$CH).

**$^{13}$C NMR:** (CDCl$_3$) δ(ppm): 157.8 ($C$(O)), 150.0, 144.0 ($C$OCH$_3$), 136.9 (N$C$H), 128.6, 117.4, 116.6, 112.0 (CH$C$H$C$HO), 104.5 ($C$H$C$H$C$H), 102.0 (O$C$HO), 62.1, 55.7, 55.6, 55.5 (O$C$H$_3$), 52.9, 52.7 (O$C$H$_3$), 46.1 (N$C$H$_2$), 31.4 (CH$_2$$C$H$_2$CH).

## 1-(3,3-Dimethoxy-propyl)-3-methoxy-2-oxo-1,2-dihydro-pyridine-4-carboxylic acid ethyl ester (21)



Pyridinone **7** (0.56 g, 2.84 mmol) was dissolved in dry DMF (50 mL) under inert atmosphere. Potassium carbonate (1.57 g, 11.4 mmol) was added and the reaction mixture was stirred for 1 h at r.t. Then 3-bromo-1,1-dimethoxypropane (1.16 mL, 8.52 mmol) was added. The reaction mixture was stirred at 100 $^0$C for 24 h. The solvent was evaporated, the residue dissolved in DCM and washed with water. The organic phase was dried over sodium sulfate, concentrated under reduced pressure and purified by column chromatography (DCM:MeOH; 95:5) to give acetal **21** (0.51 g, 60% yield) as a brown oil.

**$^1$H NMR:** (acetone-d$_6$) δ(ppm): 7.42 (d, 1H, $J$=7.2 Hz, NC$H$), 6.27 (d, 1H, $J$=7.2 Hz, CHCHC$H$), 4.46 (t, 1H, $J$=5.5 Hz, OC$H$O), 4.33 (q, 2H, $J$=7.2 Hz, C$H_2$CH$_3$), 4.03 (t, 2H, $J$=7.2 Hz, NC$H_2$), 3.93 (s, 3H, OC$H_3$), 3.30 (s, 6H, OC$H_3$), 2.04 (m, 2H, $J$=6.4, 7.2 Hz, CH$_2$C$H_2$CH), 1.35 (3H, t, $J$=7.2 Hz, $J$=7.0 Hz, CH$_2$C$H_3$).

**$^{13}$C NMR:** (acetone-d$_6$) δ(ppm): 165.7 ($C$(O)), 159.6 (N$C$(O)), 148.8 ($C$OCH$_3$) 133.9 (N$C$H), 131.1 ($C$C(O)), 103.5 (CH$C$HCH), 103.0 (O$C$HO), 61.9 ($C$H$_2$CH$_3$), 60.1, 55.0 (O$C$H$_3$ pyridinone), 53.0 (O$C$H$_3$ acetal), 46.8 (N$C$H$_2$), 32.3 (CH$_2$$C$H$_2$CH), 14.5 (CH$_2$$C$H$_3$).
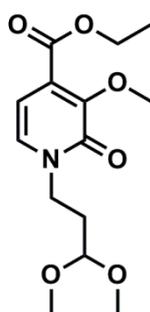
**HR-MS:** calc. 322.126109 [M+Na]$^+$, found 322.126235 [M+Na]$^+$.

## 3-Methoxy-2-oxo-1-(3-oxo-propyl)-1,2-dihydro-pyridine-4-carboxylic acid ethyl ester (22)
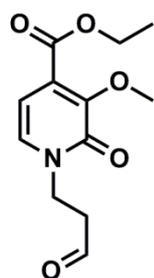
15% Sulphuric acid (0.61 mL, 1.70 mmol) was added to a suspension of silica gel (1.53 g, 25.5 mmol) in DCM (50 mL). The suspension was stirred until the sulphuric acid was taken up by the silica. Acetal **21** (0.51 g, 1.70 mmol) in DCM (5 mL) was added and the reaction mixture was stirred for 48 h at r.t. The suspension was filtered on a sintered funnel and the filtrate was concentrated under reduced pressure to give aldehyde **22** (0.38 g, 90% yield) as a yellow oil.

**$^1$H NMR:** (CDCl$_3$) δ(ppm): 9.71 (s, 1H, CHO); 7.18 (1H, overlapped with CHCl$_3$, NC*H*), 6.26 (d, 1H, *J*=7.2 Hz, NCHC*H*), 4.29 (q, 2H, *J*=6.5 Hz, NC*H*$_2$), 4.16 (t, 2H, *J*=6.0 Hz, C*H*$_2$CH$_3$), 3.92 (m, 4H, OC*H*$_3$ pyridinone), 2.99 (t, 2H, *J*=6.0 Hz, C*H*$_2$CHO), 1.30 (t, 3H, *J*=7.2 Hz, CH$_2$C*H*$_3$).

**$^{13}$C NMR**: (acetone-d$_6$) δ(ppm): 199.0 (*C*HO), 164.0 (*C*(O)O ester), 158.3 (N*C*(O)), 155.0, 144.9 (*C*OCH$_3$ pyridinone), 137.2 (N*C*H pyridinone), 133.8 (*C*C(O)), 114.2 (CH*C*HC), 70.1, 63.2 (*C*H$_2$CH$_3$), 61.9, 58.4 (O*C*H$_3$), 55.4 (N*C*H$_2$), 49.8 (CHO*C*H$_2$), 14.3 (CH$_2$*C*H$_3$).

**HR-MS:** calc. 308.110458 [M+Na+MeOH]$^+$, found 308.110270 [M+Na+MeOH]$^+$.

**1-{3-[(2-{2-[2-(Bis-*tert*-butoxycarbonylmethyl-amino)-ethoxy]-ethoxy}-ethyl)-*tert*-butoxycarbonylmethyl-amino]-propyl}-3-methoxy-2-oxo-1,2-dihydro-pyridine-4-carboxylic acid ethyl ester (23)**
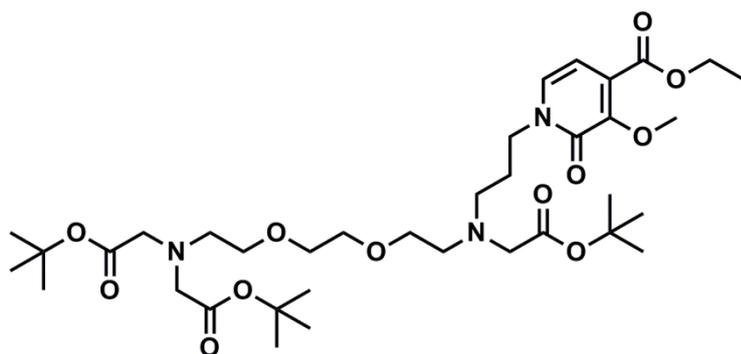
Aldehyde **22** (1.0 g, 3.95 mmol) and secondary amine **17** (2.9 g, 5.92 mmol) were dissolved in dry DMF (50 mL) under inert atmosphere. Sodium triacetoxyborohydride (2.6 g, 12.2 mmol) was added and the reaction mixture was stirred at 100 °C for 3 days. Then the solvent was evaporated, the residue dissolved in DCM and washed with water. The organic phase was dried over sodium sulfate, concentrated under reduced pressure and

purified by column chromatography (DCM:MeOH; 90:10) to give conjugate **23** (1.5 g, 52 % yield)  as a brown oil.

**$^1$H NMR:** (acetone-d6) δ(ppm): 7.39 (d, 1H, $J$=7.2 Hz, NC*H* pyridinone), 6.12 (d, 1H, $J$=7.0 Hz, NCHC*H* pyridinone), 4.19 (q, 2H, $J$= , C*H*$_2$CH$_3$), 3.94 (m, 2H, NC*H*$_2$ pyridinone), 3.78 (s, 3H, OC*H*$_3$), 3.35-3.47 (m, 15H, NC*H*$_2$ *tert*-butyl ester), 2.79-2.58 (m, 6H, C*H*$_2$ tertiary amine), 1.82-1.72 (m, 3H, CH$_2$C*H*$_2$CH$_2$ alkyl linker), 1.35-1.19 (m, 34H, C(C*H*$_3$)$_3$, CH$_2$C*H*$_3$).

**$^{13}$C NMR**: (acetone-d$_6$) δ(ppm): 171.6, 171.4 (*C*(O) $^t$Bu ester), 165.8 (*C*(O) ethyl ester), 159.7 (N*C*(O) pyridinone), 148.8 (*C*OCH$_3$), 134.5 (N*C*H), 131.1 (*C*C(O) pyridinone), 103.3 (NCH*C*H), 81.0, 80.9, 80.8, 80.7 (*C*(CH$_3$)$_3$), 71.2, 71.1, 71.0, 70.5 (*C*H$_2$O*C*H$_2$ EGTA), 61.9 (*C*H$_2$CH$_3$), 60.1, 57.1, 56.5, 54.4, 54.2, 52.0, 49.3, 48.5 (*C*H$_2$ at tertiary amine, N*C*H$_2$ at pyridinone, O*C*H$_3$) , 28.4 (C(*C*H$_3$)$_3$), 27.5, 21.4 (CH$_2$*C*H$_2$CH$_2$), 14.5 (CH$_2$*C*H$_3$).

**ESI-MS:** calc. 727.4, found 728.4 [M+H]$^+$, 750.4 [M+Na]$^+$, 766.4 [M+K]$^+$.

## Dibenzyl-{2-[2-(2-benzylamino-ethoxy)-ethoxy]-ethyl}-amine (25)
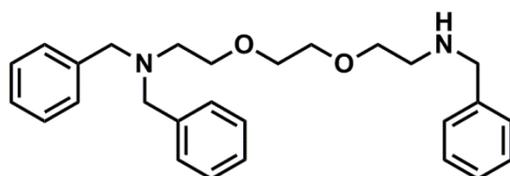


Dibenzylamine **24** (10.0 g, 30.4 mmol) was dissolved in dry DMF (100 mL) under inert atmosphere. Then potassium carbonate (4.21 g, 30.4 mmol) was added and the reaction mixture was cooled to     -40 $^0$C. Benzyl bromide (4.0 mL, 33.5 mmol) was slowly added. The reaction mixture was stirred for 24 h gradually returning to r.t. The solvent was evaporated under reduced pressure, the residue dissolved in DCM and washed with water. The organic phase was dried over sodium sulfate, concentrated under reduced pressure and purified by flash column chromatography (DCM:MeOH; 90:10) to give amine **25** as a yellow oil (7.4 g, 60%).

**$^1$H NMR** (CDCl$_3$): δ: 7.45-7.26 (15H, m, Ph), 3.84 (2H, s, NHC*H*$_2$Ph), 3.71-3.59 (12H, m, N(C*H*$_2$Ph)$_2$, C*H*$_2$OC*H*$_2$C*H*$_2$OC*H*$_2$ ), 2.87-2.74 (4H, m, C*H*$_2$N, C*H*$_2$NH).

**$^{13}$C NMR** (CDCl$_3$):  δ: 139.8, 128.3, 128.2, 127.0, 126.8 (Ph), 70.5, 70.4, 70.2, 70.0 (*C*H$_2$O*C*H$_2$*C*H$_2$O*C*H$_2$), 59.0 (*C*H$_2$Ph), 53.8 (*C*H$_2$N), 52.7 (*C*H$_2$Ph), 48.6 (*C*H$_2$NH).

**ESI-MS**: calc. 418.3, found 419.2 [M+H]$^+$.

**HR-MS:** calc. 419.269305 [M+H]$^+$, found 419.269392 [M+H]$^+$.


**1-[3-(Benzyl-{2-[2-(2-dibenzylamino-ethoxy)-ethoxy]-ethyl}-amino)-propyl]-3-methoxy-2-oxo-1,2-dihydro-pyridine-4-carboxylic acid ethyl ester (26)**
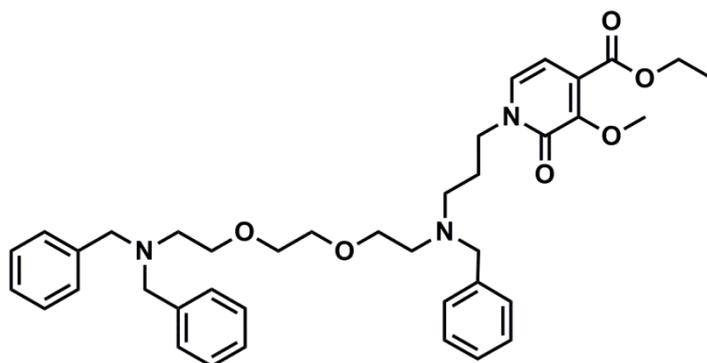


Compound **25** (0.49g, 1.17 mmol), compound **22** (0.27g, 1.07 mmol), and sodium triacetoxyborohydride (0.70 g, 3.32 mmol) were dissolved in dry DMF (20 mL) under inert atmosphere. The reaction mixture was stirred for 3 days at 100 $^0$C. The solvent was

evaporated under reduced pressure, the residue was dissolved in DCM and washed with water. The organic phase was dried over sodium sulfate, concentrated under reduced pressure and purified by column chromatography (DCM:MeOH; 95:5) to give conjugate **26** as a brown oil (0.35 g, 30%)

$^1$**H NMR** (CDCl$_3$): δ (ppm): 7.37-7.19 (15H, m, Ph), 6.85 (1H, d, *J*=7.2 Hz, NC*H*), 6.17 (1H, d, *J*=7.2 Hz, CHC*H*C), 4.33 (2H, q, *J*=7.2, 7.0 Hz, C*H*$_2$ ester), 3.97 (3H, s, OC*H*$_3$), 3.91 (2H, t, *J*=6.8 Hz, NC*H*$_2$ pyridinone), 3.62-3.48 (16H, m, C*H*$_2$Ph, C*H*$_2$OC*H*$_2$C*H*$_2$OC*H*$_2$), 2.69-2.65 (6H, m, C*H*$_2$N), 1.85 (2H, m, CH$_2$C*H*$_2$CH$_2$), 1.35 (3H, t, *J*=7.2 Hz, 7.0 Hz, C*H*$_3$ ester).

$^{13}$**C NMR** (CDCl$_3$): δ (ppm): 165.0 (C(O) ester), 159.4 (C(O) pyridinone), 148.8 (*C*OCH$_3$), 139.6 (N*C*H), 128.7 (aromatic *C*H), 126.8 (*C*C(O)), 103.6 (CH*C*HC), 70.3, 69.9, 69.6 (*C*H$_2$O*C*H$_2$*C*H$_2$O*C*H$_2$), 60.2 (*C*H$_2$CH$_3$), 59.2 (O*C*H$_3$), 58.9 (*C*H$_2$Ph), 53.2, 52.7 (N*C*H$_2$*C*H$_2$O), 50.2, 48.1 (N*C*H$_2$CH$_2$*C*H$_2$N), 26.3 (NCH$_2$*C*H$_2$CH$_2$N), 14.1 (*C*H$_3$ ester).

**ESI-MS**: calc. 655.4, found 656.4 [M+H]$^+$.

**1-[3-(Benzyl-{2-[2-(2-dibenzylamino-ethoxy)-ethoxy]-ethyl}-amino)-propyl]-3-methoxy-2-oxo-1,2-dihydro-pyridine-4-carboxylic acid (27)**
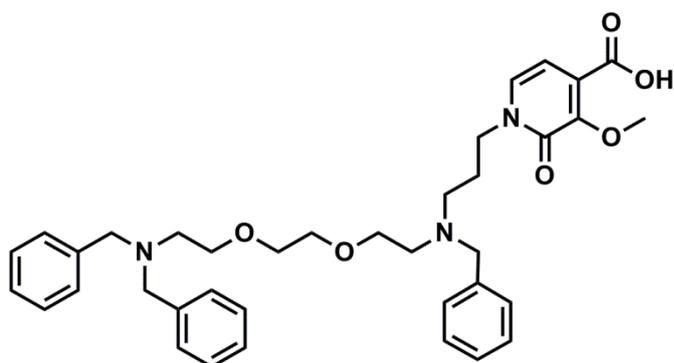
Ester **26** (1.17 g, 1.78 mmol) was suspended in water (100 mL). Sodium hydroxide (3.57 g, 89 mmol) was added and the suspension was heated at reflux overnight. After cooling to r.t. the pH was adjusted to 1. The product was extracted with ethyl acetate, the organic phase dried over sodium sulfate and concentrated under reduced pressure to give acid **27** (0.78 g, 69% yield) as a brown oil.

**$^1$H NMR:** (CDCl$_3$) δ (ppm): 7.20 (m, 18H, Ph), 6.81 (d, 1H, $J$=7.0 Hz, NC*H*), 6.16 (d, 1H, $J$=7.0 Hz, CHC*H*C), 3.87-3.46 (m, 23H, C*H$_2$*Ph, OC*H$_3$*, NC*H$_2$* pyridinone, C*H$_2$*OC*H$_2$*C*H$_2$*OC*H$_2$*), 2.80 (t, 2H, $J$=4.7 Hz, NBn$_2$C*H$_2$*), 2.66 (t, 4H, $J$=5.9 Hz, NC*H$_2$*), 1.92 (bm, 2H, NCH$_2$C*H$_2$*CH$_2$N).

**$^{13}$C NMR**: (CDCl$_3$) δ (ppm): 168.3 (*C*(O) acid), 158.4 (*C*(O) pyridinone), 144.7 (*C*OCH$_3$), 136.8 (Ph), 134.1 (N*C*H), 130.7, 128.7, 127.9, 127.0 (Ph), 126.0 (*C*COOH), 103.6 (CH*C*HC), 69.1, 68.9, 68.1, 66.8 (*C*H$_2$O*C*H$_2$*C*H$_2$O*C*H$_2$), 58.9 (O*C*H$_3$), 57.3 (Ph*C*H$_2$), 57.1 (NBn*C*H$_2$), 50.9, 50.8 (NBn$_2$*C*H$_2$), 49.1 (BnN*C*H$_2$CH$_2$CH$_2$N), 46.4 (BnNCH$_2$CH$_2$*C*H$_2$N), 24.1 (BnNCH$_2$*C*H$_2$CH$_2$N).

**ESI-MS:** calc. 627.3, found 628.4 [M+H]$^+$, 626.4 [M-H]$^-$.

**HR-MS:** calc. 628.33811 [M+H]$^+$, found 628.33810 [M+H]$^+$.

**1-(2,11-dibenzyl-1-phenyl-5,8-dioxa-2,11-diazatetradecan-14-yl)-3-methoxy-N-(2-(2-(3-methoxy-1-methyl-2-oxo-1,2-dihydropyridine-4-carboxamido)ethylamino)ethyl)-2-oxo-1,2-dihydropyridine-4-carboxamide (28)**
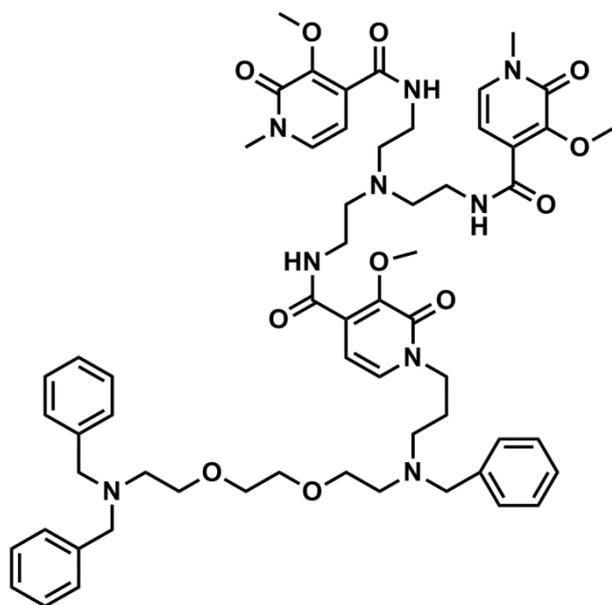
A solution of acid **27** (0.2 g, 0.319 mmol) and pyridine (0.08 mL, 0.96 mmol) in dry DMF (2ml) was cooled to 0 °C. Then perfluorophenyl 2,2,2-trifluoroacetate (0.07 mL, 0.41 mmol) was added dropwise. The cooling bath was removed and the reaction mixture was stirred for overnight at r.t. Then the reaction mixture was diluted with ethyl acetate and washed with water. The organic phase was dried over sodium sulfate, filtered and concentrated under reduced pressure. The crude product was used without further purification. HOPO substituted amine **12** (0.09 g, 0.16 mmol) and DIPEA (0.14 mL, 0.79 mmol) were dissolved in dry DMF (2 mL). The activated ester (0.25 g, 0.32 mmol) in DMF (2 mL) was added dropwise and the reaction mixture was stirred overnight at r.t. The solvent was evaporated under reduced pressure, the residue was dissolved in DCM and washed with water. The organic phase was dried over sodium sulfate, concentrated under reduced pressure and purified by column chromatography (DCM:MeOH; 90:10) to give tris-HOPO derivative **28** (0.05 g, 29% yield) as a brown oil.

**$^1$H NMR:** (acetone-$d_6$) δ (ppm): 8.14 (m, 3H, N*H* amide), 7.26-7.06 (m, 19H, Ph, NC*H*), 6.37-6.33 (m, 3H, CHC*H*C), 3.86-3.83 (m, 12H, OCH$_3$, N(pyridinone)C*H*$_2$), 3.54-3.33 (m, 29H, NC*H*$_3$, C*H*$_2$Ph, C*H*$_2$ scaffold, C*H*$_2$OC*H*$_2$C*H*$_2$OC*H*$_2$), 2.74-2.70 (m, 6H, NC*H*$_2$), 1.90-1.76 (m, 3H, NCH$_2$C*H*$_2$CH$_2$N).

**$^{13}$C NMR:** (acetone-$d_6$) δ (ppm): 164.3 (*C*(O) amide), 159.9, 159.5 (*C*(O) pyridinone), 147.8, 147.7 (*C*OCH$_3$), 140.8 (N*C*H), 133.7, 133.3, 131.4, 130.0, 129.6, 129.1, 129.0, 127.8 (Ph), 127.6 (*C*C(O)), 104.4, 104.3 (CHC*H*C), 71.1, 70.4, 70.0 (O*C*H$_2$), 60.2 (*C*H$_2$Ph), 59.7, 59.4 (O*C*H$_3$), 54.0, 53.8, 53.5 (N*C*H$_2$CH$_2$O), 51.9 (NH*C*H$_2$CH$_2$N), 48.4 (N*C*H2CH2CH2NBn), 41.2 (NCH$_2$CH$_2$*C*H$_2$NBn), 38.6 (N*C*H$_3$), 37.4 (NH*C*H$_2$), 27.2 (NCH$_2$*C*H$_2$CH$_2$NBn).

**ESI-MS:** calc. 1085.6, found 1086.6 [M+H]$^+$.

**Di-*tert*-butyl 2-(2-*tert*-butoxy-2-oxoethyl)-11-(3-(3-methoxy-4-(2-(2-(3-methoxy-1-methyl-2-oxo-1,2-dihydropyridine-4-carboxamido)ethylamino)ethylcarbamoyl)-2-oxopyridin-1(2*H*)-yl)propyl)-5,8-dioxa-2,11-diazadodecane-1,12-dicarboxylate (30)**
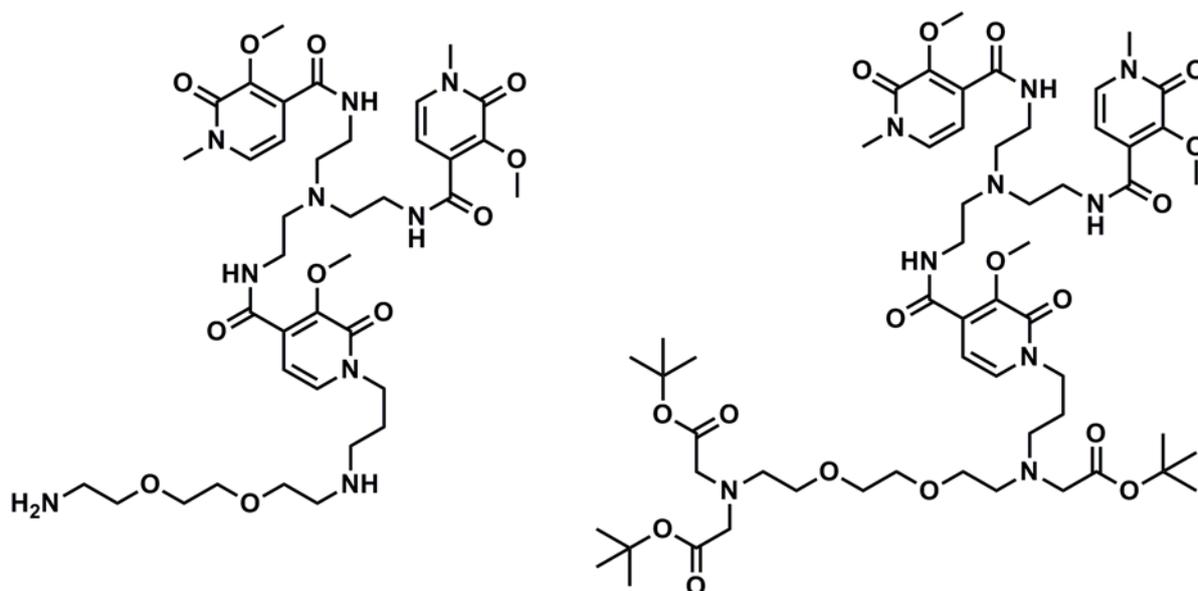


intermediate 29                    30

Tris-HOPO derivative **28** (0.05 g, 0.05 mmol) was dissolved in methanol (10 mL). Palladium on carbon (5 mg, 0.05 mmol) and ammonium formate (0.17 g, 2.76 mmol) were added. The mixture was stirred at reflux overnight. After cooling to r.t. the solution was filtered through a pad of celite. The filtrate was concentrated under reduced pressure to give amine **29** as yellow oil which was used in the further step without any purification.

**ESI-MS:** calc. 815.4, found 816.3 [M+H]$^+$, 838.3 [M+Na]$^+$.

Amine **29** (0.083 g, 0.10 mmol) was dissolved in dry DMF (5 mL) under inert atmosphere. Potassium carbonate (0.13 g, 0.92 mmol) was added and the reaction mixture was stirred for 1 h at r.t. Then *tert*-butyl 2-bromoacetate (0.06 mL, 0.41 mmol) was added and the reaction mixture was stirred for 4 days at r.t. The solvent was evaporated under reduced pressure and the residue dissolved in DCM and washed with water. The organic phase was dried over sodium sulfate and

concentrated under reduced pressure. The residue was purified by column chromatography (DCM:MeOH; 90:10) to give ester **30** (0.09 g, 76 % yield) as a brown oil.

**¹H NMR:** (CDCl₃) δ(ppm): 8.13 (m, 3H, N*H* amide), 7.03 (d, 3H, *J*=7.2Hz, NC*H*), 6.66 (d, 3H, *J*=7.2Hz, CHC*H*C), 3.97 (m, 11H, OC*H₃*, NC*H₂*CH₂CH₂NCH₂), 3.46 (m, 22H, NC*H₃*, C*H₂*C(O)OC(CH₃)₃, NCH₂ scaffold, NCH₂C*H₂*O), 3.15 (m, 4H, OC*H₂*C*H₂*O), 2.71-2.58 (m, 14H, NCH₂CH₂C*H₂*NC*H₂*, NC*H₂*CH₂O), 1.33-1.18 (m, 32H, NCH₂C*H₂*CH₂N, C(C*H₃*)₃).

**¹³C NMR:** (CDCl₃) δ(ppm): 163.5 (*C*(O) amide), 159.3 (*C*(O) ester), 156.0 (*C*(O) pyridinone), 147.4 (*C*OCH₃), 132.1, 129.9, 129.7, 128.7, 128.1, 126.9 (CH*C*H*C*), 104.5 (CH*C*HC), 79.1 (*C*(CH₃)₃), 69.9 (*C*H₂O*C*H₂*C*H₂O*C*H₂), 60.0 (O*C*H₃), 58.9 (*C*H₂C(O)OC(CH₃)₃), 53.5, 53.2 (N*C*H₂), 37.8, 37.7, 37.5 (N*C*H₃, NH*C*H₂), 29.6, 28.3, 28.2 (C(*C*H₃)₃), 23.0, 22.6 (NCH₂*C*H₂CH₂N).

**ESI-MS:** calc. 1214.6, found 1253.7 [M+Na]⁺.

**2-(Carboxymethyl)-11-(3-(3-methoxy-4-(2-(2-(3-methoxy-1-methyl-2-oxo-1,2-dihydropyridine-4-carboxamido)ethylamino)ethylcarbamoyl)-2-oxopyridin-1(2H)-yl)propyl)-5,8-dioxa-2,11-diazadodecane-1,12-dicarboxylic acid (31)**
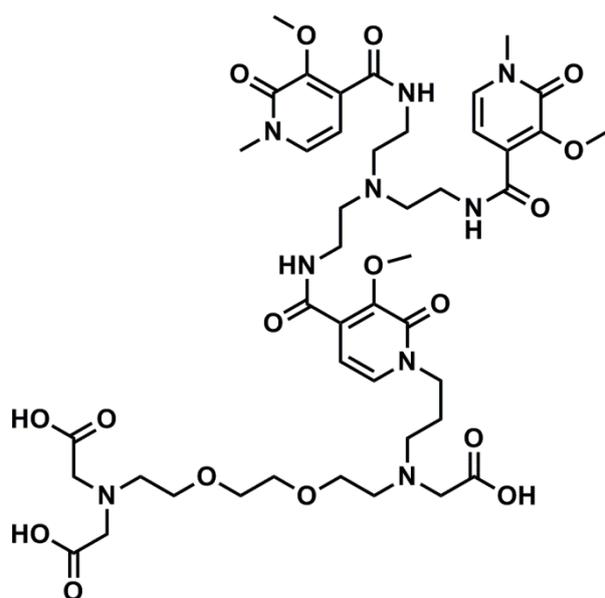


*tert*-Butyl ester **30** (0.06 g, 0.05 mmol) was dissolved in dry DCM (5 mL) and 2,2,2-trifluoroacetic acid (0.1 mL, 1.24 mmol) was added. The reaction mixture was stirred overnight at r.t., then the solvent and TFA were removed under reduced pressure to give crude triacid **31** as a brown oil which was used in the next step without further purification.

**¹H NMR:** δ(ppm): 7.31 (m, 3H, NC*H*), 7.13 (m, 3H, CHC*H*C), 6.45 (m, 3H,

COO$H$), 4.33 (m, 3H, NCH$_2$(C$H_2$COOH)$_2$), 3.94-3.44 (bm, 45H, C$H_2$ alkyl), 3.19 (m, 2H).

**$^{13}$C NMR:** δ(ppm): 170.3 (*C*(O)OH), 165.7, 165.2, 164.5 (C(O) amide), 152.6 (C(O) pyridinone), 137.8, 136.5, 134.4 (*C*OCH$_3$), 126.9, 123.1 (N*C*H), 119.2 (*CC*(O)NH), 115.4, 109.4 (CH*C*HC), 75.3, 71.6, 70.5, 70.2 (NCH$_2$*C*H$_2$O), 65.1 (O*C*H$_2$CH$_2$O), 62.9 (O*C*H$_3$), 62.1 (N*C*H$_2$CH$_2$O), 58.9 (N*C*H$_2$C(O)OH), 55.7 (*C*H$_2$NCH$_2$CH$_2$CH$_2$N), 53.1 (*C*H$_2$N scaffold), 43.9, 42.5 (CH$_2$N*C*H$_2$CH$_2$*C*H$_2$N), 40.3 (N*C*H$_3$), 36.9 (*C*H$_2$NH), 27.7 (CH$_2$NCH$_2$*C*H$_2$CH$_2$N).

**3-(3-(4-((2-(Bis(2-(3-hydroxy-1-methyl-2-oxo-1,2-dihydropyridine-4-carboxamido)ethyl)amino)ethyl)carbamoyl)-3-hydroxy-2-oxopyridin-1(2H)-yl)propyl)-12-(carboxymethyl)-6,9-dioxa-3,12-diazatetradecane-1,14-dioic   acid (L1)**
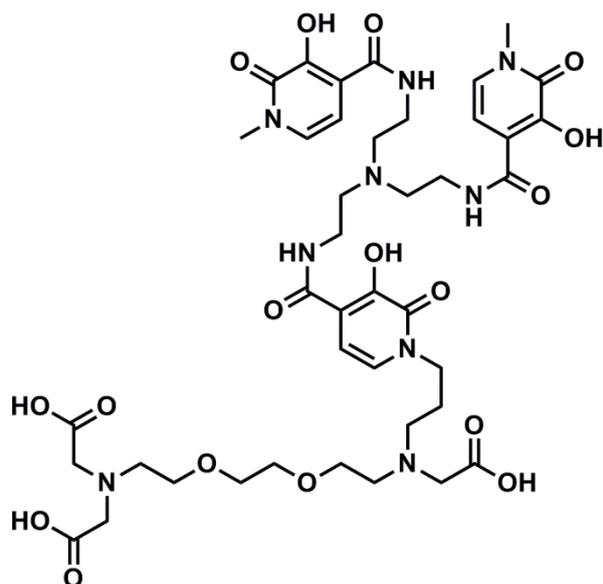


Methyl groups from phenols were removed as published by Kiessling *et al.*[102]

Triacid **31** (51 mg, 0.05 mmol) was dissolved in DMSO under inert atmosphere so the concentration was between 0.4 and 26 mM. Sodium ethanethiolate (32 mg, 0.39 mmol) was added and the reaction mixture was heated at 140 °C for 2 h. After cooling to r.t a 4-fold excess of water was added to quench the thiolate. All solvents were evaporated under reduced pressure to give **L1** as sodium salt which was further purified by HPLC (RT 18.8 min).

**FAB-MS:** (NBA) calc. 947.3, found 472.6 [M-2H]$^{2-}$.

**3-Methoxy-2-oxo-1,2-dihydro-pyridine-4-carboxylic acid (32)**
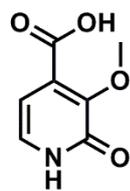
Ester **7** (0.11 g, 0.57 mmol) was dissolved in methanol (10 mL) Potassium hydroxide (0.2 g, 3.52 mmol) was added and the reaction mixture was refluxed for 24 h. After cooling to r.t. the solution was acidified until pH=1 with concentrated HCl. The solvent was evaporated and the brownish residue was dried on high vacuum to give acid **32** (0.3 g, 312% yield) as a fine tan powder due to presence of KCl.

**$^1$H NMR:** (DMSO-d$_6$) δ(ppm): 12.01 (bs, 1H, C(O)O*H*), 7.16 (d, 1H, *J*=6.8 Hz, NHC*H*), 6.17 (d, 1H, *J*=6.8 Hz, CHC*H*C), 3.79 (s, 3H, OC*H*$_3$).

**$^{13}$C NMR:** (DMSO-d$_6$) δ(ppm): 166.5 (*C*(O)OH), 159.0 (C(O) pyridinone), 146.8 (*C*OCH$_3$), 132.5 (*C*C(O)OH), 129.6 (NH*C*H), 102.9 (CH*C*HC), 59.2 (O*C*H$_3$).

**N,N'-(((2-(3-methoxy-2-oxo-1,2-dihydropyridine-4-carboxamido)ethyl)azanediyl)bis(ethane-2,1-diyl))bis(3-methoxy-1-methyl-2-oxo-1,2-dihydropyridine-4-carboxamide) (33)**
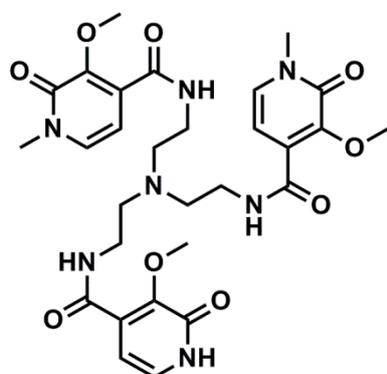
Acid **32** (0.4 g, 2.36 mmol) was dissolved in dry DMF (5 mL) under inert atmosphere and pyridine (0.6 mL, 7.09 mmol) followed by perfluorophenyl 2,2,2-trifluoroacetate (0.6 mL, 3.55 mmol) were slowly added. The reaction mixture was stirred overnight at r.t. The next day the solution was diluted with ethyl acetate and washed with water. The organic phase was dried over sodium sulfate and concentrated under reduced pressure. The crude product was used in the next step without any further purification.

Primary amine **12** (0.27 g, 0.46 mmol) was dissolved in dry DMF (2 mL) under inert atmosphere. DIPEA (0.3 mL, 1.85 mmol) was added and a solution of the activated ester in dry DMF (2 mL) was slowly added. The reaction mixture was stirred at r.t. for 72 h. The solvent was evaporated, the residue dissolved in DCM and washed with water. The organic phase was dried over sodium sulfate, concentrated under

reduced pressure and purified by column chromatography (DCM:MeOH; 90:10) to give tris-HOPO derivative **33** (0.16 g, 56% yield) as a brown oil.

**$^1$H NMR:** (CDCl$_3$) δ(ppm): 10.53 (bs, 1H, N*H* pyridinone), 8.17 (m, 3H, N*H* amide), 7.05 (d, 3H, *J*=7.2 Hz, NC*H*), 6.64 (d, 3H, *J*=7.2 Hz, CH*CH*C), 3.97 (m, 9H, OC*H$_3$*), 3.48 (m, 10H, NC*H$_3$*), 3.05 (m, 6H, NC*H$_2$* scaffold), 2.73 (m, 6H, NHC*H$_2$*).

**$^{13}$C NMR:** (CDCl$_3$) δ(ppm): 163.6 (*C*(O) amide), 159.3, 156.1 (*C*(O) pyridinone), 147.3 (*C*OCH$_3$), 132.2, 130.0 (N*C*H), 104.6 (CH*C*HC), 60.0 (O*C*H$_3$), 53.6, 53.1 (N*C*H$_2$ scaffold), 50.2, 42.0 (N*C*H$_3$), 37.5 (NH*C*H$_2$ scaffold).

## 1-(3-Dibenzylamino-propyl)-3-methoxy-2-oxo-1,2-dihydro-pyridine-4-carboxylic acid ethyl ester (34)
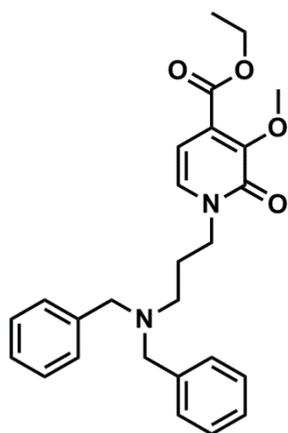
Pyridinone **7** (1.0 g, 5.07 mmol) was dissolved in dry DMF (50 mL) under inert atmosphere. Potassium carbonate (1.75 g, 12.68 mmol) was added and the reaction mixture was stirred at r.t. for 1 h. Then N,N-dibenzyl-3-bromopropan-1-amine[122] (1.94 g, 6.09 mmol) was added and the reaction mixture was heated to 100 °C overnight. The solvent was evaporated under reduced pressure and the residue was dissolved in DCM and washed with water. The organic phase was dried over sodium sulfate, concentrated under reduced pressure and purified by silica gel chromatography (DCM:MeOH; 95:5) to give dibenzylamine **34** (0.96 g, 44% yield) as a brown oil.

**$^1$H NMR:** (acetone-d$_6$) δ(ppm): 7.42-7.22 (m, 13H, Ph), 7.08 (d, 1H, *J*=7.0 Hz, NC*H*), 6.11 (d, 1H, *J*=7.2 Hz, CHC*H*C), 4.32 (m, 2H, C*H$_2$*CH$_3$), 3.99-3.89 (m, 6H, OC*H$_3$*, NC*H2*CH2CH2NBn2), 3.60 (s, 5H, C*H$_2$*Ph), 2.51 (m, 2H, NCH$_2$CH$_2$C*H$_2$*NBn$_2$), 1.96 (m, 3H, NCH$_2$C*H$_2$*CH$_2$NBn$_2$), 1.35 (m, 4H, CH$_2$C*H$_3$*).

**$^{13}$C NMR:** (acetone-d$_6$) δ(ppm): 165.8 (*C*(O) ester), 159.6 (*C*(O) pyrdinone), 148.9 (*C*OCH$_3$), 140.6 (N*C*H), 133.6, 130.9, 129.8, 129.6, 129.1, 129.0, 127.7, 127.6 (Ph, *C*C(O)O), 103.3 (CH*C*HC), 61.9 (*C*H$_2$Ph), 60.0 (*C*H$_2$CH$_3$), 59.0 (O*C*H$_3$), 51.0

(N*CH*$_2$CH$_2$*CH*$_2$NBn$_2$), 48.6 (N*CH*$_2$CH$_2$CH$_2$NBn$_2$), 27.1 (NCH$_2$*CH*$_2$CH$_2$NBn$_2$), 14.5 (CH$_2$*CH*$_3$).

**ESI-MS:** calc. 434.2, found 435.1 [M+H]$^+$, 457.1 [M+Na]$^+$, 473.1 [M+K]$^+$.

**1-(3-Dibenzylamino-propyl)-4-dihydroxymethyl-3-methoxy-1*H*-pyridin-2-one (35)**
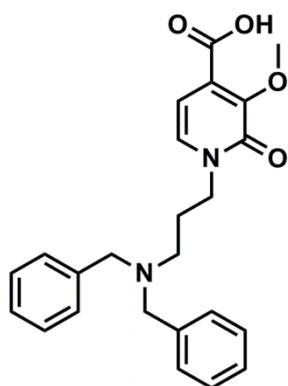


Ester **34** (0.71 g, 1.64 mmol) was suspended in water (100 mL). Sodium hydroxide (3.29 g, 82 mmol) was added and the suspension was heated at reflux overnight. After cooling down to r.t the pH was adjusted to 1. The crude product was extracted with ethyl acetate. The organic phase was dried over sodium sulfate and concentrated under reduced pressure to give the acid **35** (0.45 g, 67% yield) as a brown oil which was used in the next reaction without further purification.

**$^1$H NMR:** (acetone-d$_6$/CDCl$_3$) δ(ppm): 7.51-7.25 (m, 18H, Ph), 6.93 (s, 1H, NC*H*), 6.22 (s, 1H, CHC*H*C), 3.99-3.90 (m, 11H, NC*H*$_2$, OC*H*$_3$, C*H*$_2$Ph), 2.71 (s, 3H, C*H*$_2$NBn), 1.92 (s, CH$_2$C*H*$_2$CH$_2$)

**$^{13}$C NMR:** (acetone-d$_6$/CDCl$_3$) δ(ppm): 177.6 (*C*(O) acid), 171.1 (*C*OCH3), 164.3 (*C*(O) pyridinone), 153.1 (CHCH*C*), 137.4 (N*C*H), 135.4, 133.9, 133.6 (Ph), 109.5 (CH*C*HC), 65.4 (*C*H2Ph), 62.9 (O*C*H$_3$), 54.4 (*C*H$_2$NBn), 52.7 (N*C*H$_2$), 30.1, 25.5 (CH$_2$*C*H$_2$CH$_2$).

**ESI-MS:** calc. 406.2, found 405.0[M-H]$^-$.

**N,N'-(((2-(1-(3-(Dibenzylamino)propyl)-3-methoxy-2-oxo-1,2-dihydropyridine-4-carboxamido)ethyl)azanediyl)bis(ethane-2,1-diyl))bis(3-methoxy-1-methyl-2-oxo-1,2-dihydropyridine-4-carboxamide) (36)**
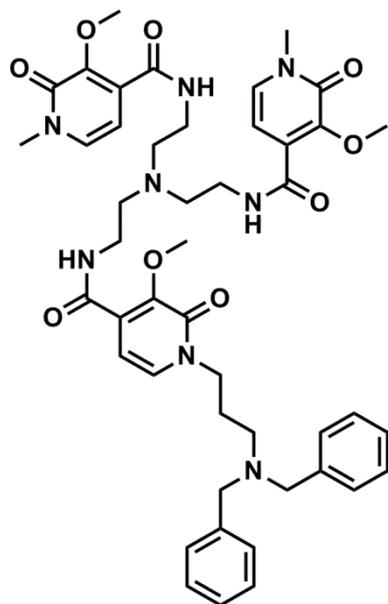
Pyridine (0.27 mL, 3.32 mmol) was added to the crude acid **35** (0.45 g, 1.11 mmol) dissolved in dry DMF (5 mL) under inert atmosphere. Perfluorophenyl 2,2,2-trifluoroacetate (0.25 mL, 1.44 mmol) was added dropwise. The solution was stirred at r.t. overnight. The next day it was diluted with ethyl acetate and washed with water. The organic phase was dried over sodium sulfate and concentrated to dryness to give crude active ester as a brown oil which was used in the next step without further purification.

Amine **12** (0.31 g, 0.52 mmol) was dissolved in dry DMF (2 mL) under inert atmosphere and DIPEA (0.4 mL, 2.10 mmol) was added before a solution of the activated ester in dry DMF (2 mL) was added dropwise. The solution was stirred overnight at r.t. The solvent was evaporated under reduced pressure. The residue was dissolved in DCM and washed with water. The organic phase was dried over sodium sulfate, concentrated under reduced pressure and purified by column chromatography (DCM:MeOH; 90:10) to give amide **36** (0.24 g, 53% yield) as a brown foam.

**$^1$H NMR:** (acetone-d$_6$) δ(ppm): 7.26-7.06 (m, 13H, Ph), 6.88 (t, 1H, $J$=6.7, NC*H*), 6.40-6.22 (m, 3H, CHC*H*C), 3.89-3.76 (m, 11H, OC*H$_3$*, NC*H$_2$*CH$_2$CH$_2$NBn$_2$), 3.45-3.30 (m, 16H, NC*H$_3$*, NHC*H$_2$* scaffold, C*H$_2$*Bn), 2.73-2.59 (m, 7H, NC*H$_2$* scaffold), 2.33 (t, 2H, $J$=6.6Hz, NCH$_2$CH$_2$C*H$_2$*NBn$_2$), 1.84-1.73 (m, 3H, NCH$_2$C*H$_2$*CH$_2$NBn$_2$).

**$^{13}$C NMR:** (acetone-d$_6$) δ(ppm): 170.4, 164.3, 164.2, 164.1(C(O) amide), 159.8, 159.3 (C(O) pyridinone), 147.9, 147.8, 147.7 (*C*OCH$_3$), 140.5, 133.6, 133.0, 131.4, 129.8, 129.1, 127.8 (Ph, N*C*H, CHCH*C*,), 104.3, 104.2 (CH*C*HC), 60.1 (*C*H$_2$Bn), 58.9 (O*C*H$_3$), 54.5, 54.4, 54.0 (N*C*H$_2$CH$_2$CH$_2$NBn$_2$), 51.04, 49.8, 48.5 (N*C*H$_2$ scaffold, NCH$_2$*C*H$_2$*C*H$_2$NBn$_2$), 38.6, 37.4 (N*C*H$_3$, NH*C*H$_2$ scaffold), 27.1 (NCH$_2$*C*H$_2$CH$_2$NBn$_2$).

**ESI-MS:** calc. 864.4, found 865.3 [M+H]$^+$, 887.2 [M+Na]$^+$, 903.2 [M+K]$^+$.

## 1-[3-(1,3-Dioxo-1,3-dihydro-isoindol-2-yl)-propyl]-3-methoxy-2-oxo-1,2-dihydro-pyridine-4-carboxylic acid methyl ester (37)
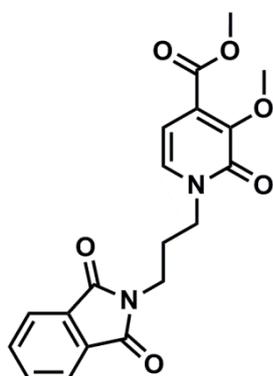


Pyridinone **7** (0.5 g, 2.73 mmol) was dissolved in dry DMF (20 mL) under inert atmosphere. Potassium carbonate (1.13 g, 8.19 mmol) was added and the reaction mixture was stirred at r.t. for 1 h. Then 2-(3-bromopropyl)isoindoline-1,3-dione (1.46 g, 5.46 mmol) was added. The reaction was stirred at 100 $^0$C for 24 h. The solvent was evaporated under reduced pressure, the residue was dissolved in DCM and washed with water. The organic phase was dried over sodium sulfate and concentrated under reduced pressure. The residue was purified by column chromatography (DCM:acetone; 6:1) to give phthalimide **37** as a cream amorphous powder (0.5 g, 50% yield).

**$^1$H NMR**: (acetone-d$_6$) δ (ppm): 7.73-7.63 (5H, m, Ph), 7.32 (1H, d, *J*=7.2 Hz, NC*H*), 6.20 (1H, d, *J*=7.2 Hz, CHC*H*C), 3.97 (2H, t, *J*=7.0 Hz, NC*H$_2$*), 3.84 (3H, s, OC*H$_3$*), 3.76 (3H, s, C*H$_3$* ester), 3.65 (2H, t, *J*=6.6 Hz, C*H$_2$*pht), 2.07 (2H, t, *J*=7.2 Hz, NCH$_2$C*H$_2$*CH$_2$N)).

**$^{13}$C NMR**: (acetone-d$_6$) δ (ppm): 168.9 (*C*(O) ester), 166.0 (C(O) pht), 159.9 (C(O) pyridinone), 149.6 (*C*OCH$_3$), 134.9 (N*C*H), 133.0, 130.3, 123.9 (Ph), 114.9 (*C*C(O)O), 104.3, (CH*C*HC), 60.6 (O*C*H$_3$ ether), 53.0 (C(O)O*C*H$_3$), 48.4 (N*C*H$_2$CH$_2$CH$_2$Npht), 35.0 (NCH$_2$CH$_2$*C*H$_2$Npht), 28.8 (NCH$_2$*C*H$_2$CH$_2$Npht).

## 1-(3-Benzyloxycarbonylamino-propyl)-3-methoxy-2-oxo-1,2-dihydro-pyridine-4-carboxylic acid ethyl ester (38)
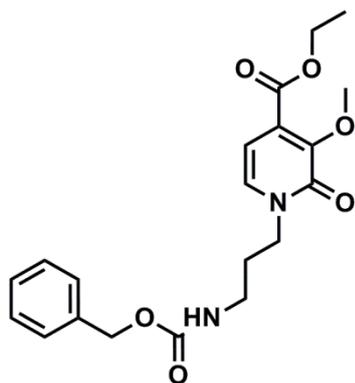


Comound **7** (1.0 g, 5.07 mmol) was dissolved in dry DMF (50 mL) under inert atmosphere. Potassium carbonate (2.1 g, 15.2 mmol) was added and the suspension was stirred at r.t for 1 h. Then potassium iodide (0.42 g, 2.54 mmol) followed by benzyl (3-bromopropyl)carbamate (1.66 g, 6.09 mmol) were added and the reaction mixture

was stirred at 100 °C for 24h. The solvent was evaporated and the residue was dissolved in DCM and washed with water. The organic phase was dried over sodium sulfate, concentrated under reduced pressure and purified by column chromatography (DCM:MeOH; 95:5) to give carbamate **38** (0.9 g, 46% yield) as a brown oil.

**$^{1}$H NMR:** (acetone-d$_6$) δ(ppm): 7.31-7.16 (m, 6H, Ph, NC*H*), 6.38 (m, 1H, N*H* carbamate), 6.14 (d, 1H, *J*=7.2Hz, CHC*H*C), 4.93 (s, 2H, NCH$_2$CH$_2$C*H$_2$*NH), 4.16 (q, 2H, *J*=7.2 Hz, NC*H$_2$*CH$_2$CH$_2$NH), 3.90 (t, 2H, *J*=7.0 Hz, C*H$_2$*CH$_3$), 3.76 (s, 3H, OC*H$_3$*), 3.04 (q, 2H, *J*=6.4Hz, C*H$_2$*Ph), 1.79 (kw, 2H, *J*=6.8 Hz, NCH$_2$C*H$_2$*CH$_2$NH), 1.18 (t, 3H, *J*=7.2 Hz, CH$_2$C*H$_3$*).

**$^{13}$C NMR:** (acetone-d$_6$) δ(ppm): 165.7 (*C*(O) ester), 159.9 (C(O) carbamate), 157.3 (C(O) pyridinone), 148.9 (*C*OCH$_3$), 138.4, 133.7, 131.2, 129.2, 128.7, 128.6 (Ar*C*H), 103.9 (CH*C*HC), 66.5 (*C*H$_2$Ph), 62.0 (*C*H$_2$CH$_3$), 60.2 (O*C*H$_3$), 47.7 (N*C*H$_2$CH$_2$CH$_2$NH), 38.6 (NCH$_2$CH$_2$*C*H$_2$NH), 29.1 (NCH$_2$*C*H$_2$CH$_2$NH), 14.5 (CH$_2$*C*H$_3$).

**ESI-MS:** calc. 388.2, found 411.0 [M+Na]$^{+}$.

## 1-(3-*tert*-Butoxycarbonylamino-propyl)-3-methoxy-2-oxo-1,2-dihydro-pyridine-4-carboxylic acid ethyl ester (40)
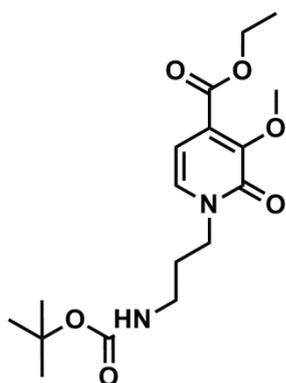


Pyridinone **7** (0.5 g, 2.54 mmol) was dissolved in dry DMF (30 mL) under inert atmosphere. Potassium carbonate (1.05 g, 7.61 mmol) was added and the suspension stirred for 1 h at r.t. Potassium iodide (0.21 g, 1.268 mmol) followed by *tert*-butyl (3-bromopropyl)carbamate[123] (0.91 g, 3.80 mmol) were added and the reaction mixture was stirred at 100 °C for 24 h. The solvent was evaporated under reduced pressure, the residue was dissolved in DCM and washed with water. The organic phase was dried over sodium sulfate, concentrated under reduced pressure and purified by column chromatography (DCM:MeOH; 95:5) to give carbamate **40** (0.5 g, 56% yield) as a brown oil.

**¹H NMR:** (CDCl₃) δ (ppm): 7.10 (d, 1H, *J*=7.2Hz, NC*H*), 6.28 (d, 1H, *J*=7.2Hz, CHC*H*C), 4.27 (m, 2H, C*H₂*CH₃), 3.94 (m, 5H, NC*H₂*CH₂CH₂NH, OC*H₃*), 3.03 (m, 2H, NCH₂CH₂C*H₂*NH), 1.83 (m, 2H, NCH₂C*H₂*CH₂NH), 1.30 (m, 14H, C(C*H₃*)₃, CH₂C*H₃*).

**¹³C NMR:** (CDCl₃) δ (ppm): 164.7 (*C*(O) ester), 159.7 (C(O) carbamate), 157.7, 156.0(C(O) pyridinone), 148.1 (*C*OCH₃), 141.2, 135.1, 131.6 (N*C*H), 129.9, 128.4 (CH*C*HC), 104.5 (CH*C*HC), 78.9 (*C*(CH₃)₃), 65.1, 61.6 (*C*H₂CH₃), 60.2 (O*C*H₃), 46.9 (N*C*H₂CH₂CH₂NH), 36.8 (NCH₂CH₂*C*H₂NH), 29.7 (NCH₂*C*H₂CH₂NH), 28.3 (C(*C*H₃)₃), 14.0 (CH₂*C*H₃).

**ESI-MS:** calc. 354.2, found 355.2 [M+H]⁺, 363.1 [M+Li]⁺, 377.2 [M+Na]⁺.

**HR-MS:** calc. 377.16831 [M+Na]⁺, found 377.16807 [M+Na]⁺.

**1-(3-Amino-propyl)-3-methoxy-2-oxo-1,2-dihydro-pyridine-4-carboxylic acid ethyl ester (39)**
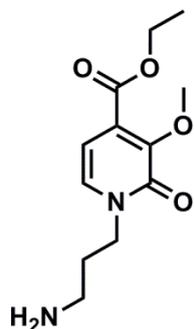


Carbamate **40** (0.5 g, 1.41 mmol) was dissolved in dry DCM (5 mL) under inert atmosphere and cooled to 0 °C. Trifluoroacetic acid (0.87 ml, 11.3 mmol) was added and the solution was stirred at r.t. for 3h. The solvent was evaporated and the crude amine salt **39** (0.53 g, 102 % yield) as a brown oil was used in the next step without further purification.

**¹H NMR:** (CDCl₃) δ(ppm): 7.15 (d, 1H, *J*=7.2 Hz, NC*H*), 6.42 (d, 1H, *J*=7.2 Hz, CHC*H*C), 5.58 (bs, 2H, N*H₂*), 4.27 (q, 2H, *J*=7.0, 7.2 Hz, C*H₂*CH₃), 4.03 (m, 2H, NC*H₂*CH₂CH₂NH₂), 3.80 (s, 3H, OC*H₃*), 2.93 (m, 2H, NCH₂CH₂C*H₂*NH₂), 2.08 (m, 2H, NCH₂C*H₂*CH₂NH₂), 1.29 (t, 3H, *J*=7.2 Hz, CH₂C*H₃*).

**¹³C NMR:** (CDCl₃) δ(ppm): 164.2 (*C*(O) ester), 160.8 (*C*(O) pyridinone), 148.6 (*C*OCH₃), 131.6 (CH*C*HC), 131.2 (*C*HCHC), 106.7 (CH*C*HC), 62.1 (*C*H₂CH₃), 60.8 (O*C*H₃), 46.6 (N*C*H₂CH₂CH₂NH₂), 37.1, 36.7 (NCH₂CH₂*C*H₂NH₂), 31.9, 27.0 (NCH₂*C*H₂CH₂NH₂), 13.9, 13.8 (CH₂*C*H₃).

**ESI-MS:** calc. 254.1, found 255.0 [M+H]⁺.

**HR-MS:** calc. 255.13393 [M+H]⁺, found 255.13380 [M+H]⁺.

**(3-{4-[2-(Bis-{2-[(3-methoxy-1-methyl-2-oxo-1,2-dihydro-pyridine-4-carbonyl)-amino]-ethyl}-amino)-ethylcarbamoyl]-3-methoxy-2-oxo-2*H*-pyridin-1-yl}-propyl)-carbamic acid *tert*-butyl ester (42)**



intermediate 41                     42
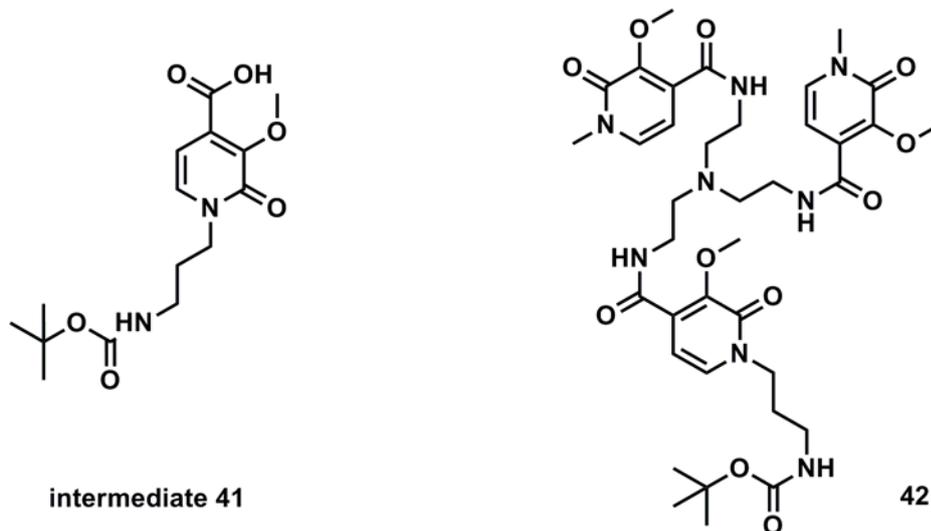
Ester **40** (0.66 g, 1.88 mmol) was dissolved in water (50 mL). Sodium hydroxide (3.76 g, 94 mmol) was added and the solution was stirred at reflux overnight. After cooling to r.t the pH was adjusted to 1 and the acid was extracted with ethyl acetate. The organic phase was dried over sodium sulfate and concentrated to dryness to give the intermediate acid **41** (0.15 g, 25% yield) as a brown oil which was used in next step without any further purification.

The crude acid **41** (0.15 g, 0.47 mmol) was dissolved in dry DMF (5 mL) under inert atmosphere. Pyridine (0.11 mL, 1.41 mmol) followed by perfluorophenyl 2,2,2-trifluoroacetate (0.12 mL, 0.70 mmol) were added and the solution was stirred at r.t overnight. The solution was diluted with ethyl acetate and washed with water. The organic phase was dried over sodium sulfate and concentrated to dryness to give the activated ester as a brown oil which was used in the next step without further purification.

Amine **12** (0.14 g, 0.24 mmol) and DIPEA (0.16 mL, 0.94 mmol) were dissolved in dry DMF (2 mL). A solution of the activated ester in dry DMF (2 mL) was added dropwise and the reaction mixture was stirred at r.t. overnight. The solvent was evaporated, the residue dissolved in DCM and washed with water. The organic

phase was dried over sodium sulfate, evaporated under reduced pressure and purified by column chromatography (DCM:MeOH; 90:10) to give amide **42** (0.04 g, 22% yield) as a brown oil.

**$^1$H NMR:** (acetone-d$_6$) δ(ppm): 7.28-7.19 (dd, 3H, *J*=7.2, 18.7 Hz, NC*H*), 6.42-6.35 (dd, 3H, *J*=7.1, 14.9 Hz, CHC*H*C), 3.91-3.28 (m, 12H, OC*H$_3$*, NC*H$_2$*CH$_2$CH$_2$NH), 3.43-3.35 (m, 12H, NC*H$_3$*, NCH$_2$CH$_2$C*H$_2$*NH), 2.97-2.63 (m, 13H, C*H$_2$* scaffold), 1.79-1.75 (m, 2H, NCH$_2$C*H$_2$*CH$_2$NH), 1.28 (s, 9H, C(C*H$_3$*)$_3$).

**$^{13}$C NMR:** (acetone-d$_6$) δ(ppm): 164.2 (C(O) amide), 159.8, 159.7 (C(O) carbamate), 156.7 (C(O) pyridinone), 147.8, 147.7 (*C*OCH$_3$), 133.6, 132.9 (N*C*H), 131.3 (CH*C*HC), 104.7, 104.2, 104.1 (CH*C*HC), 78.6 (*C*(CH$_3$)$_3$), 60.2, 60.1 (O*C*H$_3$), 54.0 (N*C*H$_2$ scaffold), 47.5 (N*C*H$_2$CH$_2$CH$_2$NH), 39.7 (N*C*H$_3$), 38.5, 38.1 (NCH$_2$*C*H$_2$CH$_2$NH), 37.3 (*C*H$_2$NH scaffold), 28.6 (C(*C*H$_3$)$_3$).

**ESI-MS:** calc. 784.4, found 785.2 [M+H]$^+$, 807.2 [M+Na]$^+$, 823.2 [M+K]$^+$.

## 1-[3-(2-Bromo-acetylamino)-propyl]-3-methoxy-2-oxo-1,2-dihydro-pyridine-4-carboxylic acid ethyl ester (43)
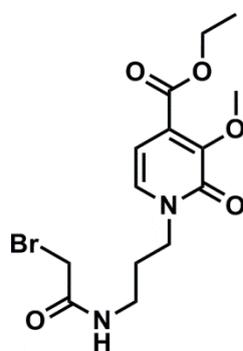


Amine **39** (0.6 g, 1.63 mmol) was dissolved in DCM (50 mL). Solution of potassium carbonate (0.22 g, 1.63 mmol) in water (50 mL) was added and the biphasic mixture was cooled to 0 °C. Bromoacetyl bromide (0.42 mL, 4.89 mmol) in dry DCM (5 mL) was added dropwise until pH reached 5. Then the pH was re-adjusted to 7 with 1.6 M water solution of potassium carbonate and the addition of bromoacetyl bromide in DCM was continued.

After all bromoacetyl bromide was added, the reaction mixture was stirred at r.t for 5 h. The phases were separated and the organic phase was additionally washed water. The organic phase was dried over sodium sulphate and concentrated under reduced pressure. The crude bromoacetyl derivative **43** (0.4 g, 65 % yield) as a yellow oil was used in the next step without further purification.

**$^1$H NMR:** (CDCl$_3$) δ (ppm): 7.03 (d, 1H, *J*=7.2 Hz, NC*H*), 6.33 (d, 1H, *J*=7.2 Hz, CHC*H*C), 4.30 (q, 2H, *J*=7.0 Hz, C*H$_2$*CH$_3$), 3.97 (m, 5H, OC*H$_3$*, NC*H$_2$*CH$_2$CH$_2$NH),

3.80 (s, 2H, C$H_2$Br), 3.20 (q, 2H, $J$=6.2 Hz, NCH$_2$CH$_2$C$H_2$NH), 1.88 (quin, 2H, $J$=6.2 Hz, NCH$_2$C$H_2$CH$_2$NH), 1.31 (m, 3H, CH$_2$C$H_3$).

**$^{13}$C NMR:** (CDCl$_3$) δ (ppm): 166.2 ($C$(O) amide), 164.7 ($C$(O) ester), 160.1 ($C$(O) pyridinone), 149.0 ($C$OCH$_3$), 131.2 (N$C$H), 130.2 (CH$C$HC), 105.0 (CH$C$HC), 61.8 ($C$H$_2$CH$_3$), 60.4 (O$C$H$_3$), 53.4, 46.6 (N$C$H$_2$CH$_2$$C$H$_2$NH), 36.2 (NCH$_2$$C$H$_2$CH$_2$NH), 29.2 ($C$H$_2$Br), 29.0 (NCH$_2$$C$H$_2$CH$_2$NH), 14.1 (CH$_2$$C$H$_3$).

**ESI-MS:** calc. 394.0, found 413.0 [M+K]$^+$.

**HR-MS:** calc. 397.036955 [M+Na]$^+$, found 397.037139 [M+Na]$^+$.

### 1-{3-[2-(Benzyl-{2-[2-(2-dibenzylamino-ethoxy)-ethoxy]-ethyl}-amino)-acetylamino]-propyl}-3-methoxy-2-oxo-1,2-dihydro-pyridine-4-carboxylic acid ethyl ester (44)
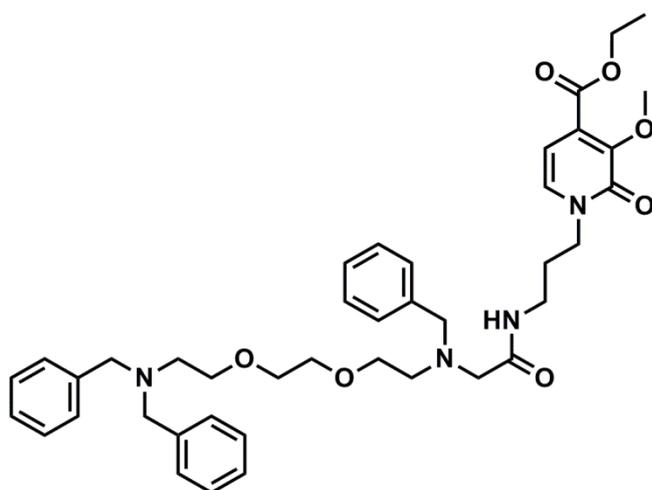


Compound **25** (0.67 g, 1.60 mmol) was dissolved in dry DMF (10 mL) under inert atmosphere. Potassium carbonate (0.33 g, 2.40 mmol) was added and the suspension was stirred at r.t. for 2 h. Compound **43** (0.3 g, 0.80 mmol) in dry DMF (10 mL) was added and the reaction mixture was stirred at r.t. overnight. The solvent was evaporated, the residue was dissolved in DCM and washed with water. The organic phase was dried over sodium sulfate, evaporated under reduced pressure and purified by column chromatography (DCM:MeOH; 98:2) to give **44** (0.3 g, 53% yield) as a brown oil.

**$^1$H NMR:** (acetone-d$_6$) δ(ppm): 7.61 (m, 17H, Ph, NC$H_2$), 6.28 (d, 1H, $J$=7.0 Hz, CHC$H$C), 4.32 (q, 2H, $J$=7.0 Hz, C$H_2$CH$_3$), 3.97 (m, 5H, OC$H_3$, NC$H_2$CH$_2$CH$_2$NH), 3.6 (m, 14H, C$H_2$Ph, C$H_2$O), 3.19 (q, 2H, $J$=6.4 Hz, NCH$_2$CH$_2$C$H_2$NH), 3.07 (s, 2H, C$H_2$C(O)), 2.69 (dt, 4H, $J$=5.5, 21.9 Hz, C$H_2$NBn$_2$, C$H_2$NBn), 1.87 (m, 2H, NCH$_2$C$H_2$CH$_2$NH), 1.34 (t, 3H, $J$=7.0 Hz, CH$_2$C$H_3$).

**$^{13}$C NMR:** (acetone-d$_6$) δ(ppm): 171.3 (C(O) amide), 165.5 (C(O) ester), 159.6 (C(O) pyridinone), 148.6 (COCH$_3$), 140.6, 139.7 (Ph), 133.5, 131.0, 129.6, 129.3, 128.7, 127.4 (aromatic CH), 103.5 (CHCHC), 70.8, 70.1, 69.6 (OCH$_2$), 61.7 (OCH$_3$), 59.7 (CH2C(O)NH), 59.2 (CH$_2$CH$_3$), 58.7, 55.2 (CH$_2$Ph), 53.2 (CH$_2$NBn$_2$), 47.5 (NCH$_2$CH$_2$CH$_2$NH), 36.0 (NCH$_2$CH$_2$CH$_2$NH), 28.8 (NCH$_2$CH$_2$CH$_2$NH), 14.2 (CH$_2$CH$_3$).

**ESI-MS:** calc. 712.4, found 713.4 [M+H]$^+$.

**HR-MS:** calc. 713.39088 [M+H]$^+$, 735.37282 [M+Na]$^+$, found 713.39122 [M+H]$^+$, 735.37277 [M+Na]$^+$.

**1-{3-[2-(Benzyl-{2-[2-(2-dibenzylamino-ethoxy)-ethoxy]-ethyl}-amino)-acetylamino]-propyl}-3-methoxy-2-oxo-1,2-dihydro-pyridine-4-carboxylic acid (45)**
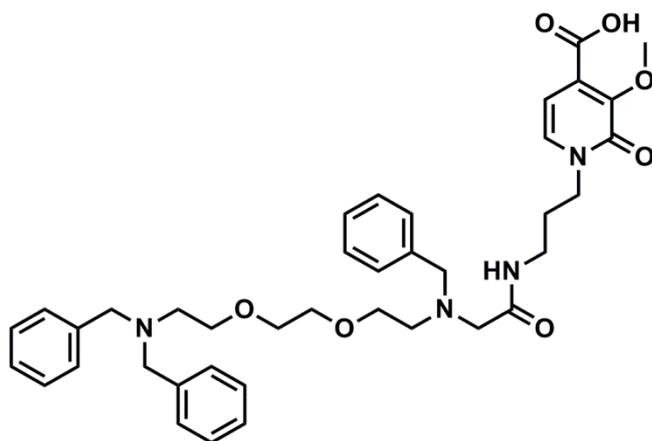


Ester **44** (0.3 g, 0.42 mmol) was suspended in water (25 mL) and potassium hydroxide (1.18 g, 21.0 mmol) was added. The solution was heated at reflux overnight. The pH of the solution was adjusted to 1 and the crude product was extracted with ethyl acetate. The organic phase were dried over sodium sulfate and evaporated under reduced ressure to give crude acid **45** (0.28 g, 99% yield) as a brown oil.

**$^1$H NMR:** (acetone-d$_6$) δ (ppm): 7.42 (m, 1H, NH amide), 7.32-7.04 (m, 17H, Ph), 3.83-3.35 (m, 18H, alkyl), 3.02-2.90 (m, 2H, CH$_2$C(O)), 2.58-2.46 (m, 4H, CH$_2$N), 1.81-1.68 (m, 2H, NCH$_2$CH$_2$CH$_2$NH).

**$^{13}$C NMR:** (acetone-d$_6$) δ (ppm): 170.6 (C(O) amide), 169.8 (C(O) acid), , 158.7 (C(O) pyridinone), 139.5, 138.3, 135.9, 131.5, 129.1, 127.9, 127.3, 125.9, (Ph), 117.0, 115.9 (CHCHC), 103.3 (CHCHC), 69.4, 68.6, 68.0 (CH$_2$O), 65.9 (CH$_2$C(O)),

58.3, 57.7, 57.3 (O*C*H$_3$), 53.7 (*C*H$_2$N), 51.8 (*C*H$_2$Ph), 47.9 (N*C*H$_2$CH$_2$CH$_2$NH), 34.4 (NCH$_2$*C*H$_2$CH$_2$NH), 19.0 (NCH$_2$*C*H$_2$CH$_2$NH).

**ESI-MS:** calc. 684.4, found 685.4 [M+H]$^+$, 683.3 [M-H]$^-$.

**HR-MS:** calc. 685.35959 [M+H]$^+$, found 685.35936 [M+H]$^+$.

**N,N'-(((2-(1-(2,11-Dibenzyl-13-oxo-1-phenyl-5,8-dioxa-2,11,14-triazaheptadecan-17-yl)-3-methoxy-2-oxo-1,2-dihydropyridine-4-carboxamido)ethyl)azanediyl)bis(ethane-2,1-diyl))bis(3-methoxy-1-methyl-2-oxo-1,2-dihydropyridine-4-carboxamide) (46)**
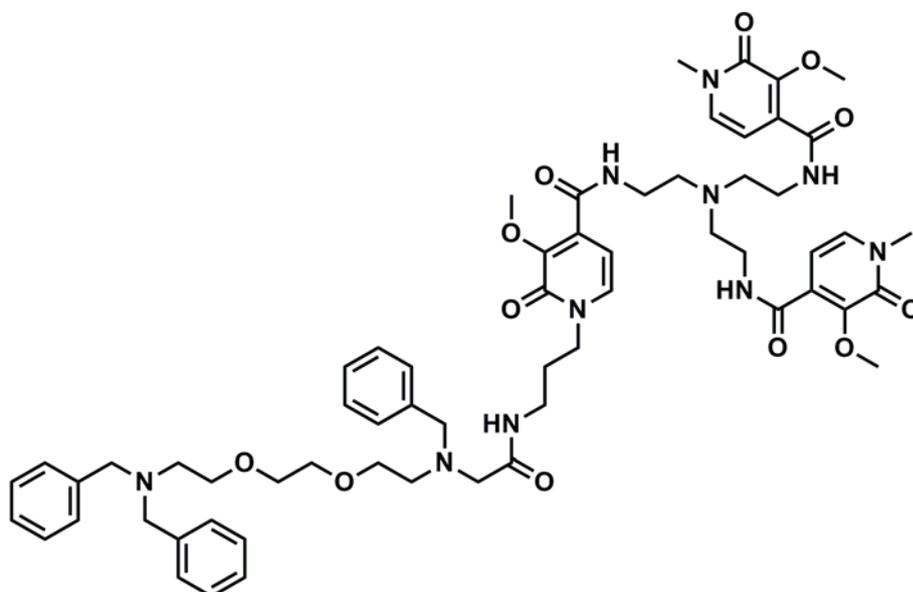


Crude acid **45** (0.45 g, 0.66 mmol) was dissolved under inert atmosphere in dry DMF (5 mL). Pyridine (0.16 mL, 1.97 mmol) followed by perfluorophenyl 2,2,2-trifluoroacetate (0.16 mL, 0.92 mmol) were added and the solution was stirred overnight. The next day the reaction mixture was diluted with ethyl acetate and the organic phase was washed with water, dried over sodium sulfate and evaporated under reduced pressure to give the crude activated ester which was used in the next step without further purification.

Amine **12** (0.20 g, 0.34 mmol) and DIPEA (0.23 mL, 1.34 mmol) were dissolved in dry DMF (2 mL) under inert atmosphere and a solution of the activated ester in dry

DMF 92 mL) was added. The reaction mixture was stirred at r.t overnight. The next day the solvent was evaporated, the residue dissolved in DCM and washed with water. The organic phase was dried over sodium sulfate, concentrated under reduced pressure and purified by column chromatography (DCM:MeOH; 90:10) to give amide **46** (0.18 g, 47% yield) as a brown oil.

**¹H NMR:** (acetone-d$_6$) δ (ppm): 7.70-7.30 (m, 18H, Ph), 6.42-6.34 (m, 3H, CHC*H*C), 3.88-3.78 (m, 10H, OC*H$_3$*, NC*H$_2$*CH$_2$CH$_2$NH), 3.58-2.93 (m, 33H, alkyl C*H$_2$*), 2.74-2.51 (m, 10H, C*H$_2$*N), 1.72 (m, 2H, NCH$_2$C*H$_2$*CH$_2$NH).

**¹³C NMR:** (acetone-d$_6$) δ (ppm): 171.3 (*C*(O) amide), 164.2, 164.1(*C*(O) scaffold amide), 159.8, 159.7 (*C*(O) pyridinone), 147.9, 147.7 (*C*OCH$_3$), 140.0, 133.6, 131.5, 131.3, 129.8, 129.8, 129.6, 129.0, 127.6 (Ph), 104.7, 104.2 (CH*C*HC), 71.1, 70.3, 69.9 (*C*H$_2$O), 60.2, 60.1, 59.4, 59.0, 55.4, 54.1 (*C*H$_2$N), 53.4 (O*C*H$_3$), 47.6 (N*C*H$_2$CH$_2$CH$_2$NH), 38.5, 37.3, 36.2, 36.1 (*C*H$_2$NH), 30.6 (N*C*H$_3$), 25.7 (NCH$_2$*C*H$_2$CH$_2$NH).

**ESI-MS:** calc. 1142.6, found 1143.5 [M+H]⁺.

**HR-MS:** calc. 1143.58734 [M+H]⁺, found 1143.58646 [M+H]⁺.

**Di-*tert*-butyl-3-(2-((3-(4-((2-(bis(2-(3-methoxy-1-methyl-2-oxo-1,2-dihydropyridine-4-carboxamido)ethyl)amino)ethyl)carbamoyl)-3-methoxy-2-oxopyridin-1(2*H*)-yl)propyl)amino)-2-oxoethyl)-12-(2-(*tert*-butoxy)-2-oxoethyl)-6,9-dioxa-3,12-diazatetradecane-1,14-dioate (48)**



**intermediate 47**
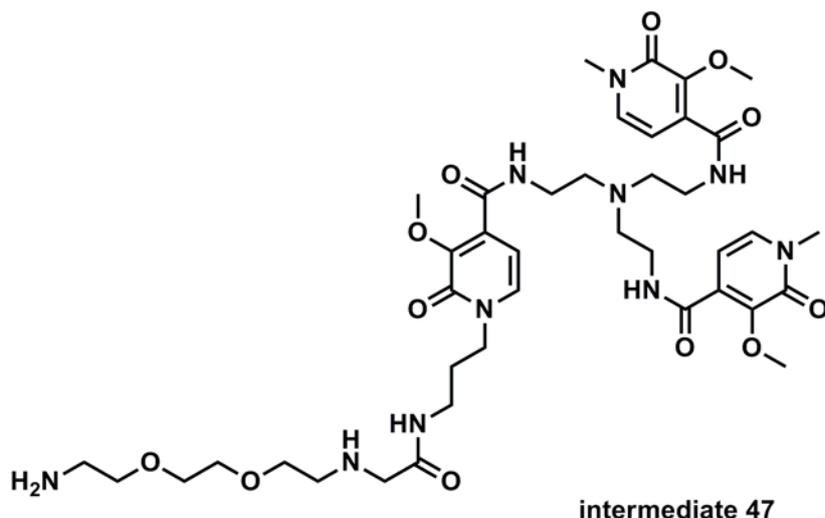
Tribenzylamine **46** (0.18 g, 0.16 mmol) was dissolved in methanol (20 mL). Palladium on carbon (0.017 g, 0.157 mmol) and ammonium formate (0.59 g, 9.45 mmol) were added and the reaction was refluxed overnight. The suspension was filtered through a pad of celite and the filtrate was evaporated under reduced pressure to give amine **47** as yellow oil which was used in the next reaction without any purification.

**ESI-MS:** calc. 872.4, found 873.5 [45%, M$^+$].



**48**
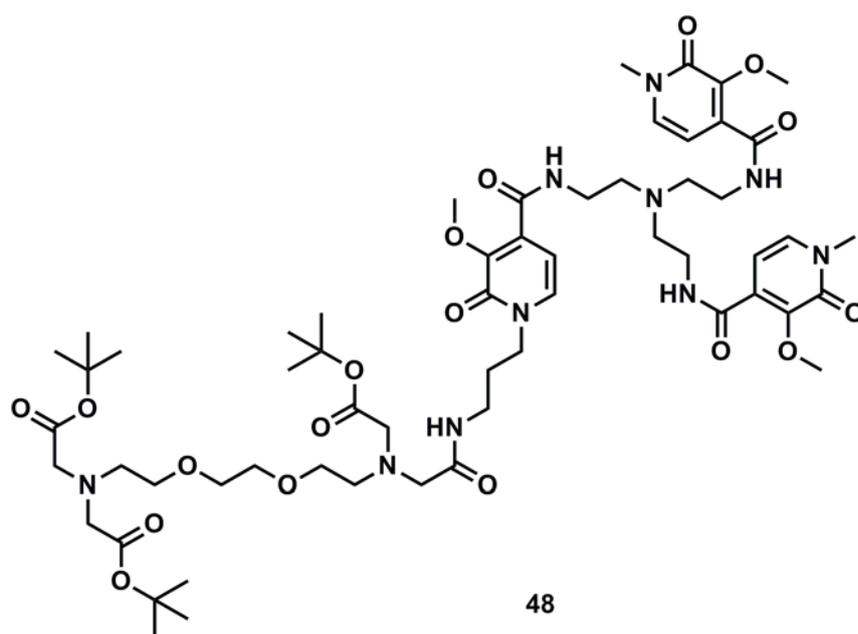
Amine **47** (0.13 g, 0.16 mmol) was dissolved in dry DMF (5 mL) under inert atmosphere. Potassium carbonate (0.19 g, 1.39 mmol) was added and the suspension was stirred for 1 h at r.t. Then *tert*-butyl bromoacetate (0.1 mL, 0.62 mmol) was added and the reaction mixture was stirred for 4 days at r.t. The solvent was evaporated, the residue dissolved in DCM and washed with water. The organic phase was dried over sodium sulfate, evaporated under reduced pressure and purified by column chromatography (DCM:MeOH; 90:10) to give triester **48** (0.11 g, 56% yield) as a brown oil.

**$^1$H NMR:** (acetone-d$_6$) δ (ppm): 8.12 (bs, 3H, aromatic N*H*); 7.21 (d, 3H, *J*=7.37 Hz, NC*H*)); 6.41 (d, 3H, J=7.18 Hz, CHC*H*C); 5.81 (bs, 1H, aliphatic N*H*); 3.83-3.92 (m, 10H, OC*H$_3$*, NC*H$_2$*CH$_2$CH$_2$NH); 3.47-3.34 (m, 18H, NC*H$_3$*, C*H$_2$*C(O), C*H$_2$*O); 3.11-

3.05 (m, 4H, OC$H_2$C$H_2$O); 2.72-2.57 (m, 19H, C$H_2$N, C$H_2$NH); 1.32-1.16 (m, 30H, NCH$_2$C$H_2$CH$_2$NH, C(C$H_3$)$_3$).

**$^{13}$C NMR:** (CDCl$_3$) δ (ppm): 173.0, 172.8, 172.6, 171.4 (C(O)NH), 165.3, 162.8 (C(O) pyridinone), 133.8 (COCH$_3$), 129.7, 129.0 (NCH$_2$), 127.8 (CHCHC), 104.2 (CHCHC), 85.1, 82.2, 81.8, 81.7, 81.0, 80.9 (C(CH$_3$)$_3$), 70.8, 70.6, 70.6, 70.4, 70.4, 70.2 (OCH$_2$), 69.3, 69.1, 68.5, 65.1, 62.3, 59.8, 59.6, 58.4, 58.0, 57.0, 56.9, 56.6, 56.3, 55.8, 55.0, 54.4, 53.9, 49.7 (CH$_2$N), 36.2 (CH$_2$NH), 31.1 (NCH$_3$), 28.3, 28.2 (C(CH$_3$)$_3$), 12.3 (NCH$_2$CH$_2$CH$_2$NH).

**ESI-MS:** calc. 1214.6, found 1253.7 [M+Na]$^+$.

**3-(2-((3-(4-((2-(bis(2-(3-methoxy-1-methyl-2-oxo-1,2-dihydropyridine-4-carboxamido)ethyl)amino)ethyl)carbamoyl)-3-methoxy-2-oxopyridin-1(2H)-yl)propyl)amino)-2-oxoethyl)-12-(carboxymethyl)-6,9-dioxa-3,12-diazatetradecane-1,14-dioic acid (49)**
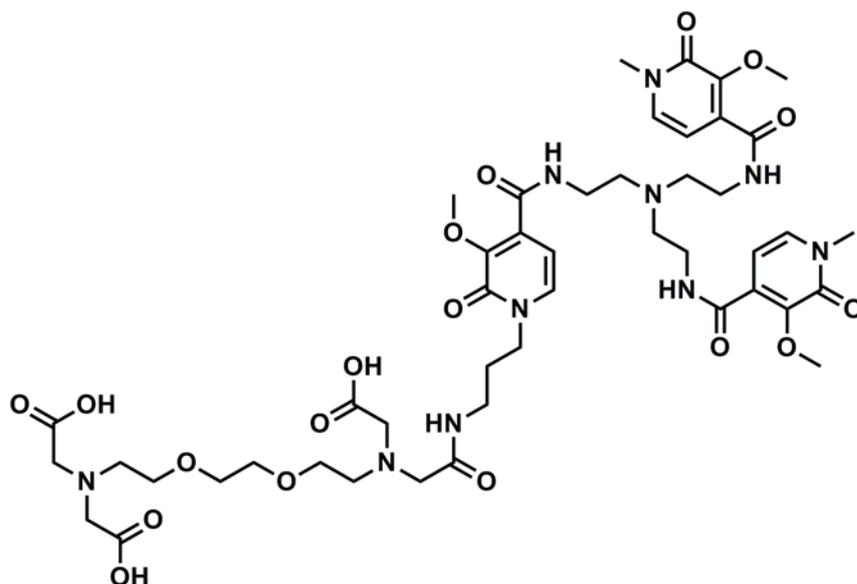


*tert*-Butyl ester **48** (0.11 g, 0.09 mmol) was dissolved in dry DCM (5 mL) and TFA (0.22 mL, 2.79 mmol) was added. The reaction was stirred at r.t overnight. The solvent and TFA were removed under reduced pressure. The crude triacid as a brown oil was used in the next step without further purification.

**$^1$H NMR:** (acetone-d$_6$) δ (ppm): 7.50-7.44 (m, 2H, N*H* amide), 7.33-7.30 (m, 3H, NC*H*), 7.14-7.12 (m, 3H, CHC*H*C), 6.47-6.43 (m, 3H, O*H*), 4.35-4.29 (m, 3H, alkyl C*H$_2$*), 3.94-3.44 (m, 45H, alkyl C*H$_2$*), 3.21-3.18 (m, 2H, alkyl C*H$_2$*).

**$^{13}$C NMR:** (acetone-d$_6$) δ (ppm): 170.3 (*C*(O) acid), 165.7, 165.2, 164.5 (*C*(O) amide), 152.6 (*C*(O) pyridinone), 137.8, 136.5, 134.3 (*C*OCH$_3$), 126.9, 123.1(N*C*H), 119.2 (CH*C*HC), 115.4, 109.4 (*C*HCHC), 75.3 (O*C*H$_2$), 65.1, 62.6, 62.1 (N*C*H$_2$), 58.9, 55.7 (O*C*H$_3$), 53.1(*C*H$_2$N scaffold), 43.9, 42.5(N*C*H$_2$CH$_2$CH$_2$NH), 40.3 (N*C*H$_3$), 36.9 (*C*H$_2$NH), 27.7 (NCH$_2$*C*H$_2$CH$_2$NH).

**{(2-{2-[2-(Bis-carboxymethyl-amino)-ethoxy]-ethoxy}-ethyl)-[(3-{4-[2-(bis-{2-[(3-hydroxy-1-methyl-2-oxo-1,2-dihydro-pyridine-4-carbonyl)-amino]-ethyl}-amino)-ethylcarbamoyl]-3-hydroxy-2-oxo-2*H*-pyridin-1-yl}-propylcarbamoyl)-methyl]-amino}-acetic acid (L2)**
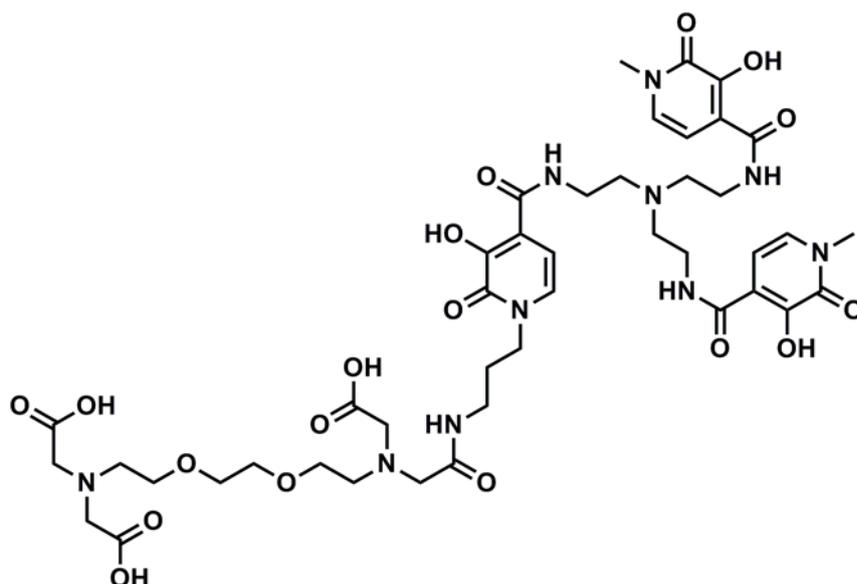


HOPO derivative **49** (0.091 g, 0.09 mmol) was dissolved under nitrogen in dry DMSO so that the concetration was approximately . Sodium ethanethiolate (0.055 g, 0.65 mmol) was added and the solution was stirred at 140 °C for 2 h. After cooling to r.t., water (50 ml) were added. All solvents were evporated under reduced pressure and the product was purified by HPLC (RT 18.9 min)to give **L2**.

**ESI-MS:** calcd. 1004.4, found 541.3 $[M+2K]^{2+}$, 627.4 $[M+2Na^{+}+3HCOONa]^{2+}$, 643.3 $[M+2K^{+}+3HCOONa]^{2+}$.

**N,N'-(3-(2-(3-Methoxy-1-methyl-2-oxo-1,2-dihydropyridine-4-carboxamido)ethyl)-3-nitropentane-1,5-diyl)bis(3-methoxy-1-methyl-2-oxo-1,2-dihydropyridine-4-carboxamide) (51)**
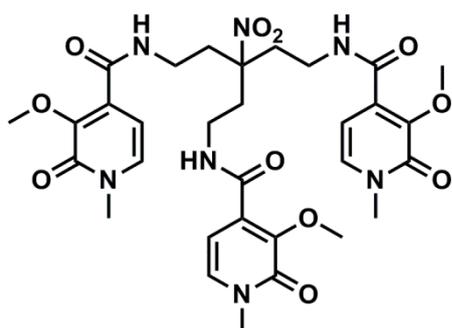
HOPO acid **9** (0.46 g, 2.51 mmol) was dissolved in dry DMF (5 mL) under inert atmosphere and pyridine (0.61 mL, 7.53 mmol) followed by perfluorophenyl 2,2,2-trifluoroacetate (0.65 mL, 3.77 mmol) were added. The reaction mixture was stirred overnight at r.t. The next day the solution was diluted with ethyl acetate and the organic phase was washed with water. The organic phase was dried over sodium sulfate and evaporated under reduced pressure. The crude product was used in the next step without further purification.

Triamine **50**[112] (0.114 g, 0.382 mmol) was suspended in dry DMF (2 mL) under inert atmosphere. DIPEA (2.0 mL, 11.45 mmol) was added and the suspension was stirred at r.t. for 1 h. Then a solution of activated ester in dry DMF (2 mL) was slowly added and the reaction mixture was stirred at r.t. for 72 h. The solvent was evaporated, the residue dissolved in DCM and washed with water. The organic phase was dried over sodium sulfate, evaporated under reduced pressure and the residue was purified by column chromatography (DCM:MeOH; 90:10) to give HOPO derivative **51** (0.118 g, 45% yield) as a brown oil.

**$^{1}$H NMR:** (CDCl$_3$) δ (ppm): 8.17 (m, 3H, N*H* amide), 7.06 (d, 3H, *J*=7.0 Hz, NC*H*), 6.62 (d, 3H, *J*=7.0 Hz, CHC*H*C), 3.99 (s, 9H, OC*H$_3$*), 3.47 (m, 15H, NC*H$_3$*, C*H$_2$*NH), 2.32 (m, 6H, C*H$_2$*C).

**$^{13}$C NMR:** (CDCl$_3$) δ (ppm): 163.7 (*C*(O) amide), 159.3 (*C*(O) pyridinone), 147.5 (*C*OCH$_3$), 132.2 (N*C*H), 129.5 (CH*C*HC), 104.3 (CH*C*HC), 90.4 (*C*(CH$_2$)$_3$NO$_2$), 60.1 (O*C*H$_3$), 37.5 (N*C*H$_3$), 35.1, 34.8 (*C*H$_2$).

### N,N'-(3-(2-(3-Hydroxy-1-methyl-2-oxo-1,2-dihydropyridine-4-carboxamido)ethyl)-3-nitropentane-1,5-diyl)bis(3-hydroxy-1-methyl-2-oxo-1,2-dihydropyridine-4-carboxamide) (L3)
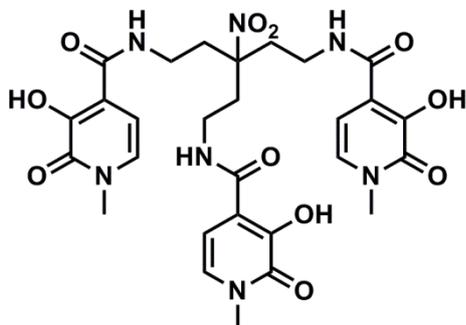
Methyl ether **51** (0.118 g, 0.17 mmol) was dissolved in dry DMSO under nitrogen to make a final solution 0.4 and 26 mM. Sodium ethanethiolate (0.109 g, 1.29 mmol) was added and the solution was stirred at 140 °C for 2 h. After cooling to r.t., 5-fold excess of water was added. All solvents were evporated under reduced pressure and the product was purified by HPLC (RT 17.1 min) to give **L3** (0.066 g, 54%) as a brown oil.

### [3-*tert*-Butoxycarbonylamino-1,1-bis-(2-tert-butoxycarbonylamino-ethyl)-propyl]-carbamic acid benzyl ester (53)
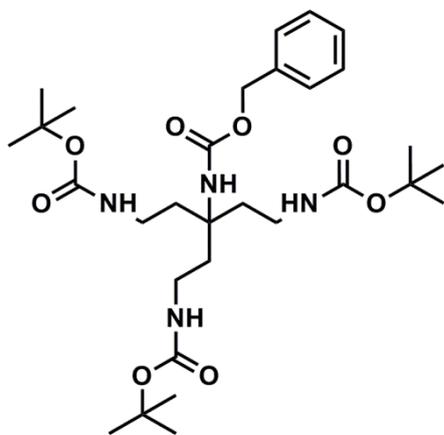
Amine **52**[124] (1.0 g, 2.17 mmol) was suspended in a mixture of ethyl acetate (10 mL0 and water (5 mL). Then sodium bicarbonate (0.365 g, 4.34 mmol) was added followed by slow addition of benzyl chloroformate (0.46 mL, 3.26 mmol). The reaction mixture was stirred at r.t overnight. Then the phases were separated and the water phase was extracted with ethyl acetate. The combined organic layers were dried over sodium sulfate and evaporated to dryness to give carbamate **53** (1.28 g, 99% yield) as a yellow oil.

**¹H NMR:** (CDCl$_3$) δ (ppm): 7.28-7.20 (m, 10H, Ph), 4.94-4.87 (m, 4H, C$H_2$Ph), 3.02 (m, 6H, C$H_2$NH), 1.79-1.74 (m, 6H, C(C$H_2$)$_3$), 1.37-1.33 (m, 27H, C(C$H_3$)$_3$).

**¹³C NMR:** (CDCl$_3$) δ (ppm): 156.1, 154.8 (C(O) carbamate), 141.2, 136.6, 128.7, 128.5, 128.4, 128.4, 126.9 (Ph), 79.2 ($C$(CH$_3$)$_3$), 66.1, 64.8 (C$H_2$Ph), 60.4, 55.5 ($C$(CH$_2$)$_3$), 35.7 (C$H_2$NH), 28.7, 28.4, 28.2 (C(C$H_3$)$_3$).

**ESI-MS:** calc. 594.4, found 633.3 [M+K]$^+$.

**HR-MS:** calc. 595.37014 [M+H]$^+$, found 595.37016 [M+H]$^+$.

## [3-Amino-1,1-bis-(2-amino-ethyl)-propyl]-carbamic acid benzyl ester (54)
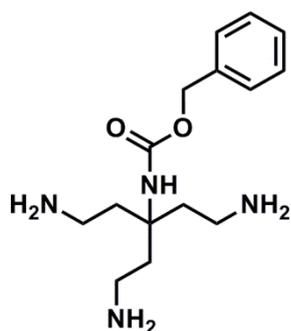
N-Boc carbamate **53** (1.18 g, 1.99 mmol) was dissolved in dry DCM (10 mL) and the solution was cooled with an ice bath. TFA (3.7 mL, 47.7 mmol) was added, the ice bath removed and the solution was stirred at r.t. over the weekend. Then the solvent was evaporated and the residue washed with methanol. After drying the reaction gave triamine **54** (1.0 g, 79% yield) as a yellow oil which was used in the next step without further purification.

$^1$**H NMR:** (CDCl$_3$) δ (ppm): 8.05 (bs, 2H, N*H*), 7.25-7.19 (m, 7H, Ph), 4.93 (s, 2H, C*H*$_2$Ph), 2.89-2.78 (m, 7H, C(C*H*$_2$)$_3$), 2.02-1.85 (m, 7H, C*H*$_2$NH$_2$), 1.23-1.18 (m, 3H Boc residue).

$^{13}$**C NMR:** (CDCl$_3$) δ (ppm): 155.1 (*C*(O) carbamate), 135.8, 128.4, 128.1, 127.2, 126.6 (Ph), 117.9, 114.1, 66.1, 64.0 (*C*H$_2$Ph), 53.8 (*C*(CH$_2$)$_3$), 34.2 (C(*C*H$_2$)$_3$), 31.9 (*C*H$_2$NH$_2$).

**ESI-MS:** calc. 294.2, found 295.2 [M+H]$^+$.

**HR-MS:** calc. 295.21285 [M+H]$^+$, found 295.21267 [M+H]$^+$.

## (3-[(3-Methoxy-1-methyl-2-oxo-1,2-dihydro-pyridine-4-carbonyl)-amino]-1,1-bis-{2-[(3-methoxy-1-methyl-2-oxo-1,2-dihydro-pyridine-4-carbonyl)-amino]-ethyl}-propyl)-carbamic acid benzyl ester (55)
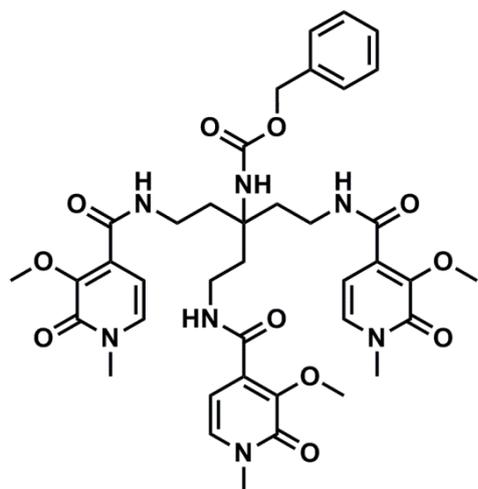
HOPO acid **9** (0.8 g, 4.37 mmol) was dissolved in dry DMF (5 mL). Pyridine (0.8 mL, 9.89 mmol) was added followed by perfluorophenyl 2,2,2-trifluoroacetate (0.8 mL, 4.64 mmol). The reaction mixture was stirred overnight at r.t. The solution was diluted with ethyl acetate and washed with water. The organic phase was dried over sodium sulphate and evaporated under reduced pressure to give the activated ester which was submitted for the next step without further purification.

Triamine **54** (0.46 g, 0.72 mmol) was dissolved in dry DMF (2 mL). DIPEA (2.5 mL, 14.3 mmol) was added and the solution was stirred at r.t for 1 h. Then a solution of the activated ester (1.5 g, 4.30 mmol) in dry DMF (2 mL) was slowly added and the reaction mixture was stirred at r.t for 24 h. The solvent was evaporated under reduced pressure, the residue was dissolved in DCM and washed with water. The organic phase was dried over sodium sulfate, evaporated under reduced pressure and the residue purified by column chromatography (DCM:MeOH, 90:10) to give HOPO derivative **55** (0.2 g, 35% yield) as a brown oil.

**^{1}H NMR:** (CDCl$_3$) δ (ppm): 8.10 (m, 3H, N*H* amide), 7.00 (d, 3H, *J*=7.2Hz, Ph), 6.63 (d, 3H, J=7.2Hz, NC*H*), 4.92 (s, 2H, C*H*$_2$Ph), 3.96 (s, 9H, OC*H*$_3$), 3.35-3.47 (m, 17H, NC*H*$_3$, C*H*$_2$NH), 2.05 (m, 6H, C(C*H*$_2$)$_3$).

**^{13}C NMR:** (CDCl$_3$) δ (ppm): 163.6, 163.5 (*C*(O) amide), 159.3 (*C*(O) pyridinone), 154.9 (*C*(O) carbamate), 147.4 (*C*OCH$_3$), 136.5, 132.2, 129.3, 128.3, 127.8, 127.6 (Ph), 104.5, 104.4 (CH*C*HC), 66.0 (*C*H$_2$Ph), 60.0 (O*C*H$_3$), 55.8, 55.7 (*C*(CH$_2$)$_3$), 50.3, 37.5 (N*C*H$_3$), 35.2 (C(*C*H$_2$)$_3$), 25.2 (*C*H$_2$NH).

**HR-MS:** calc. 790.34063 [M+H]$^+$, 812.32258 [M+Na]$^+$, found 790.34059 [M+H]$^+$, 812.32229 [M+Na]$^+$.

**N,N'-(3-Amino-3-(2-(3-hydroxy-1-methyl-2-oxo-1,2-dihydropyridine-4-carboxamido)ethyl)pentane-1,5-diyl)bis(3-hydroxy-1-methyl-2-oxo-1,2-dihydropyridine-4-carboxamide) (L4)**
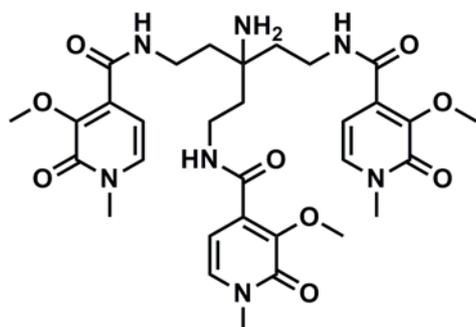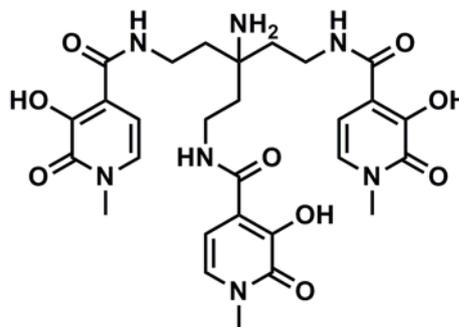


intermediate 56                                      L4

Benzyl carbamate **55** (0.1 g, 0.13 mmol) was dissolved in ethanol (5 mL). Palladium on carbon (0.1 g, 0.94 mmol) and ammonium formate (0.16 g, 2.53 mmol) were added and the reaction mixture was refluxed overnight. The next day the suspension was filtered through a pad of celite, the solvent evaporated to dryness to give amine **56** as brown oil which was used in the next step without further purification.

**ESI-MS**: calc. 655.3 found 656.3 [M+H]$^+$.

Methyl groups from phenols were removed as published by Kiessling et al.[102]

Amine **56** (83 mg, 0.13 mmol) was dissolved in DMSO under inert atmosphere so the concentration was between 0.4 and 26 mM. Sodium ethanethiolate (80 mg, 0.949 mmol) was added and the reaction mixture was heated at 140 °C for 2 h. After cooling to r.t a 4-fold excess of water was added to quench the thiolate. All solvents were evaporated under reduced pressure to give crude **L4** which was further purified by HPLC (RT 17.5 min) to give pure ligand (0.05 g, 58%) as brown oil.

**$^{13}$C NMR:** (MeOH-d$_4$) δ (ppm): 176.2 ($C$(O) amide), 161.2 ($C$(O) pyridinone), 147.7, 145.5 ($C$OH), 134.8 (N$C$H), 119.5 (CH$C$H$C$), 105.6 (CH$C$HC), 67.8, 67.6, 60.0 ($C$(CH$_2$)$_3$NH$_2$), 55.2, 40.4 (C($C$H$_2$)$_3$), 38.0, 37.8 ($C$H$_2$NH), 28.9 ($C$H$_3$N).

**General procedure for preparation of Gd-HOPO complexes.**

The procedure for preparing Gd-HOPO complexes is a modification of the one published by Kiessling *et al.*[102]

A sample of a HOPO ligand was dissolved in water with 10% $D_2O$ so that the concentration was 5 mM. Then 0.1 eq of $GdCl_3$ was added and the pH was adjusted between 7 and 8 with 0.1 M solution of NaOH 0.1 M solution of HCl, both in MilliQ water. The reaction mixture was heated for 1 h at 80 °C and then the pH was adjusted back between 7 and 8 with the above mentioned solutions. The temperature was decreased to 40 °C and the reaction was equilibrated at this temperature overnight. The next day pH was adjusted between 7 and 8 with the before mentioned solutions, the precipitate was centrifuged and the clean solution was used for further studies.

The solutions used for determining the purity of ligands **L3** and **L4** were prepared according to a published procedure.[115]

**General procedure for preparation of solutions for the thermodynamic stability determination.**

The procedure is a modification of the one published by Pierre *et al.*[83]

Varying volumes of DTPA-BMA (C.L.) stock solution were added to solutions of identical concentrations of HOPO ligand **L3**/**L4**, standardized $Gd^{3+}$ solution, electrolyte (NaCl), HEPES buffer. All solutions were brought to identical volumes. A molar ratio of 1:1 for $Gd^{3+}$/ligand, and molar ratios of 1:0.5 up to 1:500 for ligand/C.L. were used. Typical final concentrations were 50 µM of ligand and metal, 0.1 M NaCl, and 1 mM HEPES. All samples were equilibrated in an oven at 40 °C for at least 12 h.

# Chapter 7

# References

# References

(1)     Lauffer, R. B. *Chemical Reviews* **1987**, *87*, 901.

(2)     Caravan, P.; Ellison, J. J.; McMurry, T. J.; Lauffer, R. B. *Chemical Reviews* **1999**, *99*, 2293.

(3)     Logothetis, N. K.; Wandell, B. A. *Annu. Rev. Physiol.* **2004**, *66*, 735.

(4)     Bonnet, C. S.; Toth, E. *Future Medicinal Chemistry* **2010**, *2*, 367.

(5)     Huettel S.A., S. A. W., McCarthy G. *Functional Magnetic Resonance Imaging*, 2009.

(6)     Werner, E. J.; Datta, A.; Jocher, C. J.; Raymond, K. N. *Angewandte Chemie-International Edition* **2008**, *47*, 8568.

(7)     Andre E. Merbach, Eva Toth *The chemistry of contrast agents in medical magnetic resonance imaging*; John Wiley & Sons, LTD, 2001.

(8)     Idee, J.-M.; Port, M.; Robic, C.; Medina, C.; Sabatou, M.; Corot, C. *Journal of Magnetic Resonance Imaging* **2009**, *30*, 1249.

(9)     Sherry, A. D.; Caravan, P.; Lenkinski, R. E. *Journal of Magnetic Resonance Imaging* **2009**, *30*, 1240.

(10)    Cacheris, W. P.; Quay, S. C.; Rocklage, S. M. *Magnetic Resonance Imaging* **1990**, *8*, 467.

(11)    Zhang, X.; Chang, C. A.; Brittain, H. G.; Garrison, J. M.; Telser, J.; Tweedle, M. F. *Inorganic Chemistry* **1992**, *31*, 5597.

(12)    Kumar, K.; Chang, C. A.; Francesconi, L. C.; Dischino, D. D.; Malley, M. F.; Gougoutas, J. Z.; Tweedle, M. F. *Inorganic Chemistry* **1994**, *33*, 3567.

(13)    Baranyai, Z.; Uggeri, F.; Giovenzana, G. B.; Bényei, A.; Brücher, E.; Aime, S. *Chemistry – A European Journal* **2009**, *15*, 1696.

(14)    Aime, S.; Calabi, L.; Cavallotti, C.; Gianolio, E.; Giovenzana, G. B.; Losi, P.; Maiocchi, A.; Palmisano, G.; Sisti, M. *Inorganic Chemistry* **2004**, *43*, 7588.

(15)    Kim, W. D.; Kiefer, G. E.; Maton, F.; McMillan, K.; Muller, R. N.; Sherry, A. D. *Inorganic Chemistry* **1995**, *34*, 2233.

(16)    Aime, S.; Botta, M.; Geninatti Crich, S.; Giovenzana, G. B.; Jommi, G.; Pagliarin, R.; Sisti, M. *Inorganic Chemistry* **1997**, *36*, 2992.

(17)    Kim, W. D.; Hrncir, D. C.; Kiefer, G. E.; Sherry, A. D. *Inorganic Chemistry* **1995**, *34*, 2225.

(18)    Laus, S.; Ruloff, R.; Toth, E.; Merbach, A. E. *Chemistry-a European Journal* **2003**, *9*, 3555.

(19)    Jaszberenyi, Z.; Sour, A.; Toth, E.; Benmelouka, M.; Merbach, A. E. *Dalton Transactions* **2005**, 2713.

(20)    Polasek, M.; Rudovsky, J.; Hermann, P.; Lukes, I.; Vander Else, L.; Muller, R. N. *Chemical Communications* **2004**, 2602.

(21)    Rudovsky, J.; Kotek, J.; Hermann, P.; Lukes, I.; Mainero, V.; Aime, S. *Organic & Biomolecular Chemistry* **2005**, *3*, 112.

(22)    Aime, S.; Botta, M.; Crich, S. G.; Giovenzana, G.; Pagliarin, R.; Sisti, M.; Terreno, E. *Magnetic Resonance in Chemistry* **1998**, *36*, S200.

(23)    Zech, S. G.; Eldredge, H. B.; Lowe, M. P.; Caravan, P. *Inorganic Chemistry* **2007**, *46*, 3576.

(24)    Muller, R. N.; Raduchel, B.; Laurent, S.; Platzek, J.; Pierart, C.; Mareski, P.; Vander Elst, L. *European Journal of Inorganic Chemistry* **1999**, 1949.

(25)    Nicolle, G. M.; Toth, E.; Schmitt-Willich, H.; Raduchel, B.; Merbach, A. E. *Chemistry-a European Journal* **2002**, *8*, 1040.

(26)    Dhingra, K.; Maier, M. E.; Beyerlein, M.; Angelovski, G.; Logothetis, N. K. *Chemical Communications* **2008**, 3444.

(27)    Atanasijevic, T.; Shusteff, M.; Fam, P.; Jasanoff, A. *Proceedings of the National Academy of Sciences of the United States of America* **2006**, *103*, 14707.

(28)    Sherry, A. D.; Woods, M. In *Annual Review of Biomedical Engineering* 2008; Vol. 10, p 391.

(29)    Chauvin, T.; Durand, P.; Bernier, M.; Meudal, H.; Doan, B.-T.; Noury, F.; Badet, B.; Beloeil, J.-C.; Toth, E. *Angewandte Chemie-International Edition* **2008**, *47*, 4370.

(30)    Aime, S.; Barge, A.; Castelli, D. D.; Fedeli, F.; Mortillaro, A.; Nielsen, F. U.; Terreno, E. *Magnetic Resonance in Medicine* **2002**, *47*, 639.

(31)    Grienberger, C.; Konnerth, A. *Neuron* **2012**, *73*, 862.

(32)    Li, W.-h.; Fraser, S. E.; Meade, T. J. *Journal of the American Chemical Society* **1999**, *121*, 1413.

(33)    Dhingra, K.; Fouskova, P.; Angelovski, G.; Maier, M. E.; Logothetis, N. K.; Toth, E. *Journal of Biological Inorganic Chemistry* **2008**, *13*, 35.

(34)    Angelovski, G.; Fouskova, P.; Mamedov, I.; Canals, S.; Toth, E.; Logothetis, N. K. *Chembiochem* **2008**, *9*, 1729.

(35)    Hanaoka, K.; Kikuchi, K.; Urano, Y.; Narazaki, M.; Yokawa, T.; Sakamoto, S.; Yamaguchi, K.; Nagano, T. *Chemistry & Biology* **2002**, *9*, 1027.

## References

(36)    Esqueda, A. C.; Lopez, J. A.; Andreu-de-Riquer, G.; Alvarado-Monzon, J. C.; Ratnakar, J.; Lubag, A. J. M.; Sherry, A. D.; De Leon-Rodriguez, L. M. *Journal of the American Chemical Society* **2009**, *131*, 11387.

(37)    Vallee, B. L.; Falchuk, K. H. *Physiological Reviews* **1993**, *73*, 79.

(38)    Frederickson, C. J.; Koh, J. Y.; Bush, A. I. *Nature Reviews Neuroscience* **2005**, *6*, 449.

(39)    Hanaoka, K.; Kikuchi, K.; Urano, Y.; Nagano, T. *Journal of the Chemical Society-Perkin Transactions 2* **2001**, 1840.

(40)    Major, J. L.; Boiteau, R. M.; Meade, T. J. *Inorganic Chemistry* **2008**, *47*, 10788.

(41)    Zecca, L.; Youdim, M. B. H.; Riederer, P.; Connor, J. R.; Crichton, R. R. *Nature Reviews Neuroscience* **2004**, *5*, 863.

(42)    Ruloff, R.; Koten, G. v.; Merbach, A. E. *Chemical Communications* **2004**, 842.

(43)    Livramento, J. B.; Toth, E.; Sour, A.; Borel, A.; Merbach, A. E.; Ruloff, R. *Angewandte Chemie-International Edition* **2005**, *44*, 1480.

(44)    Parac-Vogt, T. N.; Elst, L. V.; Kimpe, K.; Laurent, S.; Burtea, C.; Chen, F.; Van Deun, R.; Ni, Y.; Muller, R. N.; Binnemans, K. *Contrast Media & Molecular Imaging* **2006**, *1*, 267.

(45)    Paris, J.; Gameiro, C.; Humblet, V.; Mohapatra, P. K.; Jacques, V.; Desreux, J. F. *Inorganic Chemistry* **2006**, *45*, 5092.

(46)    Chesler, M. *Physiological Reviews* **2003**, *83*, 1183.

(47)    Raghunand, N.; Altbach, M. I.; van Sluis, R.; Baggett, B.; Taylor, C. W.; Bhujwalla, Z. M.; Gillies, R. J. *Biochemical Pharmacology* **1999**, *57*, 309.

(48)    Zhang, S. R.; Wu, K. C.; Sherry, A. D. *Angewandte Chemie-International Edition* **1999**, *38*, 3192.

(49)    Garcia-Martin, M. L.; Martinez, G. V.; Raghunand, N.; Sherry, A. D.; Zhang, S. R.; Gillies, R. J. *Magnetic Resonance in Medicine* **2006**, *55*, 309.

(50)    Yuguo, L.; Sheth, V. R.; Guanshu, L.; Pagel, M. D. *Contrast Media & Molecular Imaging* **2011**, *6*, 219.

(51)    Moats, R. A.; Fraser, S. E.; Meade, T. J. *Angewandte Chemie-International Edition in English* **1997**, *36*, 726.

(52)    Louie, A. Y.; Huber, M. M.; Ahrens, E. T.; Rothbacher, U.; Moats, R.; Jacobs, R. E.; Fraser, S. E.; Meade, T. J. *Nature Biotechnology* **2000**, *18*, 321.

(53)   Arena, F.; Singh, J. B.; Gianolio, E.; Stefanìa, R.; Aime, S. *Bioconjugate Chemistry* **2011**, *22*, 2625.

(54)   Westmeyer, G. G.; Durocher, Y.; Jasanoff, A. *Angewandte Chemie-International Edition* **2010**, *49*, 3909.

(55)   Aime, S.; Delli Castelli, D.; Fedeli, F.; Terreno, E. *Journal of the American Chemical Society* **2002**, *124*, 9364.

(56)   Trokowski, R.; Zhang, S. R.; Sherry, A. D. *Bioconjugate Chemistry* **2004**, *15*, 1431.

(57)   Koretsky, A. P. *Neuroimage* **2012**, *62*, 1208.

(58)   Shapiro, M. G.; Westmeyer, G. G.; Romero, P. A.; Szablowski, J. O.; Kuester, B.; Shah, A.; Otey, C. R.; Langer, R.; Arnold, F. H.; Jasanoff, A. *Nature Biotechnology* **2010**, *28*, 264.

(59)   Lelyveld, V. S.; Brustad, E.; Arnold, F. H.; Jasanoff, A. *Journal of the American Chemical Society* **2011**, *133*, 649.

(60)   Tei, L.; Barge, A.; Crich, S. G.; Pagliarin, R.; Negri, V.; Ramella, D.; Cravotto, G.; Aime, S. *Chemistry-a European Journal* **2010**, *16*, 8080.

(61)   Mishra, A.; Schuez, A.; Engelmann, J.; Beyerlein, M.; Logothetis, N. K.; Canals, S. *ACS Chemical Neuroscience* **2011**, *2*, 578.

(62)   Mamedov, I.; Engelmann, J.; Eschenko, O.; Beyerlein, M.; Logothetis, N. K. *Chemical Communications*  **2012**, *48*, 2755.

(63)   Wu, C. W. H.; Vasalatiy, O.; Liu, N.; Wu, H.; Cheal, S.; Chen, D.-Y.; Koretsky, A. P.; Griffiths, G. L.; Tootell, R. B. H.; Ungerleider, L. G. *Neuron* **2011**, *70*, 229.

(64)   Bruce, J. I.; Dickins, R. S.; Govenlock, L. J.; Gunnlaugsson, T.; Lopinski, S.; Lowe, M. P.; Parker, D.; Peacock, R. D.; Perry, J. J. B.; Aime, S.; Botta, M. *Journal of the American Chemical Society* **2000**, *122*, 9674.

(65)   Xu, J.; Franklin, S. J.; Whisenhunt, D. W.; Raymond, K. N. *Journal of the American Chemical Society* **1995**, *117*, 7245.

(66)   Kenneth N. Raymond; Daniel M. J. Doble, T., OR ;Christopher J. Sunderland; Thompson, Andrew J.  2005; Vol. US 6,846,915 B2.

(67)   Cohen, S. M.; Xu, J. D.; Radkov, E.; Raymond, K. N.; Botta, M.; Barge, A.; Aime, S. *Inorganic Chemistry* **2000**, *39*, 5747.

(68)   Sunderland, C. J.; Botta, M.; Aime, S.; Raymond, K. N. *Inorganic Chemistry* **2001**, *40*, 6746.

(69)    Puerta, D. T.; Botta, M.; Jocher, C. J.; Werner, E. J.; Avedano, S.; Raymond, K. N.; Cohen, S. M. *Journal of the American Chemical Society* **2006**, *128*, 2222.

(70)    Jocher, C. J.; Moore, E. G.; Xu, J. D.; Avedano, S.; Botta, M.; Aime, S.; Raymond, K. N. *Inorganic Chemistry* **2007**, *46*, 9182.

(71)    Seitz, M.; Pluth, M. D.; Raymond, K. N. *Inorganic Chemistry* **2007**, *46*, 351.

(72)    Weitl, F. L.; Raymond, K. N.; Durbin, P. W. *Journal of Medicinal Chemistry* **1981**, *24*, 203.

(73)    Hajela, S.; Botta, M.; Giraudo, S.; Xu, J. D.; Raymond, K. N.; Aime, S. *Journal of the American Chemical Society* **2000**, *122*, 11228.

(74)    Hajela, S. P.; Johnson, A. R.; Xu, J. D.; Sunderland, C. J.; Cohen, S. M.; Caulder, D. L.; Raymond, K. N. *Inorganic Chemistry* **2001**, *40*, 3208.

(75)    O'Sullivan, B.; Doble, D. M. J.; Thompson, M. K.; Siering, C.; Xu, J. D.; Botta, M.; Aime, S.; Raymond, K. N. *Inorganic Chemistry* **2003**, *42*, 2577.

(76)    Werner, E. J.; Avedano, S.; Botta, M.; Hay, B. P.; Moore, E. G.; Aime, S.; Raymond, K. N. *Journal of the American Chemical Society* **2007**, *129*, 1870.

(77)    Jocher, C. J.; Botta, M.; Avedano, S.; Moore, E. G.; Xu, J. D.; Aime, S.; Raymond, K. N. *Inorganic Chemistry* **2007**, *46*, 4796.

(78)    Moore, E. G.; Jocher, C. J.; Xu, J. D.; Werner, E. J.; Raymond, K. N. *Inorganic Chemistry* **2007**, *46*, 5468.

(79)    Werner, E. J.; Botta, M.; Aime, S.; Raymond, K. N. *Contrast Media & Molecular Imaging* **2009**, *4*, 220.

(80)    Klemm, P. J.; Floyd, W. C., III; Smiles, D. E.; Frechet, J. M. J.; Raymond, K. N. *Contrast Media & Molecular Imaging* **2012**, *7*, 95.

(81)    Johnson, A. R.; O'Sullivan, B.; Raymond, K. N. *Inorganic Chemistry* **2000**, *39*, 2652.

(82)    Thompson, M. K.; Doble, D. M. J.; Tso, L. S.; Barra, S.; Botta, M.; Aime, S.; Raymond, K. N. *Inorganic Chemistry* **2004**, *43*, 8577.

(83)    Pierre, V. C.; Botta, M.; Aime, S.; Raymond, K. N. *Inorganic Chemistry* **2006**, *45*, 8355.

(84)    Majoral, J. P. *New Journal of Chemistry* **2007**, *31*, 1039.

(85)    Pierre, V. C.; Botta, M.; Raymond, K. N. *Journal of the American Chemical Society* **2005**, *127*, 504.

(86)   Floyd, W. C., III; Klemm, P. J.; Smiles, D. E.; Kohlgruber, A. C.; Pierre, V. C.; Mynar, J. L.; Frechet, J. M. J.; Raymond, K. N. *Journal of the American Chemical Society* **2011**, *133*, 2390.

(87)   Klemm, P. J.; Floyd, W. C., III; Andolina, C. M.; Frechet, J. M. J.; Raymond, K. N. *European Journal of Inorganic Chemistry* **2012**, 2108.

(88)   Behbehani, G. R.; Barzegar, L.; Savad Koohi, M. K. K.; Mohebbian, M.; Abedi, B. S.; Saboury, A. A.; Divsalar, A. *Journal of Chemistry* **2013**, *2013*, 4.

(89)   Datta, A.; Hooker, J. M.; Botta, M.; Francis, M. B.; Aime, S.; Raymond, K. N. *Journal of the American Chemical Society* **2008**, *130*, 2546.

(90)   Garimella, P. D.; Datta, A.; Romanini, D. W.; Raymond, K. N.; Francis, M. B. *Journal of the American Chemical Society* **2011**, *133*, 14704.

(91)   Pierre, V. C.; Melchior, M.; Doble, D. M. J.; Raymond, K. N. *Inorganic Chemistry* **2004**, *43*, 8520.

(92)   Pundir, C. S.; Sharma, M. *Journal of Scientific & Industrial Research* **2010**, *69*, 489.

(93)   Spitzer, N. C. *Nature* **2006**, *444*, 707.

(94)   Vizard, T. N.; O'Keeffe, G. W.; Gutierrez, H.; Kos, C. H.; Riccardi, D.; Davies, A. M. *Nature Neuroscience* **2008**, *11*, 285.

(95)   Nicholson, C.; Tenbruggencate, G.; Stockle, H.; Steinberg, R. *Journal of Neurophysiology* **1978**, *41*, 1026.

(96)   Doble, D. M. J.; Melchior, M.; O'Sullivan, B.; Siering, C.; Xu, J. D.; Pierre, V. C.; Raymond, K. N. *Inorganic Chemistry* **2003**, *42*, 4930.

(97)   Fox, R. C.; Taylor, P. D. *Synthetic Communications* **1998**, *28*, 1563.

(98)   Martin, R. *Organic Preparations and Procedures International* **1992**, *24*, 369.

(99)   Nakai, T.; Mikami, K. *Chemical Reviews* **1986**, *86*, 885.

(100)  Hanessian, S.; Saavedra, O. M.; Mascitti, V.; Marterer, W.; Oehrlein, R.; Mak, C. P. *Tetrahedron* **2001**, *57*, 3267.

(101)  Hong, S. Y.; Tobias, G.; Al-Jamal, K. T.; Ballesteros, B.; Ali-Boucetta, H.; Lozano-Perez, S.; Nellist, P. D.; Sim, R. B.; Finucane, C.; Mather, S. J.; Green, M. L. H.; Kostarelos, K.; Davis, B. G. *Nature Materials* **2010**, *9*, 485.

(102)  Allen, M. J.; Raines, R. T.; Kiessling, L. L. *Journal of the American Chemical Society* **2006**, *128*, 6534.

# References

(103) Liu, D.; Wu, W.; Qiu, Y.; Lu, J.; Yang, S. *The Journal of Physical Chemistry C* **2007**, *111*, 17713.

(104) Sterzycki, R. *Synthesis-Stuttgart* **1979**, 724.

(105) Huet, F.; Lechevallier, A.; Pellet, M.; Conia, J. M. *Synthesis-Stuttgart* **1978**, 63.

(106) Abdel-Magid, A. F.; Mehrman, S. J. *Organic Process Research & Development* **2006**, *10*, 971.

(107) Gatto, V. J.; Miller, S. R.; Gokel, G. W. *Organic Syntheses* **1990**, *68*, 227.

(108) Greene, T. W. W., P.G *Protective groups in organic synthesis*; 3rd ed.; John Wiley & Sons, Inc., 1999.

(109) Mani, T.; Tircsó, G.; Togao, O.; Zhao, P.; Soesbe, T. C.; Takahashi, M.; Sherry, A. D. *Contrast Media & Molecular Imaging* **2009**, *4*, 183.

(110) Sensi, S. L.; Paoletti, P.; Bush, A. I.; Sekler, I. *Nature Reviews Neuroscience* **2009**, *10*, 780.

(111) Botta, M.; Tei, L. *European Journal of Inorganic Chemistry* **2012**, 1945.

(112) Zhao, X.; Schanze, K. S. *Chemical Communications* **2010**, *46*, 6075.

(113) Albert, A.; Brown, D. J.; Cheeseman, G. *Journal of the Chemical Society* **1951**, 474.

(114) Kaim, W.; Schwederski, B.; Heilmann, O.; Hornung, F. M. *Coordination Chemistry Reviews* **1999**, *182*, 323.

(115) Barge, A.; Cravotto, G.; Gianolio, E.; Fedeli, F. *Contrast Media & Molecular Imaging* **2006**, *1*, 184.

(116) Kobayashi, H.; Brechbiel, M. W. *Advanced Drug Delivery Reviews* **2005**, *57*, 2271.

(117) Kalber, T. L.; Kamaly, N.; So, P.-W.; Pugh, J. A.; Bunch, J.; McLeod, C. W.; Jorgensen, M. R.; Miller, A. D.; Bell, J. D. *Molecular Imaging and Biology* **2011**, *13*, 653.

(118) Yantasee, W.; Fryxell, G. E.; Porter, G. A.; Pattamakomsan, K.; Sukwarotwat, V.; Chouyyok, W.; Koonsiripaiboon, V.; Xu, J.; Raymond, K. N. *Nanomedicine: Nanotechnology, Biology and Medicine* **2010**, *6*, 1.

(119) Corsi, D. M.; Platas-Iglesias, C.; Bekkum, H. v.; Peters, J. A. *Magnetic Resonance in Chemistry* **2001**, *39*, 723.

(120) Formica, M.; Fusi, V.; Giorgi, L.; Guerri, A.; Lucarini, S.; Micheloni, M.; Paoli, P.; Pontellini, R.; Rossi, P.; Tarzia, G.; Zappia, G. *New Journal of Chemistry* **2003**, *27*, 1575.

(121) Gérard, E.; Bessy, E.; Salvagnini, C.; Rerat, V.; Momtaz, M.; Hénard, G.; Marmey, P.; Verpoort, T.; Marchand-Brynaert, J. *Polymer* **2011**, *52*, 1223.

(122) Almiento, G. M.; Balducci, D.; Bottoni, A.; Calvaresi, M.; Porzi, G. *Tetrahedron-Asymmetry* **2007**, *18*, 2695.

(123) Vernekar, S. K. V.; Hallaq, H. Y.; Clarkson, G.; Thompson, A. J.; Silvestri, L.; Lummis, S. C. R.; Lochner, M. *Journal of Medicinal Chemistry* **2010**, *53*, 2324.

(124) Baldoli, C.; Rigamonti, C.; Maiorana, S.; Licandro, E.; Falciola, L.; Mussini, P. R. *Chemistry-a European Journal* **2006**, *12*, 4091.

# Chapter 8

# Appendix

## Synthesis of 3,2-hydroxypyridinone (3,2-HOPO) based smart contrast agents for functional magnetic resonance imaging

Over the last 20 years magnetic resonance imaging (MRI) became a very important diagnostic and research tool in biology and medicine. Recent progress of the MRI technique led to the development of new high field devices with magnetic field strengths often exceeding 300 MHz. Yet the majority of the contrast agents (CA) applied to improve the signal to noise ratio of the MR images are efficient only at lower magnetic fields (up to 100 MHz). Therefore, it is crucial to develop agents that are able to significantly improve the quality of the images at high magnetic fields. Additionally, in basic research using functional MRI (fMRI), smart contrast agents which can recognize changes in the surrounding *in vivo* environment are needed, e.g. to precisely map brain activity or mark specific cell clusters in a straightforward manner.

Recently, a novel 3,2-hydroxypyridinone-based (3,2-HOPO) system was published showing a great potential to become a high field CA due to its outstanding paramagnetic properties, dependent on high hydration number. In addition these agents have reasonable thermodynamic stability and show no interactions with endogenous anions making them a promising platform for developing responsive MRI probes. Unfortunately, the challenging synthetic procedure and the requirement of special equipment limited the application of such molecules. Here I developed a new synthetic pathway that allows synthesis of the 3,2-Hopo based molecule using techniques available in each standard chemistry laboratory. Two ion responsive 3,2-HOPO reporters with an EGTA type $Ca^{2+}$-chelator attached via an amine or an amide bond were synthesized, and their performance in presence of biologically significant ions ($Ca^{2+}$ and $Zn^{2+}$) was examined.

In addition, I developed a 3,2-HOPO MR reporter utilizing a new type of scaffold containing an additional amine group. This new scaffold allows further modifications of the agent according to needs without demanding synthesis and opens a way towards targeted contrast agents. The relaxometric and spectrophotometric characteristics of the agent were examined. Moreover, the ligand itself can be potentially applied in chelation therapies or preparation of novel medical materials.

**Synthese und Auswertung von 3,2-hydroxypyridinone (3,2-HOPO) basierenden intelligenten Kontrastmitteln zur funktionellen Magnetresonanz Tomographie**

In den letzten 20 Jahren hat sich die Magnet-Resonanz-Tomographie (MRT) zu einem der wichtigsten und weitverbreitesten Bildgebungsverfahren in der biologischen und medizinischen Forschung und Diagnostik entwickelt. Aktuelle Entwicklungen in der MRT Technik haben zur Entwicklung neuer Hoch-Feld Magnetresonanz-Tomographen geführt die nicht selten Feldstärken von über 300 MHz erreichen. Die Mehrzahl der verfügbaren Kontrastmittel zur Verbesserung des Signal-Rausch Verhältnis in der MRT sind allerdings meist nur für die Verwendung unter geringeren Feldstärken geeignet (100 MHz). Die Entwicklung neuer Kontrastmittel zur Anwendung unter hohen magnetischen Feldstärken ist daher zwingend erforderlich. In der Grundlagenforschung besteht darüber hinaus im Bereich der funktionellen MRT ein großer Bedarf an sogenannten intelligenten Kontrastmitteln, welche es ermöglichen biologische Prozesse und Abläufe, wie z.B. die Hirnaktivität oder die Markierung spezifischer-Zell Cluster, in vivo direkt sichtbar zu machen.

Ein vielversprechender Kandidat für die Entwicklung intelligenter Kontrastmittel zur Anwendung in der Hoch-Feld-MRT ist ein vor kurzem veröffentlichtes auf 3,2-Hydroxypyridinon (3,2-HOPO) basierendes System, welches aufgrund seiner hohen Hydrationszahl hervorragende paramagnetische Eigenschaften besitzt. Zusätzlich besitzen diese Stoffe eine angemessene thermodynamische Stabilität und zeigen keine Interaktionen mit endogenen Anionen, was sie zur aussichtsreichen Grundlage für die Entwicklung von responsiven MRT-Proben macht. Die Synthese dieser Moleküle ist allerdings mit großem technischem Aufwand verbunden, was ihre Anwendung erheblich einschränkt.

Hier stelle ich ein von mir entwickeltes neues Verfahren zur Synthese von auf 3,2-HOPO basierenden Molekülen vor, welches es erlaubt diese Stoffe unter Verwendung von in jedem gängigen Chemielabor zur Verfügung stehenden Techniken herzustellen. Zwei Ionen responsive 3,2-HOPO Reporter mit einem über Amin oder Amid-Bindung angeschlossenem EGTA $Ca^{2+}$ Chelator wurden

synthetisiert und hinsichtlich ihrer Eigenschaften zur Registrierung biologisch relevanter Ionen untersucht.

Zusätzlich habe ich einen 3,2-HOPO-MR-Reporter entwickelt welcher die Eigenschaften eines neuen Typs von Scaffold mit einer zusätzlichen Amin Gruppe ausnützt. Dieser neue Scaffold-Typ ermöglicht je nach Bedarf weitere Modifikationen des Stoffes ohne aufwendige Synthese und eröffnet dadurch neue Möglichkeiten zur Herstellung verschiedener targeted Kontrastmittel. Die relaxometrischen und spektrophotometrischen Eigenschaften dieses Stoffes wurden untersucht. Die möglichen Anwendungen des Liganden selbst beinhalten u.a. chelation Therapien oder die Entwicklung neuer medizinischer Materialien.